Design, Modelling and Fault Analysis of Induction Motor Drive System using ANSYS

Thesis

Submitted to the

G. B. Pant University of Agriculture & Technology

Pantnagar -263145 Uttarakhand, India

By

Rajat Sharma

B.Tech (Electrical and Electronics Engineering)

IN PARTIAL FULFILLMENT OF THE REQUIREMENTS FOR THE DEGREE OF

Master of Technology

In

Electrical Engineering

(Electrical Energy System)

August, 2018

ACKNOWLEDGEMENT

Seldom are the works which could be accomplished without the help of others hence I would like to express my sincere gratitude to my thesis advisor ***Dr. Rajiv Singh****, Assistant Professor, Department of Electrical Engineering and Chairman of Advisory Committee for his sincere support and guidance throughout my thesis work. I would like to express my deep gratitude and respect to the esteemed members of my Advisory Committee,* ***Dr. Sudha Arora****, Professor and Head, Department of Electrical Engineering,* ***Dr. A.K. Swami****, Professor, Department of Electrical Engineering and* ***Dr. Ajay Srivastava****, Professor, Department of Electrical Engineering.*

I express my sincere thanks to ***Dr. J.P. Pandey****, Dean, College of Post Graduate Studies,* ***Dr. H. C. Sharma****, Dean, College of Technology and* ***Dr. R.S. Jadaoun,*** *Dean, Student Welfare, G. B. Pant University of Agriculture & Technology, Pantnagar for providing necessary facilities to carry out the study and for giving me this wonderful opportunity to do my M.Tech. Thesis in this prestigious institute.*

I am thankful to ***Dr. H.S. Rawat****, Assistant Professor, Department of Electrical Engineering who has been an unparalleled mentor at each and every step of my M.Tech Thesis work. I am also grateful to the faculty members for their support and cooperation throughout the duration of my degree programme.*

I am overwhelmed to express profound sense of indebtedness to my beloved parents ***Shri. Lalit Sharma*** *and* ***Smt. Sunita Sharma*** *whose continuous encouragement and blessings have brought me at this stage. Thanks to my siblings* ***Ketan*** *and* ***Vandana*** *for their affection and encouragement during my studies. I would like to pay high regards to* ***Mr. DS Bisht, Harshit, Shubham*** *and all my friends for their support, pleasant company, help and care. I finally thank all beloved and respected people around me who directly or indirectly helped me during my degree programme.*

Pantnagar
August, 2018

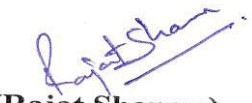

(Rajat Sharma)
Author

CERTIFICATE

This is to certify that the thesis entitled **"Design, Modelling and Fault Analysis of Induction Motor Drive System using ANSYS"**, submitted in partial fulfillment of the requirements for the degree of **Master of Technology (Electrical Engineering)** with major in **Electrical Energy System** of the College of Post Graduate Studies, G. B. Pant University of Agriculture & Technology, Pantnagar, is a record of *bona fide* research carried out by **Mr. Rajat Sharma,** Id. No. **50912** under my supervision and no part of the thesis has been submitted for any other degree or diploma.

The assistance and help received during the course of this investigation have been acknowledged.

Pantnagar
August, 2018

(Rajiv Singh)
Chairman
Advisory committee

CERTIFICATE

We, the undersigned members of the Advisory Committee of **Mr. Rajat Sharma, Id. No. 50912,** a candidate for the degree of **Master of Technology (Electrical Engineering)** with major in **Electrical Energy System** of the College of Post-Graduate Studies, G.B. Pant University of Agriculture and Technology, Pantnagar, agree that the thesis entitled **"Design, Modelling and Fault Analysis of Induction Motor Drive System using ANSYS",** may be submitted in partial fulfillment of the requirements for the degree.

(Rajiv Singh)
Chairman
Advisory Committee

(Sudha Arora)
Member

(A.K. Swami)
Member

(Ajay Srivastava)
Member

CONTENTS

LIST OF TABLES

LIST OF FIGURES

LIST OF ABBREVIATIONS AND SYMBOLS

ϕ	Phase
^{o}	Degree
N_s	Synchronous Speed
SMPS	Switched Mode Power Supply
AC	Alternating Current
DC	Direct Current
SRM	Switched Reluctance Motor
kW	kilowatt
MW	megawatt
VFD	Variable Frequency Drive
ASD	Adjustable Speed Drive
VSD	Variable Speed Drive
DSP	Digital Signal Processor
IGBT	Insulated Gate Bipolar Transistor
MOSFET	Metal Oxide Semiconductor Field Effect Transistor
SCR	Silicon Controlled Rectifier
PWM	Pulse Width Modulation
SVPWM	Space Vector Pulse Width Modulation
SPWM	Sinusoidal Pulse Width Modulation
3D	Three Dimensional
2D	Two Dimensional
DTC	Direct Torque Control
FOC	Flux Oriented Control
COMP	Comparator
SCIM	Squirrel Cage Induction Motor
IM	Induction Motor
RMxprt	Rotating Machine expert
FEA	Finite Element Analysis
DWT	Discrete Wavelet Transform

THD	Total Harmonic Distortion
DPWM	Discontinuous Pulse Width Modulation
Hz	Hertz
Op-Amp	Operational Amplifier
HV	High Voltage
FEM	Finite Element Method
FFT	Fast Fourier Transform
N-m	Newton metre
Wb	Weber
VSI	Voltage Source Inverter

INTRODUCTION

CHAPTER 1 INTRODUCTION

1.1 Overview

An electric drive can be defined as a system or machine equipment which is designed to convert electrical energy into mechanical energy and also provides the electrical control for this process. The basic electric drive system comprises a power source, power converter, an electric motor, controller and mechanical load as shown in the figure 1.1.

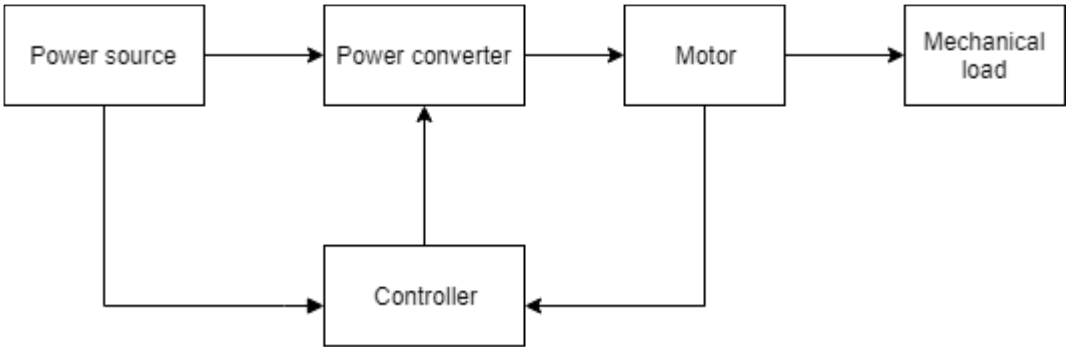

Fig. 1.1 Block diagram of a basic electric drive

1.2 Working of an Electric Drive System

The power source shown could be an ac mains supply or dc source (such as a battery) supplying the currents and voltages to the system. This power supply needs to be converted, depending upon the necessity of the machine or operation, using a power converter. The power supply available could be ac or dc and in a similar manner, the power required for the machine could be ac or dc. Therefore the conversion of power from dc to dc, dc to ac, ac to dc and ac to ac avails the various configurations for power converters depending upon the conversion operation as shown in the figure 1.2.

1. Power converter acts as SMPS (switched mode power supply) for converting dc of one level to dc of another level.
2. The conversion of ac to dc is achieved by power converters through the controlled rectification operation.

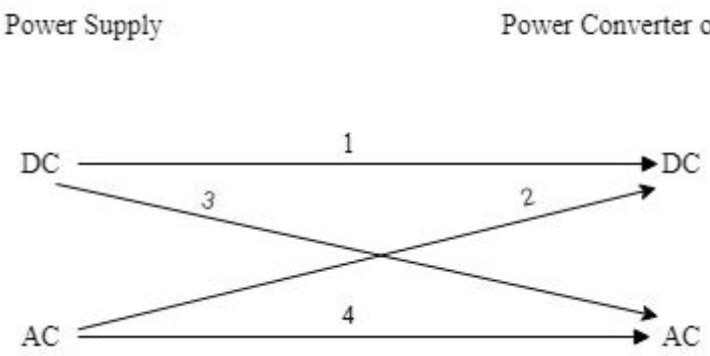

Fig. 1.2 Types of power conversion

3. The power converter operates as the inverter for the conversion of dc to ac.
4. The conversion of ac supply of some voltage and frequency to ac supply of other voltage and frequency is done by cycloconverter.

Thus, the work of power converter is to maintain the power supply as per the requirements i.e. be it the desired current magnitude, voltage magnitude, frequency, ac supply or dc supply. Consequently, this controlled power supply is fed to the motor for the electromechanical conversion i.e. electrical energy to mechanical energy. Thus, the mechanical energy fetched at the shaft end drives the mechanical load. The controller controls the parameters of the power converter unit as one do not have control over the power source, motor parameters and load as these are either already defined and can't be modified. Thus, this electronics controller in order to control the power converter requires the inputs which are provided to it by the power source or motor parameters. The control inputs are taken from the power source as in the cases when supply voltage or frequency varies there must be a controlled action taken by the controller for the power converter such that it mitigates the effects of fluctuating voltage or frequency and supplies the steady supply to the machine. Similar fluctuations can be encountered at the motor end i.e. change in speed, a rise in stator current or stator voltage due to the sudden changes in the mechanical load at the motor shaft. Thus, the controller senses these changes at the motor terminal part and performs the control action in order to prevent the hindrance in the system and ensures the uninterrupted operation of the drive system.

1.3 Classification of Electric Drives

Based on the usage of the type of an electric motor i.e. ac motor or dc motor in the

drive system the classification of electric drives could be done. In addition to dc motor drives and ac motor drives, there are drives using special motors like SRM however, here we focus our study only on the aforementioned drives only. Therefore, the electric drives can be broadly classified as the following:

a. **DC motor drives.**
b. **AC motor drives.**

1.3.1 DC motor drives:

Till 1950 the dc motor drives were popularly used for the variable speed applications while the ac motor drives were used for the fixed speed applications. Back then, the only way possible for obtaining the variable-voltage dc supply, which was required for the speed control of industrial dc motor, was to generate it using a dc generator. The induction motor was used for driving this dc generator at a fixed speed while the field of the generator was altered to obtain the variable generated voltage. This motor-driven-generator unit was employed in industries for each variable speed motor applications as shown in the figure 1.3. It was also known as the "Ward Leonard" drive. This drive system had few disadvantages like bulky in nature and inefficient as it included the mechanical coupling between the ac motor and dc generator.

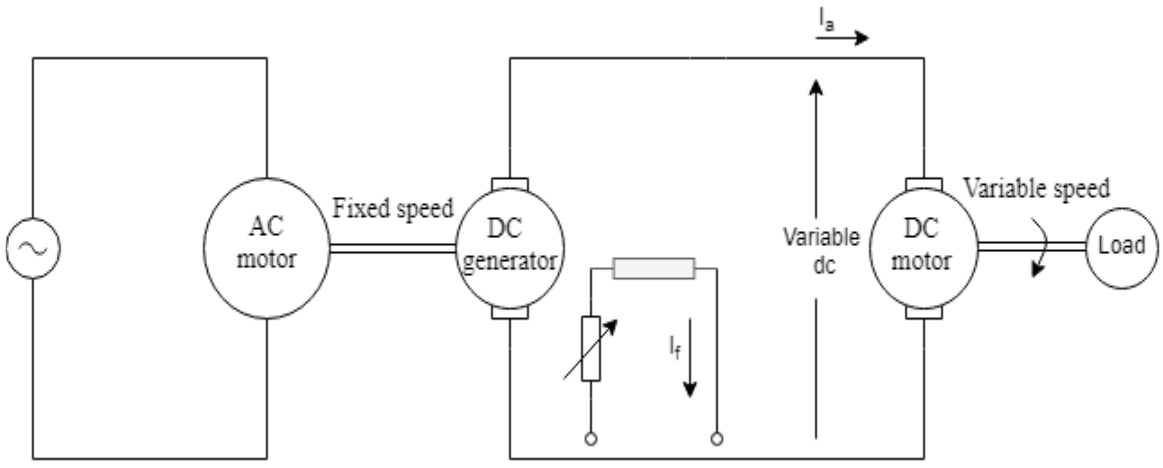

Fig. 1.3 Conventional DC motor drive

Later on, with the advent of power electronics, this conventional method was replaced by the thyristor converters offering less cost, compact size, reduced maintenance, quick response and higher efficiency. In thyristor dc drives the ac mains supply is first

rectified by thyristor rectifier and then the output dc supply is fed to the field of the motor thus by controlling the firing angles of thyristors the average of rectified voltage is varied and consequently, the speed control could be achieved. For the dc supply, chopper-fed dc motor drives are employed which reduces the armature current ripples with the high chopping frequency. The dc motor drives have advantages like adjustable speed, good speed regulation, and frequent starting, reversing and braking. The high-performance applications like tractions, elevators, servos, etc. were dominated by the dc motor drives after the semiconductors were introduced in the late 1950s. Despite these advantages of dc motor drives, the major problem encountered with them was its commutators and brushes which cause regular maintenance of the motor and resulting in higher cost of the drive system. Thus in the past, the dc drives have undergone a huge downfall in the industrial applications as the majority of the industrial requirements are now served by the ac motor drives after the vector control drives were introduced in the 1980s.

1.3.2 AC motor drives:

The ac motors act as the workhorse in the ac motor drive system converting electrical energy into mechanical energy. Traditionally, a fixed frequency sinusoidal supply fed ac motors were employed for the constant speed applications while for the variable speed applications dc motors were the first preference. However, these dc motors had many disadvantages like higher cost, regular maintenance due to commutators and brushes, and higher rotor inertia. Moreover, due to the presence of commutators and brushes, these machines had limited maximum current and machine speed hence they couldn't be operated in rough environments, and had electromagnetic interference issues. However, ac machines do not have any of the aforementioned disadvantages associated with it. An ac motor drive employs the ac motor such as induction motor, synchronous motor and variable reluctance motor. But out of these the induction motor, particularly the squirrel cage induction motor, is the leading choice for industrial applications. The induction motors are simple, rugged, cheaper in cost, reliable and are available in ratings from fractional kW to multi-MW capacity.

Thus, ac drives run 3-ϕ induction motors as they are more advantageous to use over other ac motors. An ac drive is also known in industries by the name variable frequency drive (VFD), adjustable speed drive (ASD), or variable speed drive (VSD). Although, there are different configurations for VFDs (or AC drives), but all of them work

on the same principle converting input frequency and voltage into variable frequency and voltage and thus controlling the speed and torque of the motor. A VFD comprises power converters, filter, controller (a microcontroller, a microprocessor or a DSP unit), and rest of the sensing devices. The basic block diagram of a VFD or ac drive is as shown in the figure 1.4. The variable frequency drive shown has various sections i.e. rectifier and filter, inverter, and the controller. The first section converts the 3-ϕ ac supply to dc supply using the diodes rectifier bridge with minimum ripples. This pulsating dc output of the rectifier unit is further processed by the filter unit in order to produce the fixed dc output.

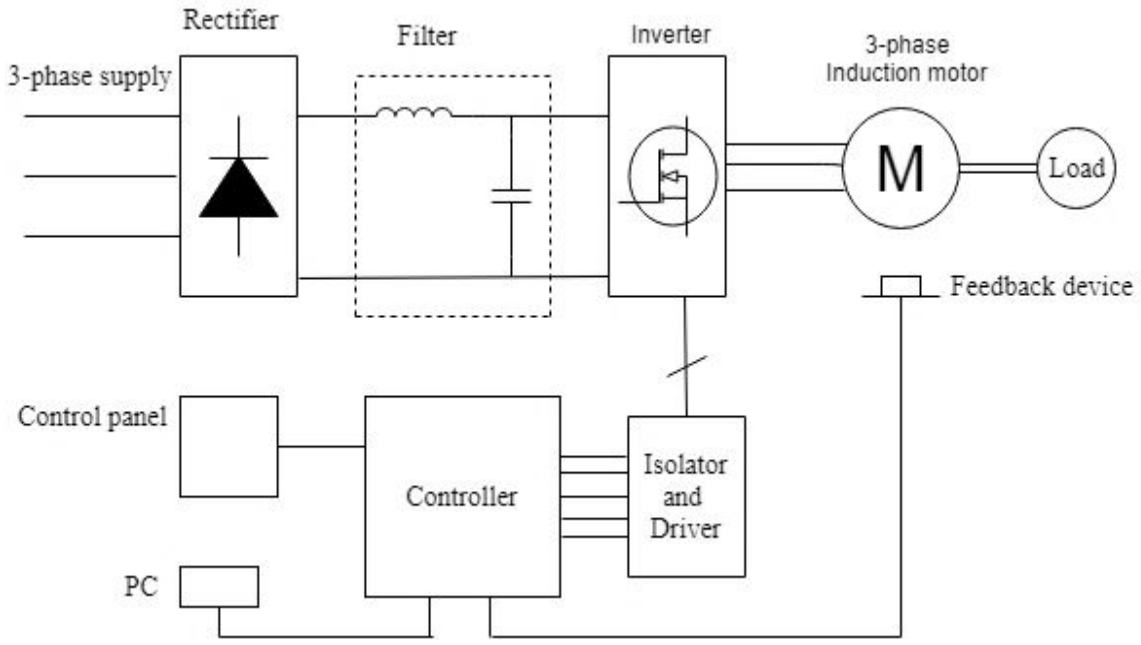

Fig.1.4 Basic block diagram of AC drive

This pulsating dc output of the rectifier unit is further processed by the filter unit in order to produce the fixed dc output. The next section i.e. inverter takes this dc input power from filter and converts it back into ac power of variable frequency and variable voltage under the control of the controller unit. This section consists of IGBTs, MOSFETs, or SCRs which are switched on and off by the control techniques from the controller unit. The controller which may be a microprocessor, a microcontroller or a DSP controller controls the switching of these transistors of inverter based on the feedback received from the motor and the sensing devices. This way the whole drive system monitors the changes in parameter of the motor and performs the control actions as desired by the user. There are various control schemes for this ac drive or VFD i.e.

1. Scalar Control
2. Vector Control
3. Direct Torque Control

In scalar control, the ratio of voltage to frequency i.e. v/f is kept constant hence known as the scalar control. The inverter is controlled by the PWM control technique thus generating variable voltage and frequency outputs for the motor. There are various ways for implementing the scalar control i.e. sinusoidal PWM technique, six-step PWM technique and space vector modulation PWM (SVPWM) technique.

The vector control method is also known as the field oriented control, flux oriented control, or indirect torque control. In this control, 3-ϕ currents are transformed to a 2-dimensional d-q rotating reference frame from the 3-dimensional reference frame using the Clarke-Park transformation. Here, the 'd' component represents the flux generating component of the stator current whereas the 'q' component denotes the torque producing component. These d-q components are controlled using the PI controllers separately and then the outputs of these PI controllers are converted back to 3-dimensional reference plane by employing the inverse of Clarke-Park transformation. The width of switching pattern is modulated using the SVM technique. Stator FOC, magnetizing FOC and rotor FOC are some of the techniques for vector control.

DTC method doesn't have any predefined switching pattern as in the above vector control method. The switching pattern for the inverter is as per the requirements of the load. This control method has better response for the sudden change in load as there is no fixed switching pattern. This method employs the adaptive motor model which makes use of the mathematical equations of basic motor theory. This model takes the inputs like dc bus voltage, line currents and current switch position and finally calculates the flux and torque value for the motor. These outputs are then fed to a two level comparator of flux and torque. The flux and torque reference signals obtained from the comparator output are given to the switch selection table where the selected switch position is provided as an input to the inverter without any modulation, thus named as the direct control method.

1.4 Induction Motor

Induction machine is the most commonly used motor for the industrial applications

due to its simple construction, reliability, robust nature, absence of commutators and brushes, high efficiency, low maintenance cost and easy speed control. On the basis of construction, this induction motor can be classified as the squirrel cage type and wound rotor or slip ring type. For our study, we have taken the case of squirrel cage induction motor only. The squirrel cage induction motor comprises a stationary part stator and a rotating part rotor. The stator is constructed with laminations having slots on the inner periphery to accommodate the stator windings. This whole laminated stator with the windings is supported inside a frame of iron or steel. The similar lamination construction is done for rotor with the slots on the outer periphery which accommodates the rotor bars which are short circuited by the end rings. This rotor is mounted over a shaft which delivers the mechanical energy during the operation of the motor.

The stator windings are displaced 120° in space thus on supplying the 3-ϕ supply through the windings, a rotating magnetic field is set in the air gap. This rotating magnetic field runs with the synchronous speed across the rotor conductors and consequently induces the voltages in them. The induced voltages set the induced currents in the short-circuited rotor bars thus these current carrying conductors placed in the rotating magnetic field experiences the force. This force produces the electromagnetic torque which results in rotation of rotor in the direction of the stator rotating magnetic fields. The rotor tries chasing the synchronous speed of rotating magnetic field however, it never attains it, and thus this motor is also named as asynchronous motor.

1.5 Open-Loop Induction Motor Drive

The open loop induction motor drive mainly comprises a power converter, VSI, induction motor and the mechanical load. The basic block diagram of the open-loop drive system is depicted in the figure1.5.

The power converter consisting of power diodes rectifies the 3-ϕ ac supply to dc supply. This dc supply is then fed to the VSI which again converts this dc supply to 3-ϕ ac supply using the sinusoidal PWM technique. The basic operation of the control technique employed for the switching of VSI transistors could be explained with the diagram given in figure 1.6.

The VSI consists of three legs each containing a pair of parallel connected power diode and IGBT. Thus, there are total of 6 IGBTs to be controlled by the SPWM circuit as

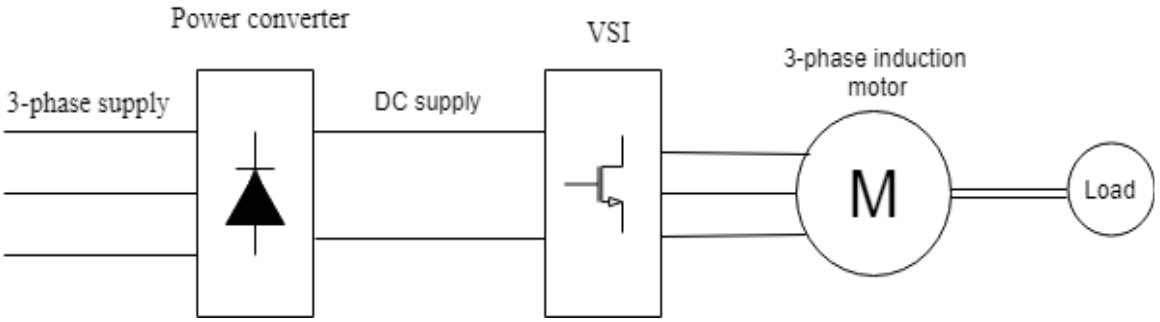

Fig. 1.5 Basic block diagram of open-loop induction motor drive

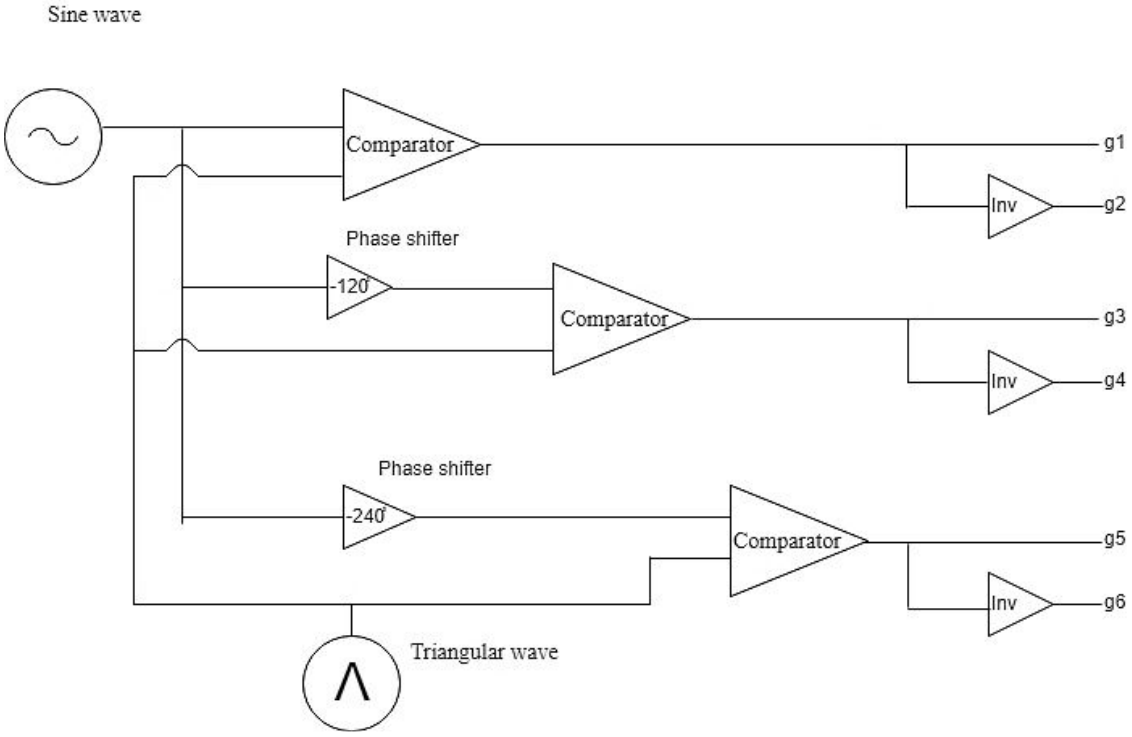

Fig. 1.6 Block diagram of SPWM control circuit for VSI

shown in figure 1.7. The main objective of the control technique is to compare the values of sine wave magnitude with the triangular wave magnitude and for the instants when sine wave is greater than triangular wave, the upper IGBT of each leg must be switched on. Whereas, when the triangular wave is greater than sine wave, at these instants the lower IGBT of each leg must be switched on. The reference sine wave for all the three legs must have a displacement of 120° with each other. Thus, this control switching of the gate pulses of IGBTs produces the 3-ϕ ac supply at the VSI output terminals. Then, the power output of this VSI is fed to 3-ϕ induction motor which finally converts the electrical energy to mechanical form for driving the mechanical load.

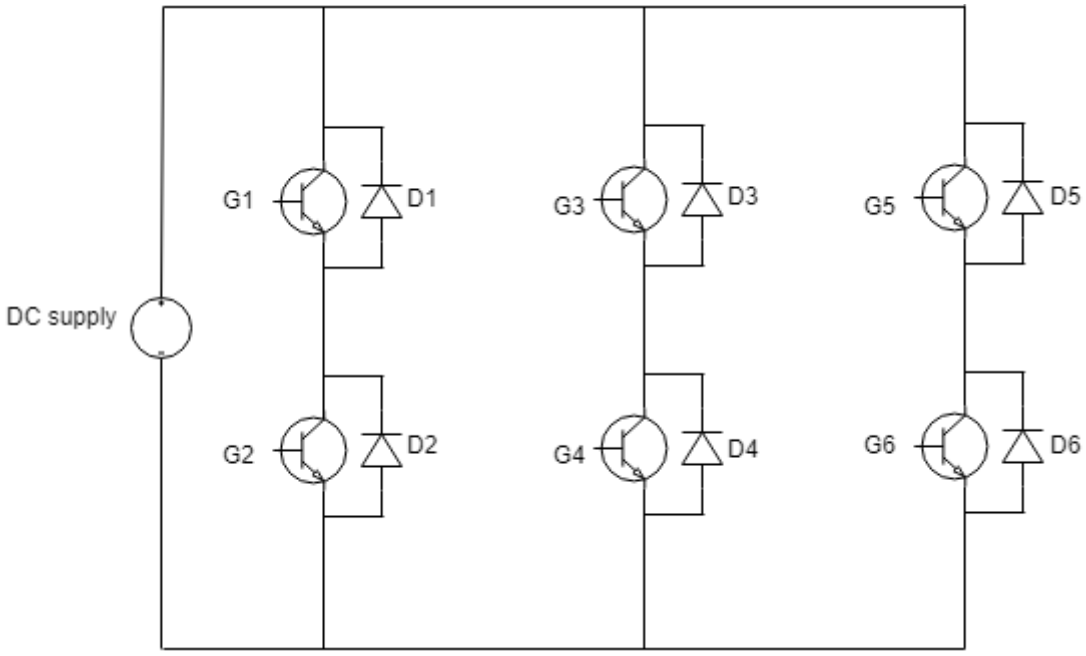

Fig. 1.7 VSI configuration for the IM drive

1.6 Objectives of the Thesis

The main aim of the study is to design the open-loop induction motor drive systemfor performance analysis. Further, the fault analysis for inverter faults in drive system has been done. The specific objectives of the study are:

1. To design 7.5 kW squirrel cage induction motor (SCIM) using RMxprt in ANSYS Electronics desktop software.
2. Design of sinusoidal PWM technique controlled VSI for SCIM in ANSYS Simplorer.
3. Performance analysis of 3-ϕ induction motor drive circuit by co-simulating ANSYS Maxwell FEA (Finite element analysis) model and Simplorer drive circuit.
4. Analysis of various inverter circuit faults of induction motor drive system using ANSYS.

1.7 Organization of the Thesis

This thesis contains five chapters including this introductory chapter. In chapter 2 review of relevant literature dealing with the IM drive is described. In chapter 3, detailed procedure for design, modeling and co-simulation of open-loop drive system is

demonstrated. In chapter 4, the results of performance of IM drive system under normal and inverter fault operation are plotted. The last chapter contains the summary and conclusions of the work and the future scope has also been discussed in chapter 5.

REVIEW OF LITERATURE

CHAPTER 2 REVIEW OF LITERATURE

2.1 General

Induction motors are susceptible to several types of faults namely rotor fault, stator fault, bearing and eccentricity faults. The fault analytic and diagnostic approaches for PWM-VSI fed induction machine have been proposed by many researchers around the world. Hence the related literature has been studied and presented below.

2.2 Literature Review

Fuchs, F. W. (2003) performed the diagnosis of faults for voltage source PWM inverters fed SCIM drive system. The author had discussed all the possible faults in VSI namely short-circuit and open-circuit faults of power switch i.e. IGBT and diode. This paper explains the after effects of the faults in the output responses of the machine and thus identifying the exact nature of the output responses during faults can help in detecting the fault location. For this, author introduced various diagnosis approaches like comparison of the phase currents of inverter under normal and fault conditions, ac current space vector trajectory slope analysis, ac current space vector average quantity approach, ac current space vector instantaneous frequency approach, ac current space vector versus rotation angle fundamental method, comparison of ac voltage actual and reference quantity approach, and current pattern recognition. In addition, to that diode rectifier faults (open-circuit) diagnosis was carried out by the author. The author tried covering the analysis of all the faults related with VSI converters of induction motor drives and still recommended further investigation of the faults.

de Araujo Ribeiro, R. L. et al. (2004) showed the implementation of various fault compensation strategies in two different configurations of 3-ϕ induction motor drive systems. The compensation strategies were designed for open-circuit and short-circuit faults of the power converter devices. For the fault compensation, the power converter topology had been reconfigured by isolating and connecting triac switches in the power converter. The triac switches were initially kept open and one of them was connected for redefining the converter circuit. The first configuration included a backup leg and for the replacement of faulty leg, the triac switches were used. While the second configuration for

drive system completely isolated faulty leg and the mid-point of the capacitor bank was connected to respective phase using triac switches. Thus, the author demonstrated the steady operation of the induction motor drive system even after segregation of the converter faulty power switch or complete leg. Though this method increased the cost of the drive system however, these fault compensation strategies ensured the uninterrupted operation of the drive system for longer time.

Klima, J. (2005) employed two distinct SVM technique for a VSI fed induction motor drive system to switch from balanced to unbalanced supply operation. The presented modulation strategy, which was based on voltage space-vector decomposition technique and thus depreciating the alternating voltage vector sequence, under fault operation showed the same symmetry as in the standard six-switch inverter. Further, the modulation strategy took into consideration the harmonics of the space-vector modulating waveforms which were reflecting in the spectrum of the PWM waveform results. The paper proposed the mathematical modelling of a space-vector modulation technique in frequency and time domain analysis for the VSI fed induction motor drive system. The author obtained the time and frequency domain results utilising the Laplace transform for the voltage space vectors. In addition, the determined experimental results showed the similar behaviour with the analytically obtained waveforms.

Yu, O. S. et al. (2006) presented a fault diagnosis scheme for the SVPWM VSI fed induction motor drive to enhance the response of power electronic system employed for commercial, industrial, military, aerospace and rolling mill applications. The author used the voltages of lower half switches in each phase leg for the fault condition in order to implement the proposed diagnosis approach. This paper proposed a reconfiguration method using a topology of four-switches which connected a faulty leg at the mid-point of dc link using bidirectional switches. The paper proposed an easy algorithm efficient in fast detection of faults of VSI within least time. Thus, the drive remained unaffected due to faults and provided continuous steady operation even after the occurrence of faults in system.

Guan, Y. et al. (2007) developed a diagnostic approach for real time inverter faults in 3-ϕ induction motor drives using calculation methods like quick mean current vector and the subtractive clustering algorithm of the stator current. The efficacy of the mean current vectors in inverter fault diagnosis was verified by employing a subtractive

clustering algorithm for analysis of the mean current vectors during normal and faulty inverter operation. The angle and amplitude values of various clusters of mean current vectors were utilised to diagnose the fault modes. In addition, the author constructed an array of mean current vector's magnitude and phase calculation for the online fault diagnosis process using a single data shifting method. Finally, the paper presented results using the proposed method which detected the faults in inverter of open loop and close loop induction motor drive system in less than $1/4^{th}$ period of fundamental period.

Lu, B., and Sharma, S. (2008) presented a comparative literature review on the various methods used for fault diagnosis and protection of IGBTs employed in 3-ϕ power inverters. The authors summarized 10 methods for short-circuit faults and 21 methods for open-circuit faults based on their performance. The paper briefly discussed the aspects of gate-misfiring faults and their methods for diagnosis. The authors found the normalized dc current method as the most effective in tracing faults with high sensitivity to false alarms. The proposed inverter control algorithm used the current deviation method that kept the inverter operate even when the open-circuit fault occurs in one device. The author made remarks on the gate-misfiring faults that these faults didn't cause any system failures when occurred and could be remedied with simple digital electronics and control equipment.

Estima, J. O., and Cardoso, A. M. (2010) examined the effects of multiple open-circuit faults in VSI fed induction motor drive system. The author discussed all the previous diagnostic methods based on the single faults and proposed the new method for real- time analysis of the drive system under multiple fault conditions. Instead of using motor phase currents average values, which most of the literature used in the past, the author took the average absolute values as the diagnostic variables. This approach overcame the problems of false alarms and provided the complete information of multiple open-circuit faults. These average absolute values together with the phase current average values provided the diagnostic approach that identified single as well as multiple open-circuit faults.

Prieto, J. et al. (2011) presented a report on current ripple analysis and flux harmonic distortion factor in numerous PWM techniques employed for the 5-ϕ inverter fed induction motor drive system. The complex space vector approach had been taken by the author for analysis. The paper showed the comparison of results for various PWM techniques of VSIs. The analysis was done for different carrier-based PWM and space

vector PWM methods. The author took the reference of already available analysis discontinuous and continuous PWM techniques to define the switching characteristics analysis in PWM VSI fed five phase induction motor drive. The paper provided a complete study on generated current ripples using discontinuous and continuous SVPWM, DPWMMIN, DPWMMAX, and DPWM0 TO DPWM3 employing (4L) and (2L+2M) vector selection methods. The simulations as well as experimental results were carried out for validating the analysis approach for 5-ϕ induction motors. The paper finally concluded that if the average switching frequency is kept same then the harmonic performance or the lowest current THD was recorded by the continuous (2L+2M) SVPWM in the domain of low modulation index values. Whereas for the prime performance was offered by the discontinuous (2L+2M) DPWM1 in the domain of high modulation index.

Georgakopoulos, I. P. et al. (2011) studied the broken rotor end-ring/bar faults in inverter fed SCIM drives. A thorough investigation had been done on the inverter input current spectrum in order to trace the fault-indicative frequency components. These frequency components or harmonics gave the detailed report of faults even for the low load and small fault condition in transient and steady-state operation. The author designed this diagnosis approach for the controlled variable frequency open-loop IM drive system. The author provided the analytic and experimental verification for the generation of harmonics during broken bar/end-ring fault in inverter input current spectrum. The frequency sidebands especially near zero frequency were extracted easily even in the low load operation. The author used the discrete wavelet transform (DWT) to diagnose the faults in motor during transient operation.

Najafabadi, T. A. et al. (2011) employed an adaptive observer with estimation of rotor resistance in sensor fault detection and isolation unit for induction motor drives. The taken VSI fed closed-loop three phase induction motor drive used a dc link voltage, a position or speed, and several sensors for the three phases. A rule base had been set which determined the faulty sensor type using a decision making unit taking inputs like estimated rotor resistance and phase currents from the fault detection and isolation unit. The unit also diagnosed the phase with erroneous sensor output in case of current sensor failure. In the proposed strategy only one current sensor employing rotor resistance estimation is enough for segregation of all the sensor faults rather than a bank of observers as presented in the

previous papers. The efficacy and the convergence of the proposed method had been verified by the authors through simulation and experimental tests.

Trabelsi, M. et al. (2011) described an improved technique for IGBTs open-circuit fault diagnosis in VSI fed IM drive system. The combination of switching pattern and the line-to-line voltage was used to extract the fault information. This technique diagnosed the single and multiple switch open-circuit faults of the VSI. Moreover, only one line-to-line voltage was enough to diagnose two inverter legs at the same time. The false diagnosis alarms were overcome by compensating the time delays, which occurred due to turn-on and turn-off operation, while acting on the switching pattern. This proposed technique had fast response as well as less cost for open-circuit fault detection in VSI fed IM drives. This improved technique had a better time delay between the occurrence of fault and its detection i.e. 0.5msec.

Apostoaia, C. M. (2012) presented the methodology to design and simulate the induction motor drive system in ANSYS and SIMULINK. The author designed a prototype of SCIM in ANSYS Maxwell, the electric and electromechanical parts in ANSYS Simplorer and the ac drive control system in Simulink/MATLAB. The author co-simulated the Maxwell 2D FEA model of induction motor with the ac drive circuit in Simulink/MATLAB using the ANSYS Simplorer as the intermediate tool. Thus, the author presented the complete step by step procedure to integrate the ANSYS tool and the MATLAB/Simulink. This paper provided the detailed report on designing an electric machine in RMxprt and discussed the problems encountered in setting the co-simulation platform for two different software.

Mini, V. P., and Ushakumari, S. (2012) designed a 3.7kW, 400V, 4 pole 3-ϕ 50Hz SCIM in RMxprt and Maxwell 2D software. This Maxwell 2D model is then used for studying the severity of rotor fault in the machine output responses. Harmonic analysis of the machine had been done by the author for various rotors' broken bar faults. The author concluded that with increase in the severity of the fault, the harmonics level increased consequently causing fluctuations in the stator current. These fluctuations in stator current resulted in rise of thermal stress on the motor. In addition, the rotor fault reduced electromagnetic torque and the starting current of the stator phases therefore contributing for the poor performance of the motor.

Islam M.S. et al. (2013) have proposed a sinusoidal pulse width modulation technique for the harmonic reduction of inverters. Literature in the past used the FPGAs, microcontrollers and microprocessors for generating the SPWM switching signals, which required the knowledge of programming and coding. However, the author presented a simple method of generating SPWM switching signals for 3-ϕ PWM-VSI using the operational-Amplifier (op-Amp) circuits/analog circuits. This PWM controlled VSI was then simulated for both standalone loads and high voltage (HV) sensitive systems/loads, for instance, micro-grid system and large industrial machines respectively connected with transformer and without a transformer. The obtained results showed less than 5% of total harmonic distortions (THD) after filtering. For the standalone inductive loads i.e. induction motor, the best results of inverter were observed. With the increase in the carrier frequency, the negligible losses were observed and the filter showed better output responses.

Estima, J. O., & Cardoso, A. J. M. (2013) in their work, proposed a novel algorithm that was applied in the Voltage fed PWM Motor drive circuits, and was applicable for the real time analysis of the diagnosis of multiple open circuit faults by considering the errors of the reference currents. Limitations of the 3-ϕ inverters, though used very commonly and extensively in industrial applications, are the fact that their extremely complex nature and stresses which they get exposed to often lead to multiple critical failures. This work aimed to suggest a novel algorithm as discussed above, and this approach simply required the measured motor currents and their corresponding reference signals. This algorithm was simple as it involved no extra addition of sensors or hardwares to be attached to the system, thereby increasing the complexity, as the signals could simply be extracted from the effective control system of the motor drive. Analysis of several results generated from the usage of a permanent magnet synchronous machine using vector controlled schemes were tabulated and final results for the effectiveness of the proposed algorithm with faster detection times and robustness was concluded.

Zhang, J. et al. (2014) developed a diagnostic approach for open-circuit fault of single switch and double switches in PWM-VSI for vector controlled IM drive system. Keeping the phase angle of a phase current as reference, the periodic operation of VSI is evenly partitioned into 6 operating states with some rules. At each state, only 3 power switches dominate the operation and the rest switches give negligible responses. The

power switch open-circuit fault causes the periodic distortions in current, this period of distortion remains identical to that of the 3-ϕ currents. These current distortions occur for the faulty state and vanish during the healthy state of operation. Each state is decided based on the recalculations done for the current vector rotating angle. The d and q axis current periodic distortions were used for detecting the faulty switches whereas the faulty states were utilized to identify the faulty switches. The author performed the simulations and experiments to demonstrate the effectiveness of the proposed method.

Sreeja V. et al. (2015) had investigated the results of SCIM drive system by introducing the switching faults in the SPWM controlled VSI. For this, the author designed the SPWM technique for the VSI in ANSYS Simplorer tool and the FEA model of the motor in ANSYS Maxwell tool. For the results, the author co-simulated both the ANSYS tools and diagnosed the after effects of introducing the fault in the VSI. The author studied the faults like short-circuiting and open-circuiting fault of power diode in the rectifier, short-circuit fault of the dc bus capacitor, short-circuit fault of IGBT in VSI, an open-circuit fault of gate signal for IGBT, and dc bus earth fault. The simulation results were observed for the dc link voltage, stator currents, line voltages, speed variation under normal and fault conditions. The author concluded that the short-circuit faults caused the severe effects on the drive system while the open-circuit faults were hard to diagnose. In addition, the open-circuit faults resulted in poor performance of the drive and if existed for longer duration could lead to further failures.

Kumar N.P. et al. (2016) presented a simulation study on analysis of radial electromagnetic field in induction motor under normal and fault condition using Finite element method (FEM). The authors observed the patterns of air gap radial flux density for the steady-state operation and line-to-line fault of the IM drive. The simulations were done for the IM directly fed from mains and the PWM-VSI fed open-loop IM drive system. For this, the author designed the IM in the ANSYS Maxwell software and the corresponding drive circuit in Simplorer and finally integrated these two tools to study the faults in machine. The author concluded that the fundamental component of air gap radial flux density remained almost same for both PWM-VSI fed IM drive as well as for directly supplied IM. The amplitude of the spatial harmonics, due to the inverter switching, was found larger for the open-loop drive system. Under the phase-to-phase short circuit condition, at 100 mm distance spatial FFT spectrum showed the dominance of the spatial

distance harmonics over the fundamental component owing to the improper distribution of air gap radial flux density.

Kumar N.P. et al. (2016) performed the electromagnetic field analysis of a 3-ϕ inverter fed IM drive system using FEM analysis during the normal and broken rotor bar fault conditions. The author added that the electromagnetic field waveform carries the details for rotor, stator and the mechanical parameters of IM, thus could be used for the diagnosis of faults in IM drive. The author presented a comparative analysis of electromagnetic fields of a healthy motor and a motor with broken rotor bar. The simulation results showed the malformation in the magnetic poles axis which resulted in torque and speed oscillations due to the saturation in the stator and rotor teeth near the broken bar site. The author drew a comparison for the air gap flux density versus FFT spectrum and air gap distance respectively for a faulty and healthy IM drive. The FFT spectrum of broken bar motor indicated the presence of magnetic noise which increased with the increase in the severity of the fault. Further, the author compared an analysis on the induced voltage and current in end-ring of a faulty and healthy rotor. This comparison showed that due to the fault there was sudden increase in the end ring current ripples and the end ring induced voltage lost its sinusoidal behaviour.

Srinivasan, J. et al. (2016) in their work considered the case of an Induction Motor. They considered an induction motor of some specific parameters with a 12 pole squirrel cage configuration type. Analysis from perspectives of considering this machine in two major cases: short pitch and full pitch winding configurations were analyzed. Their harmonic analysis results were comparatively analyzed and employed the finite element method for the purpose of verification. The ANSYS Maxwell software was used for the modelling and analysis purposes.

Kumar, P., & Isha, T. B. (2016) in their work discussed the 3-ϕ induction motor with special focus towards the most common problems faced during the efficient operation of this machine. They took up the aspect of the rotor bars being broken in an Induction Machine and thus subsequently being a factor which was responsible for failures of this machine (IM) for nearly about 7% of all cases. The approach applied in this work aimed to study the electromagnetic characteristics of the controller used in this case. The application of an open loop pulse width modulated inverter was explored in this work. The output of this was fed to the Induction machine for observation and analysis purposes using the

Finite element analysis method, wherein two major cases had been forked: the first being the case of operating the machine under perfectly healthy condition and the second being the case, where faults of the type of broken rotor bars were considered. The air-gap magnetic field monitoring method was used for the detection of faults in the machine. The output was aimed to comparatively analyze the two cases of the motor-run conditions and observe the variation in electromagnetic fields seen in both cases. This had been done using the ANSYS FEA software tool.

Kumar N.P. et al. (2017) designed the 7.5 kW 3-ϕ induction motor prototypes in ANSYS Maxwell along with the PWM-VSI in ANSYS Simplorer. The author studied the PWM VSI open-circuit fault for a 3-ϕ induction motor drive system and parameters like flux density, torque, current; flux distribution, radial flux density and speed are examined before and after the fault occurrence. The simulation results showed that the positive half of the phase current of the faulty leg gets clipped off as the IGBT switch gets open-circuited. Moreover, the line voltages (between the healthy and faulty phase) were distorted and the ripples increased in the healthy phase currents. The similar increase in ripples reflected in the torque and speed of the machine, thus reducing the average speed of the IM. The flux density, flux lines distribution and the radial air gap flux density were also distorted due to the open-circuit fault in an inverter.

Lee, S., and Yun, J. (2017) stated that the optimization of stator and rotor slot design and use of proper materials while designing an induction machine can improve the efficiency of a motor. However, while adopting low core loss electrical steel considering the magnetic flux density and harmonic core losses is important as low core loss electrical steel doesn't guarantee the reduction of core loss. By taking different electrical steel samples the core and stray losses of various motors are compared and analyzed for performance evaluation purpose. This paper analysed the core losses and verified it with finite element analysis for different types of electrical steel sheets. The experimental tests were done to analyse the variation of stray load loss and core loss for the low core loss steel. The author stated that better quality Si-steel decreased the core losses under proper magnetic flux density condition. On the contrary, the low iron loss steel increased the stray loss and core loss when magnetic flux density was not taken into consideration. Thus, the author concluded that for high-efficiency induction motors, proper analysis of magnetic flux density must be done before using different types of electrical steel material.

Vujacic, M. et al. (2018) analysed the switching ripples of voltage across dc link capacitors in 3-ϕ PWM VSIs. The author formulated the design of dc link capacitor with respect to amplitude of switching voltage ripples while taking into consideration the parameters like output current amplitude and modulation index. The calculations were acquired considering the necessities and limitations referring to the component of the high switching frequency dc link voltage ripple. The analysis was performed by taking a practical or non-ideal voltage source and a balanced load (both motor load and grid connected load) at the inverter end. The peak to peak value of dc voltage ripple was defined as a function of the modulation index, the output current amplitude and phase angle for the fundamental period. Thus, the author derived some analytical expressions for the amplitude and maximum value of dc link voltage switching ripple over the fundamental period. In addition, the paper presented various diagrams for different values of output phase angle and modulation index. The simulations as well as experimental tests were done in order to validate the results of the proposed analysis.

MATERIALS AND METHODS

CHAPTER 3 MATERIALS AND METHODS

3.1 General

This chapter contains all the methods and tools used for designing the components of the proposed work. For designing a 7.5 kW prototype of induction motor, the RMxprt tool of ANSYS electronics desktop version 18.0 is used. While for finite element analysis of this induction machine, the motor 2D FEA model is created using the ANSYS Maxwell tool. The electric drive circuit consisting of power converter, SPWM controlled VSI and the mechanical load is designed in the Simplorer design tool of ANSYS software. The Maxwell and Simplorer tools are then co-simulated for integrating the designed motor model and the drive circuit in order to analyse the complete open-loop induction motor drive system.

This chapter is divided into sections. The first section outlines the materials used in realising the study of machine i.e. ANSYS software and its tools used for the simulations. The second section covers the methodology i.e. a complete step-by-step description of designing the induction motor in RMxprt and Maxwell 2D design tool. The third section demonstrates the modelling of drive circuit of 3-ϕ induction motor in Simplorer design tool. The fourth section helps in understanding the need for co-simulating the Simplorer & Maxwell tools and its methodology.

3.2 Materials

This section elaborates the simulation software tools that have been employed in this proposed thesis work. ANSYS electromagnetics suite is the basic software which has been used in for design, modelling, and simulation of the PWM-VSI fed 3-ϕ IM drive system.

3.2.1 Software used

ANSYS is afinite element analysis software which simulates the complex designs in the disciplines of physics, fluid mechanics, structural mechanics, and electromagnetics. The software provides a virtual environment to test the prototypes of products before manufacturing them thus creates a provision for product improvement and its life computation. ANSYS software comprises various tools namely ANSYS Fluent, ANSYS

CFX, ANSYS Mechanical, ANSYS Autodyn, and ANSYS Electromagnetics for simulating designs in aforementioned disciplines. The ANSYS Electronics Desktop software provides a platform for designing and simulating various electrical and electronic systems. It comprises a unified user interface for creating electromagnetics designs and circuits. This ANSYS electronic desktop provides various design types and features as shown in figure 3.1.

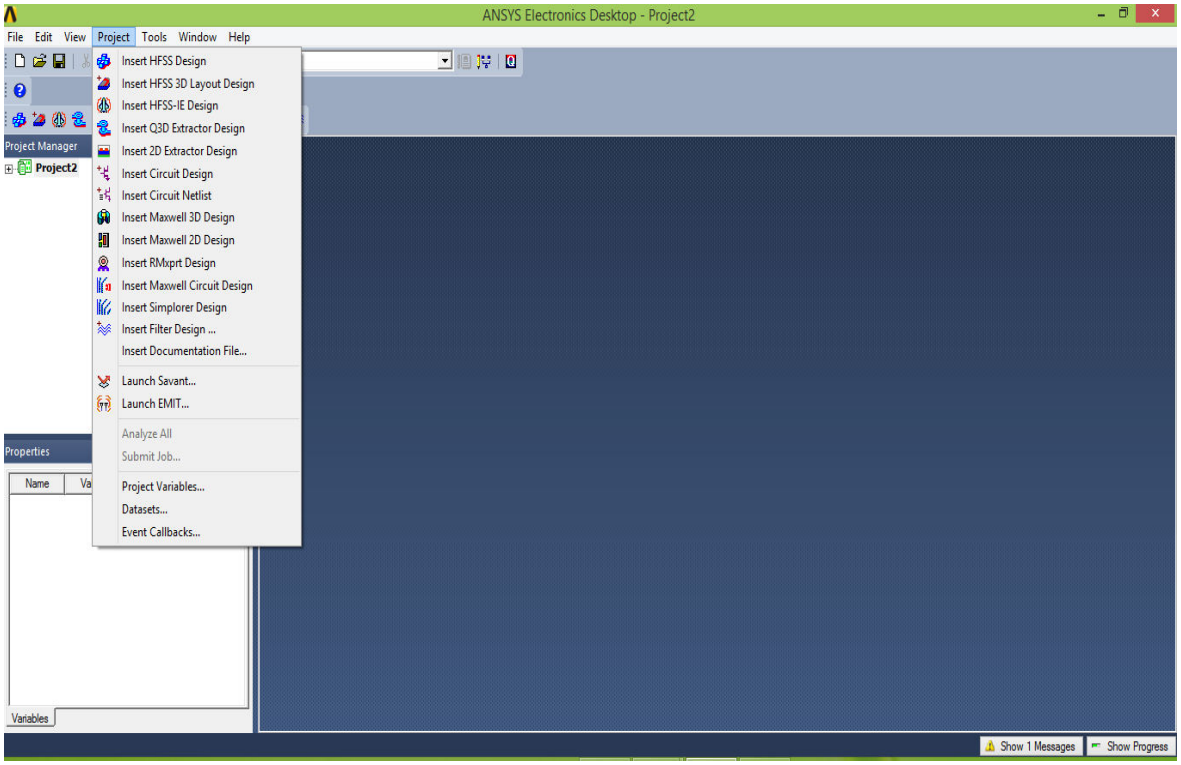

Fig. 3.1 ANSYS electronic desktop interface

- HFSS Design: high frequency structural simulation design provides a three-dimensional (3D) interface electromagnetic component design, analysis and simulation.
- HFSS 3D Layout Design: This design tool is an electromagnetic simulator based on a full wave layout providing a specialised interface for geometries prepared in layout.
- Q3D Extractor Design: allows the extraction of spice models and lumped RLGC parameters using a quasi-static 3D solver.
- 2D Extractor Design: delivers per unit length RLGC parameters of transmission lines through a two-dimensional (2D) solver.

- Maxwell 3D Design: employs finite element analysis (FEA) method to solve 3D magnetostatic, electrostatic, transient, and eddy current problems.
- Circuit Netlist: provides a text based interface for the Nexxim circuit simulator.
- Maxwell 2D Design: utilises FEA method to resolve 2D magnetostatic, electrostatic, transient, and eddy current problems.
- Maxwell Circuit Design: This tool sets up external circuit designs which supplies excitations to coil terminals of Maxwell 3D and 2D transient and eddy current designs.
- RMxprt Design: uses an electrical machine's template-based design tool providing fast, accurate and reliable evaluation of machine performance. In addition, it provides easy creation of 2-D and 3-D geometry of machine for finite element analysis in ANSYS Maxwell.
- Simplorer Design: is an integrated, mixed-signal, and multi-domain simulator for solving complex systems.
- Maxwell Circuit Design: is used for setting up external circuit designs to provide excitations for Maxwell 3D and 2D transient and eddy current designs.
- Circuit Design: a schematic-based design interface to Nexxim circuit simulator.
- Filter Design: is a schematic based design tool for designing filters employed for microwave and high frequency applications.

These above mentioned design tools are integrated in the ANSYS electronic desktop. These design tools are widely used in electrical and electronics applications. For the proposed study of open loop induction motor drive, majorly RMxprt Design, Maxwell 2D Design, and Simplorer Design tools are employed for design and simulation of the drive system.

3.3 Methodology

In this section, the methodology used in implementing the proposed work has been introduced and discussed. This section is divided into two sub-sections which provide a detailed step by step procedure used for designing the induction machine. First section demonstrates the methodology used for designing 3-ϕ induction motor in RMxprt design tool while second section describes the designing of 2D model of 3-ϕ induction motor for finite element analysis (FEA) using Maxwell 2D design tool.

3.3.1 Design of 3-ϕ induction motor in RMxprt tool

The rotating machine expert (RMxprt) is a template-based design tool which contains the predefined structures of electric machines. It provides the virtual environment for designing the machine parameters like stator geometry, rotor geometry, stator and rotor slots dimensions, and winding configuration for analyzing the machine performance. The present study describes the step-by-step procedure for designing the 7.5 kW prototype of 3-ϕ induction motor in RMxprt tool as follows:

Step 1: Creating a new project and including an RMxprt Design.

- Click **File** and select **New**. This loads a new project in the project tree named as projectn, where n is the order of project currently added to the present session.
- Click **Project** and insert the **RMxprt Design** or select the **RMxprt icon** in the tool--bar. Then choose the machine i.e. three-phase induction motor from the Select Machine Type window as shown in figure 3.2.
- After loading a new project, the project tree in project manager window shows the machine geometries like stator, stator slot, stator winding type, rotor, rotor slot, rotor winding type, shaft and analysis setup as shown in figure 3.3.

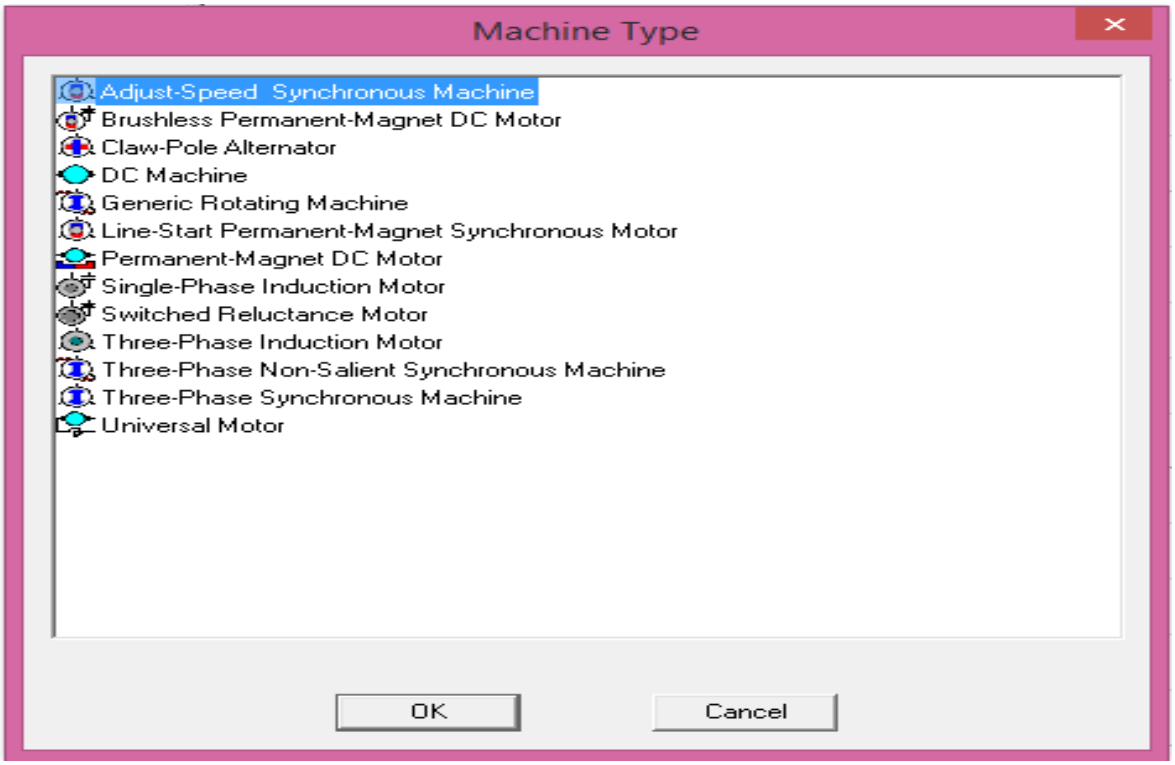

Fig. 3.2 RMxprt design machine types

Step 2: Defining the stator geometry.

The stator geometry comprises stator dimensions, stator slot, and stator winding. For the 7.5 kW of induction motor following data has been taken:

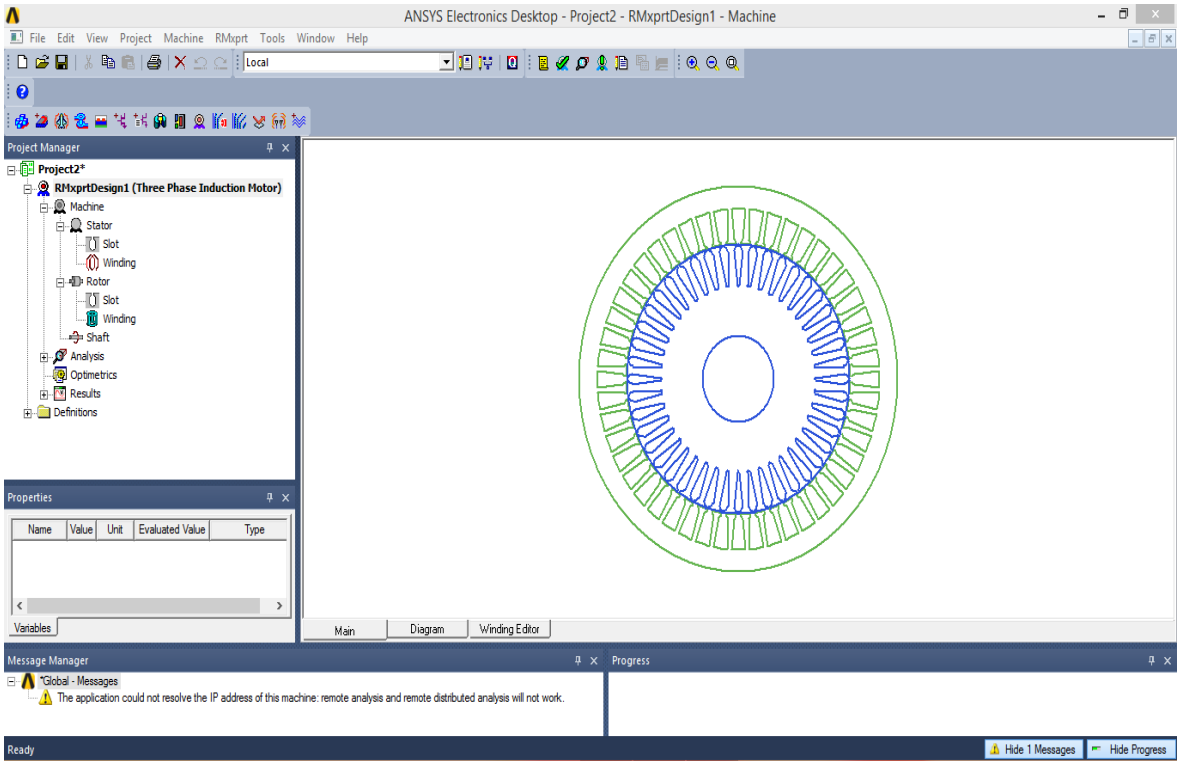

Fig. 3.3 RMxprt design schematic

- Stator dimensions:-

Table 3.1 Stator dimensions

Outer Diameter	210 mm
Inner Diameter	148 mm
Length of stator core	250 mm
Stacking factor	0.95
Steel type	M19_24G
Number of slots	48
Slot type	3
Number of lamination sectors	0 (for auto design)
Magnetic press board thickness (0 since for non-magnetic materials)	0
Skew width (measured in slot number)	0 (for auto design)

- Stator slot:-

Table 3.2 Stator slot dimensions

Bs0	3.5 mm
Hs0	0.9 mm
Hs1	1.3 mm
Bs1	6.1 mm
Bs2	9.5 mm
Hs2	16.5 mm
Rs	0 mm

.

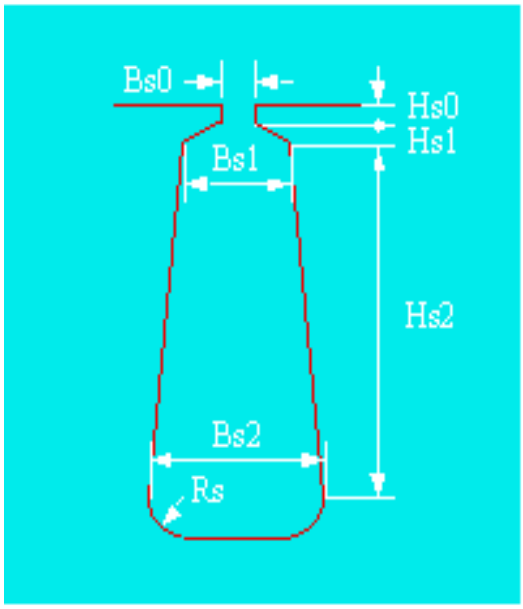

Fig. 3.4 Stator slot

The stator slot design taken for the stator of machine model is as shown in fig. 3.3.

Note: This stator slot type configuration accommodates the stator 3-ϕ winding and the dimensions for this slot should be taken in such a way that it satisfies the condition of limited slot fill factor. The predefined value for this limited slot fill factor is 75% and the conductors slot fill factor should less than this otherwise the machine model would not be feasible.

- Stator winding:-

Table 3.3 Stator winding parameters

Number of winding layers	1
Winding type	Whole coiled
Number of parallel branches of stator winding	2
Number of conductors per slot	30
Number of strands (numbers of wires/conductor)	0 (for auto design)
Wire wrap	0 (for auto design)
Wire size	0 mm (for auto design)
Base inner radius	10 mm
Tip inner diameter	2 mm
End clearance	1 mm
Slot liner	0.5 mm
Wedge thickness	0.5 mm
Limited fill factor	0.75

Using the above procedure the stator geometry is created and the stator windings are placed in the stator slots. The stator design and its winding connections are as shown in the figures below.

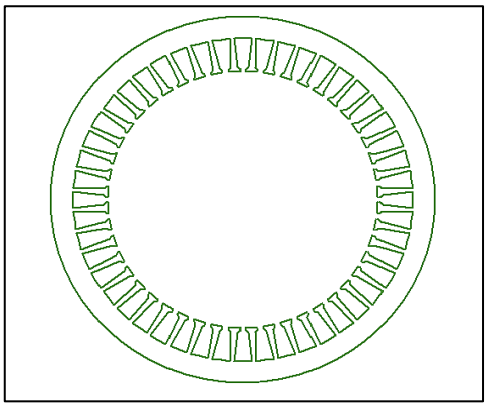

Fig. 3.5 Stator design of 3-ϕ IM

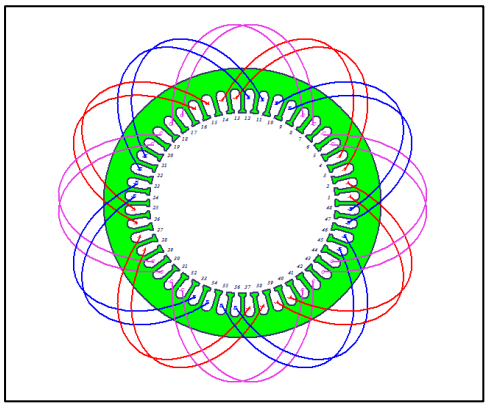

Fig. 3.6 Stator winding connections

Step 3: Defining the rotor geometry.

The rotor design of SCIM has simple construction as it is simply a stacked set of cylindrical stampings with metal conductors embedded in its slot surface.The rotor geometry comprises rotor dimensions, rotor slot design, and rotor winding configuration. The squirrel cage configuration for rotor has been taken for the present 3-ϕ induction motor model.

- Rotor dimensions:

Table 3.4 Rotor dimensions

Outer diameter	147.3 mm
Inner diameter	48 mm
Stacking factor	0.95
Number of slots	44
Slot type	1
Length of rotor core	250 mm
Steel type	M19_24G
Skew width (measured in number of slots)	0 (for auto design)
Cast rotor (rotor squirrel-cage winding is cast)	Ticked

- Rotor slot:

Table 3.5 Rotor slot dimensions

Bs0	1.5 mm
Hs01	0 mm
Hs0	0.75 mm
Bs1	6 mm
Bs2	2.2 mm
Hs2	18.75 mm

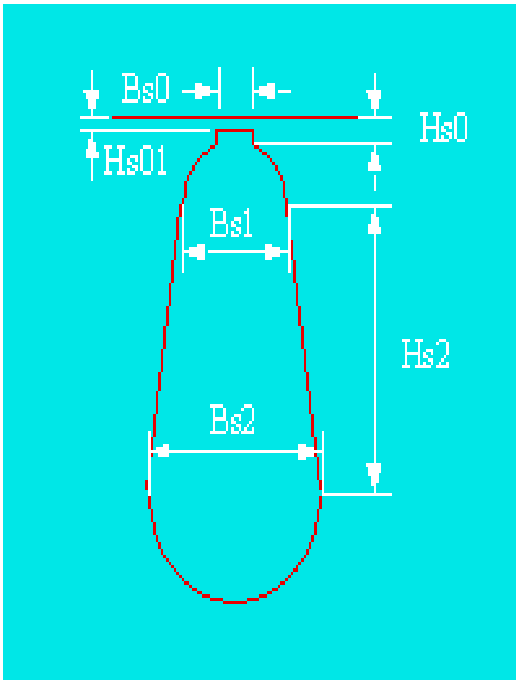

Fig. 3.7 Rotor slot

- Rotor winding:

Table 3.6 Rotor winding parameters

Bar conductor type	Copper
End length	5 mm
End ring width	10.5 mm
End ring height	29 mm
End ring conductor type	Copper

Using the above procedure the rotor geometry has been designed as shown in the figure 3.7.

Step 4: Choosing shaft material.

The shaft taken for the induction machine model is non-magnetic in nature. For this, select shaft in the project tree under project manager window and apply the required settings.

- Magnetic shaft: Unticked.

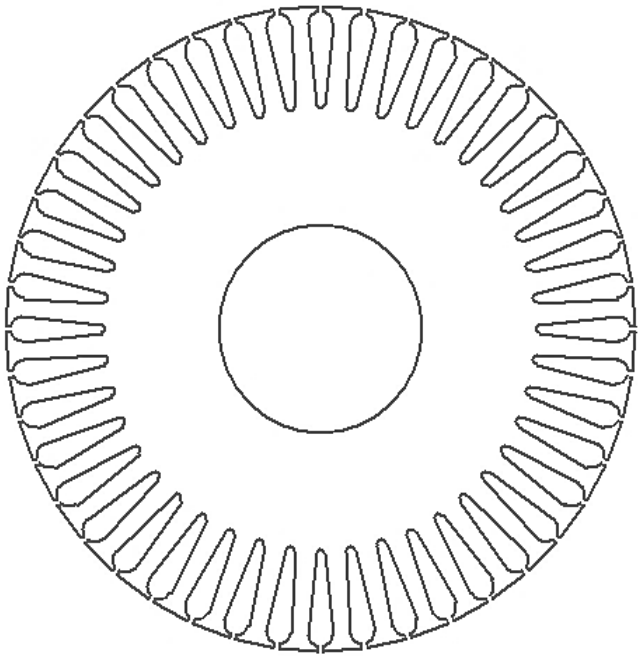

Fig. 3.8 Rotor design of 3-ϕ induction motor

Step 5: Designing the machine parameters:

Machine parameters here refer to number of poles, stray loss factor, frictional loss, windage loss and reference speed of the motor. The synchronous speed of the machine has been taken as the reference speed i.e.

$$Ns = \frac{120f}{P} = \frac{120 \times 50}{4} = 1500\ rpm \qquad (3.1)$$

where, 'f' and 'P' are the supply frequency and number of poles of the machine respectively.

Table 3.7 Machine parameters

Machine type	3-phase induction motor
Number of poles	4
Stray loss factor	0.01
Frictional loss (measured at rated speed)	50 W
Windage loss (measured at rated speed)	50 W
Reference speed	1500 rpm

Step 6: Setting the analysis setup for machine:

Table 3.8 Analysis setup

Operation type	Motor
Load type	Constant power
Rated output power (the rated mechanical or electrical output power)	7500 W
Rated voltage (line-to-line ac rms or dc voltage)	440 V
Rated speed	1360 rpm
Operating temperature	75° C
Winding connection	Wye
Source frequency	50 Hz

Step 7: Running the setup for results:

After setting the machine parameters as shown in above steps, the machine parameters are validated using the **Validate** icon in the tool bar. The RMxprt tool examines the complete machine parameters while checking for the errors in the system, if any. After the validation, the machine is analysed using the **Analyse all** icon in the tool bar and evaluated results could be fetched from the data sheets and curves in the tool bar

.

3.3.2 Design of 3-ϕ induction motor in Maxwell 2D design tool

Maxwell software utilises finite element analysis (FEA) method to solve 3D and 2D magnetostatic, electrostatic, transient and eddy current problems. The Maxwell 2D design tool provides a platform for designing the 2D geometry of electrical machines and components. It contains the user defined primitive designs for the rotating machines wherein it provides the provision of customising the dimensions for stator, rotor, stator & rotor slots, winding type configurations, boundaries, excitations, meshing, and solver-solution type. For the presented transient study of induction machine, a 2D design has been constructed in Maxwell 2D design tool using the step by step procedure as shown below in figure 3.9.

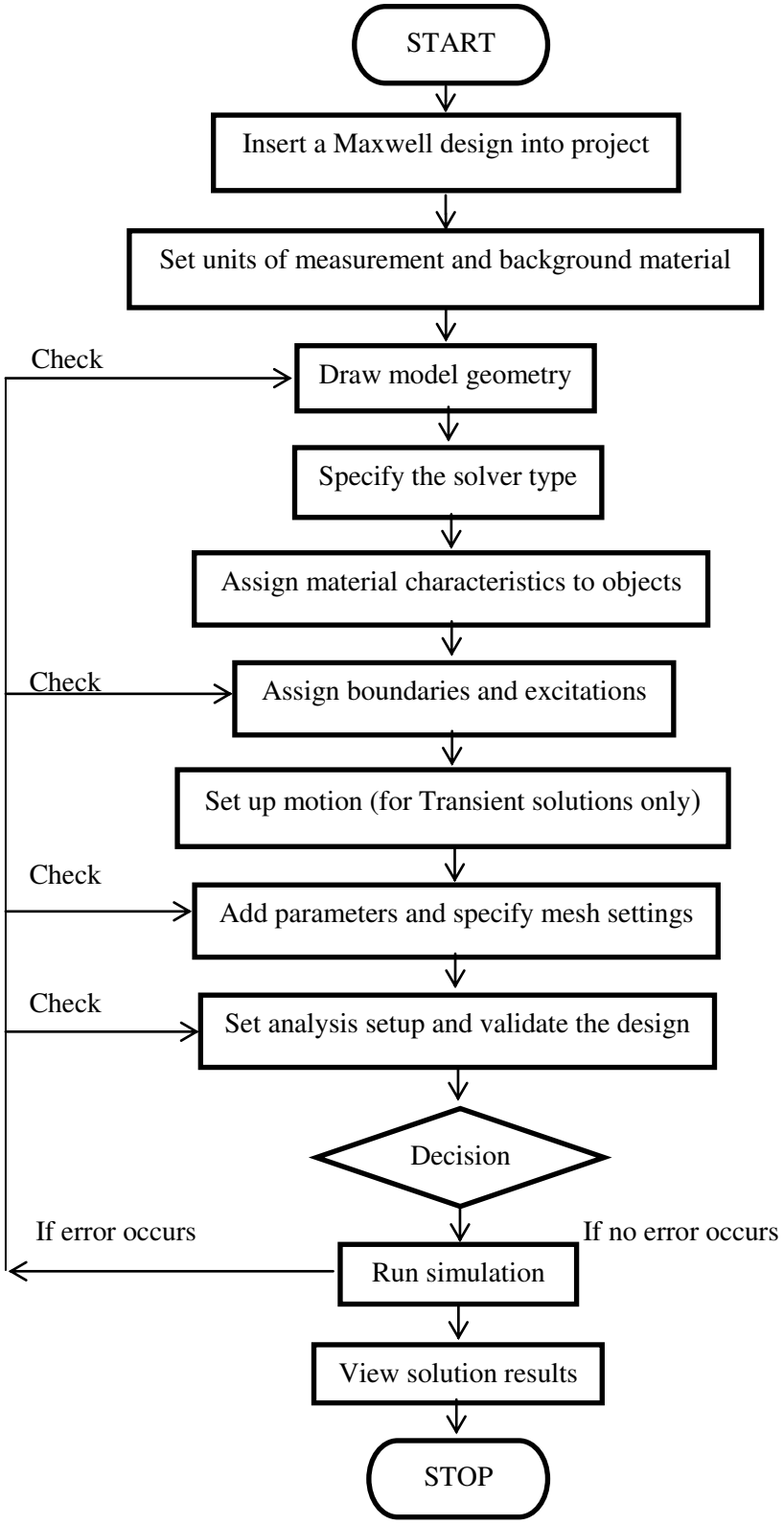

Fig. 3.9 Flowchart for designing a Maxwell 2D design

Following the above procedure the induction machine model has been prepared in Maxwell 2D Design tool as shown below:

Step 1: Creating a new project and including a Maxwell 2D design.

- Click File and select **New** to load the new project.
- Click **Project** and insert the **Maxwell 2D Design**.

After loading a new project, the project tree in project manager window shows the icons for motion setup, boundaries, Excitations, parameters, mesh operations, optimetrics, and analysis setup as shown in figure 3.5.

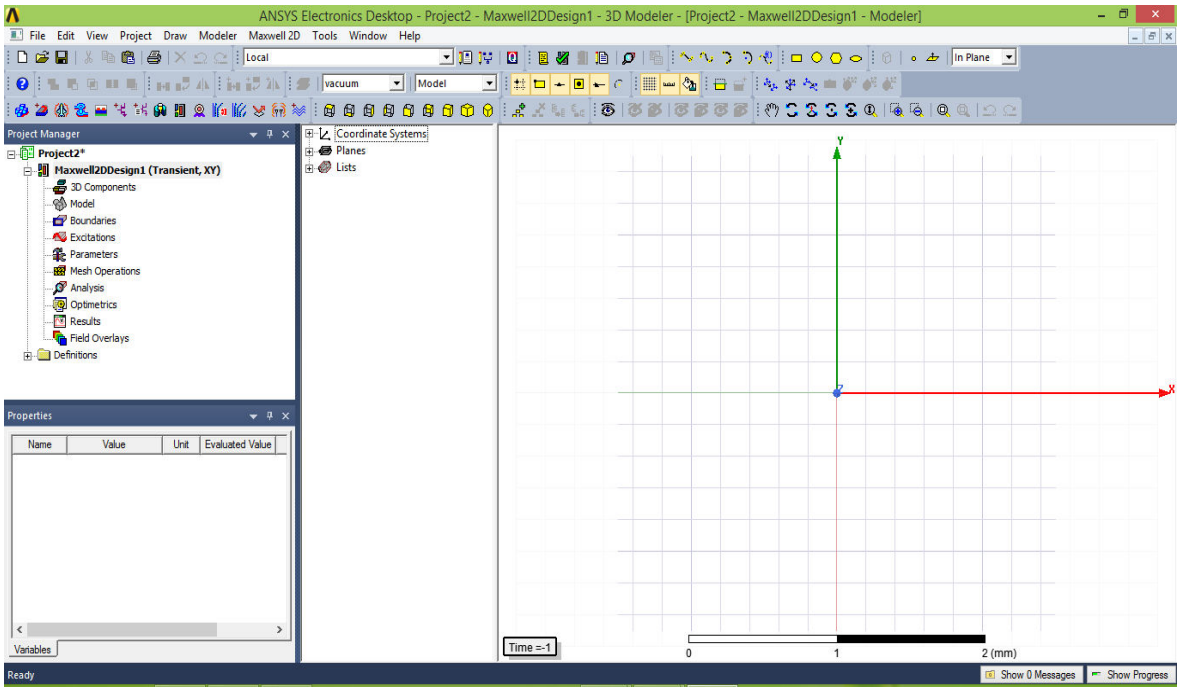

Fig. 3.10 Maxwell schematic

Step 2: Select solution type and units of measurements.

- The Maxwell Schematic is as show in the figure 3.10.
- Select solution type i.e. **Transient**

Maxwell 2D>Solution type>Magnetic (Transient)

- Select units

Modeler>units>select units (mm)

Step 3: Design stator geometry.

- **Draw>user defined primitive>RMxprt>slot core**
- Input the stator parameters i.e.

Table 3.9 Stator dimensions

Dia Gap (Inner diameter of stator core)	148 mm
Dia Yoke (outer diameter of stator core)	210 mm
Length of stator core	0 mm
Material of stator core	M19_24G
Skew	0 deg
Slots	48
Slot type	3
Hs0	0.9 mm
Hs01	0 mm
Hs1	1.3 mm
Hs2	16.5 mm
Bs0	3.5 mm
Bs1	6.1 mm
Bs2	9.5 mm
Rs	0 mm
Seg angle	15 degree
LenRegion	0 mm
Info core	0

Step 4: Define rotor geometry.

- **Draw>user defined primitive>RMxprt>slot core**
- Input the rotor parameters i.e

Table 3.10 Rotor dimensions

Dia Gap (Outer diameter of rotor core)	147.3 mm
Dia Yoke (Inner diameter of rotor core)	48 mm
Length of rotor core	0 mm
Skew	0 deg
Slots	44
Slot type	1
Hs0	0.75 mm
Hs01	0 mm
Hs1	0 mm
Hs2	18.75 mm
Bs0	1.5 mm
Bs1	6 mm
Bs2	2.2 mm
Rs	0 mm
Seg Angle	15 degree
Len Region	0 mm
Info core	0

Step 5: Designing the rotor windings or bars.

The rotor configuration taken for the present model is squirrel cage type thus rotor conductors or bars are to be placed in the rotor slots. Thus, the cage dimensions like ring diameter, ring length,ring height and material type have to be defined for the rotor bars.

- **Draw>user defined primitive>RMxprt>Squirrel Cage**
- Dimensions like diameter of gap, diameter of yoke, length etc. for squirrel cage bars remains same as in the step 4 and remaining parameters are as shown in the Table 3.11.

Table 3.11 Rotor bar parameters

Material	Copper
Bar End Ext	5 mm
Ring length	10.5 mm
Ring height	29 mm
Ring Diagap	0 mm
Cast rotor	1
Info coil	0

Step 6: Designing the stator coil.

- **Draw>user defined primitive>RMxprt>Lap coil**
- Dimensions for stator winding remains same as in the step 3 and remaining parameters are as shown in Table 3.12.

Table 3.12 Stator coil parameters

Layers	1
EndExt	0
Span Ext	0
Bend Angle	0
Seg Angle	10 degree
Len Region	0
Info coil	2

Step 7: Duplicating the stator coil.

After the execution of step 6 only one coil gets placed in the stator slots so in order to accommodate rest of the coils, duplication of coils is done. In order to duplicate the stator coils across the stator periphery i.e.

- **Select coil_0>Duplicate around the axis**
- Keep the angle equal to 7.5° as all the stator slots are displaced by this angle across the stator core (since 360°/48 = 7.5°). And the number of duplicates is equal to 48.

Step 8: Connecting the stator coils.

For a 3-ϕ induction motor comprising of 48 stator slots, each phase winding will be placed in 16 slots in a set of 4 consecutive slots. The 3-phase, 1-layer winding can be arranged in 48 slots as below:

Slot 1 to 24: AAAA-C-C-C-CBBBB-A-A-A-ABBBB-C-C-C-C

Slot 25 to 48: AAAA-C-C-C-CBBBB-A-A-A-ACCCC-B-B-B-B

Here, the negative sign shows the direction of currents carried by the stator windings. Therefore, for the model, if the stator cross-section is sub divided into four quadrants (each comprise of 12 slots) then every first coil of all the quadrants is to be united i.e.coil_0, coil_12, coil_24, and coil_36 are united. Similarly, rest of the coils of stator is united.

Step 9: Separating the rotor bar conductors.

- For separating the bar conductors:

  Select all bars>Modeler>Boolean>separate the bodies

Step 10: Defining the machine shaft.

- **Draw>user defined primitive>RMxprt>Band**
- Input the following dimensions as shown in Table 3.13.

Table 3.13 Shaft dimensions

Dia Gap	147.65 mm
Dia Yoke	48 mm
Length of shaft	0 mm
Seg angle	0.9375 degree
Fractions	1
Half axial	0
Info core	100

Step 11: Defining the Inner region for machine.

- **Draw>user defined primitive>RMxprt>Slot core**
- Input the inner region parameters as shown in Table 3.14:

Table 3.14 Inner region dimensions

Dia Gap	147.3 mm
Dia Yoke	48 mm
Length	0 mm
Skew	0
Slots	44
Slot type	1
Slot dimensions	Same as the rotor slot dimensions
Seg angle	15 degree
Len Region	0
Info core	100

Step 12: Defining the outer region for machine.

- **Draw>user defined primitive>RMxprt>Band**
- Input the outer region parameters as shown in Table 3.15.

Table 3.15 Outer region dimensions

Dia Gap	147.65 mm
Dia Yoke	210 mm
Length	0 mm
Seg angle	0.9375 degree
Fractions	1 (for circular region)
Half axial	0
Info core	100

Step 14: Defining band for the circular motion.

- **Draw>user defined primitive>RMxprt>Band**
- Input the band dimensions as shown in Table 3.16.

Table 3.16 Band dimensions

Dia Gap	147.65 mm
Dia Yoke	48 mm
Length of band	0 mm
Seg angle	0.9375 degree
Fractions	1
Half axial	0
Info core	0

Step 15: Defining boundaries for the machine.

- Select the outer periphery of the stator.
- **Maxwell 2D>Boundaries>Assign>Vector Potential**

Step 16: Assign excitations.

For the rotor conductors:

- Select all the rotor bar conductors.
- **Maxwell 2D>Excitations>Assign>End coonection**
- Put end resistance = $5.47454e^{-007}$ ohm and end inductance = $2.2014e^{-009}$ H.

For the stator coils:

- **Select coil>Maxwell 2D>Excitations>Assign>Coil Terminal**
- Keep the number of conductors equal to 30.
- Repeat the same process for the remaining coils.
- Now in the project manager window, all the coil excitations defined above are listed under **Excitations** icon**.** Right click on the **Excitations** under project manager and add winding.

- Specify a name as for this winding viz phase_A. Keep the type of conductor - stranded, type of excitation-external, initial current- 0A, and number of parallel branches- 2.
- Add all the coils named A as shown in the **step 8** under this **phase_A** winding.
- Repeat the same process for defining **phase_B** and **phase_C** and add the respective coils as in the aforementioned case.

Step 17: Specify the mesh settings.

For rotor bars:

- Select all the rotor bars.
- **Project Manager>Mesh operations>inside selection>Length based**
- Keep maximum number of elements equal to 1.1 mm.

For stator coils:

- Select all the stator coils.
- **Project Manager>Mesh operations>inside selection>Length based**
- Keep maximum number of elements equal to 3.9 mm.

For the stator and rotor length:

- Select rotor and stator.
- **Project Manager>Mesh operations>inside selection>Length based**
- Keep maximum number of elements equal to 6.27 mm.

For the stator and rotor surface:

- Select rotor and stator.
- **Project Manager>Mesh operations>surface approximation**
- Put surface deviation= 0.105 mm and normal deviation= 15 degree.

Step 18: Defining the motion setup for machine.

- **Select Band>Click Maxwell 2D>Model>Motion setup>Assign Band**
- Keep the motion type as rotational in motion setup window.
- Put the moving vector- Global: Z positive.

- And the initial position= 0 degree.

Step 19: Set analysis setup for the design.

- Keep the values for **Stop time** and **Time step** in the **General** tab of analysis setup window.
- Also, set the values for sweep setup in **Save Fields** tab.

Step 20: Validate the design.

- Validate the design by clicking validate icon in the tool bar.

Following the above procedure, the design of 3-ϕ induction motor has been created in Maxwell 2D design tool. This created 2D design is further integrated with the drive circuit, which is designed in Simplorer design tool, for the performance analysis of the machine. The Maxwell 2D design of the 3-phase induction motor is as shown in figure 3.11.

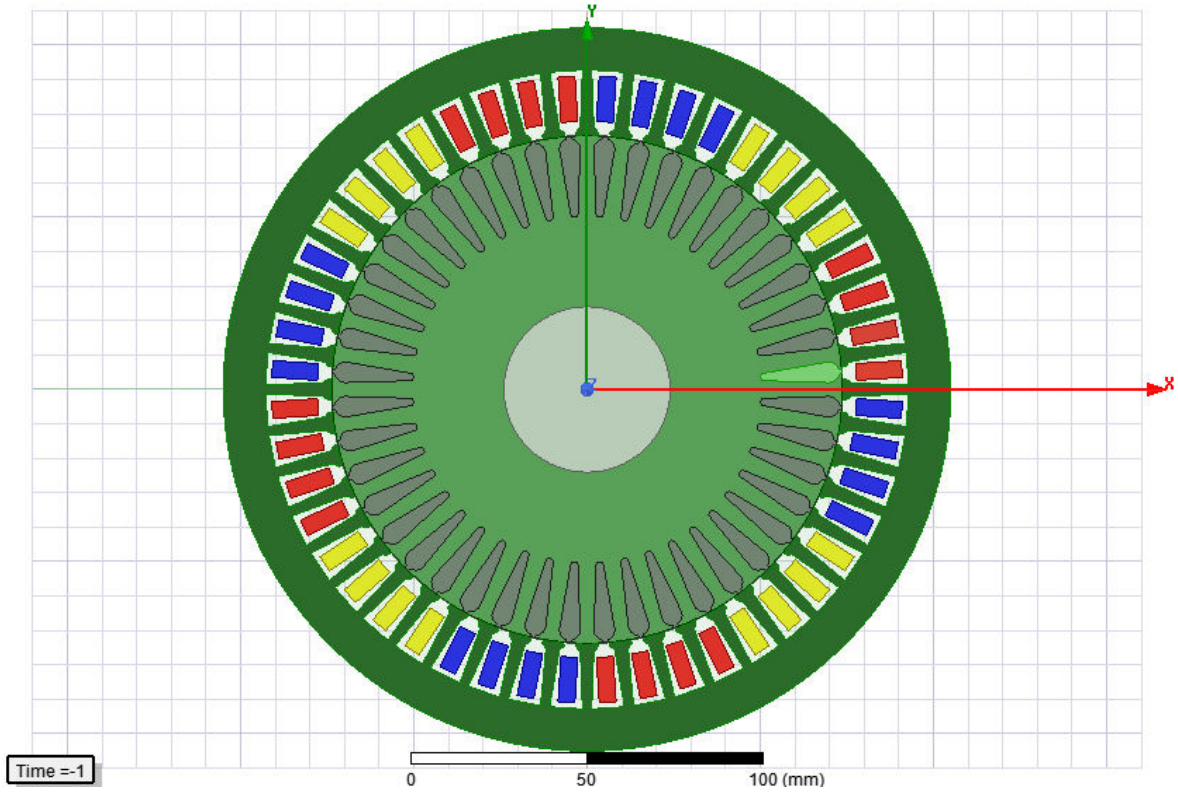

Fig. 3.11 Maxwell 2D design of 3-ϕ induction motor

3.3.3 Design of drive circuit in Simplorer design tool

ANSYS Simplorer is an integrated, mixed-signal, multi-domain simulator for complex electrical circuits. It provides fast, accurate and reliable environment for designing the simulation models of electrical circuits. In addition, it can dynamically interact with other ANSYS design tools such as Maxwell and RMxprt and with third party applications like Simulink and Mathcad. The open-loop PWM VSI drive circuit has been prepared in the Simplorer design tool by following the procedure given below.

Step 1: Insert a Simplorer design and create a new project.

- On the **File** menu, click **New.** A new project named as **Projectn** is listed in the project tree.
- Go to **Project** menu and click **Insert Simplorer Design.** Thus, a simplorer design named as **Simplorer1** is created under the project.

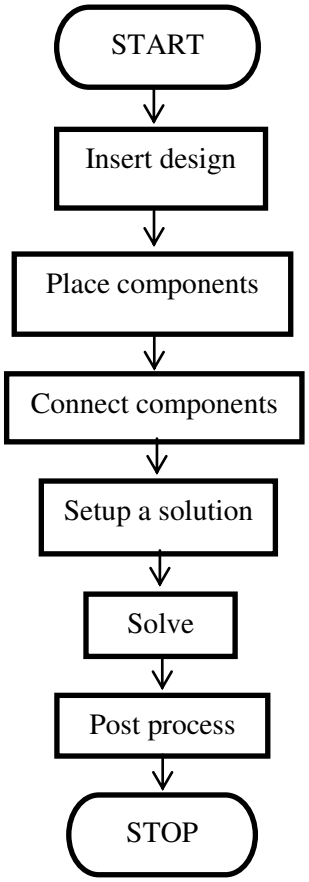

Fig. 3.12 Flowchart for designing a Simplorer design

Step 2: Place components and connect them.

- Select the components like IGBT, Diode, voltage source, voltmeter, ammeter, resistance, inductor etc. from the component libraries (as shown in figure 3.12).
- Connect these components as per the required circuit design.

Step 3: Setting the component parameters.

- Keep the IGBT and Diode parameters as shown in Table. 13.17.
- Keep the frequencies of sine wave source and triangular wave source as 50 Hz and 2 kHz respectively.

Table 3.17 IGBT and diode parameters

Forward voltage	0.8 V
Bulk resistance	0.001 ohm
Reverse resistance	0.1 Megaohm

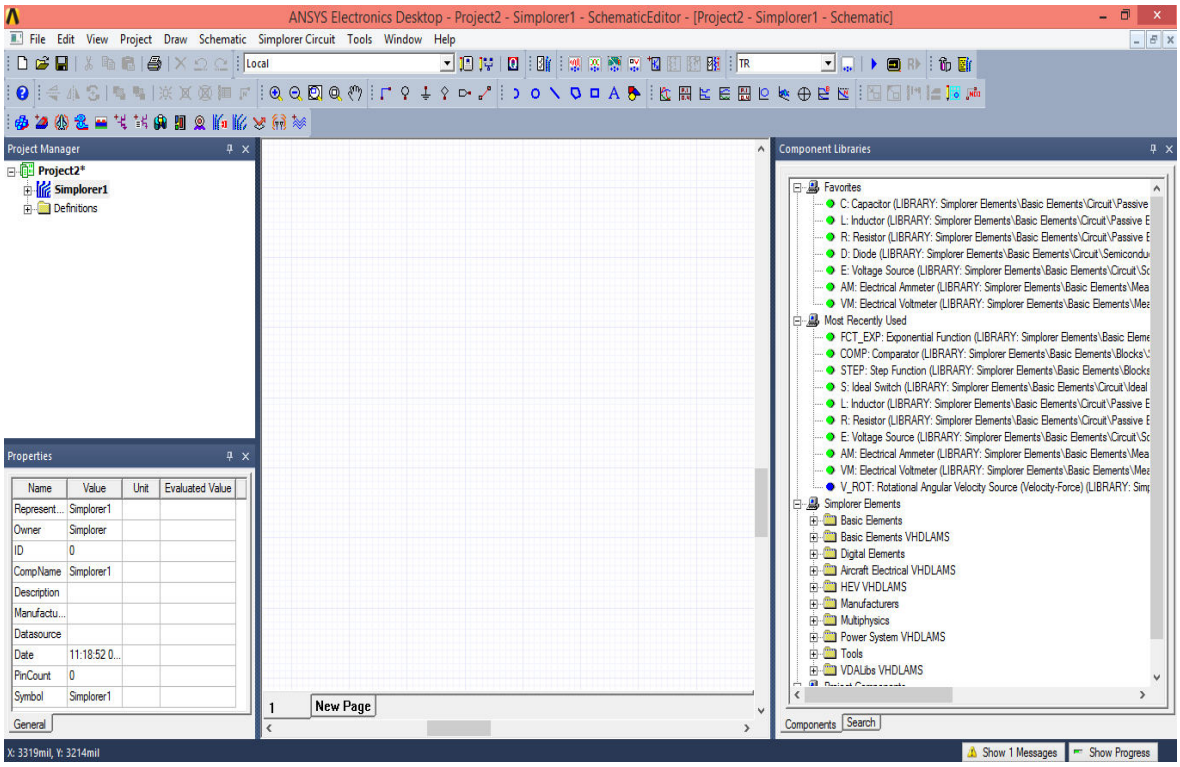

Fig. 3.13 Simplorer design schematic

Step 4: Set the analysis setup for Simplorer Design.

- Add the **Transient analysis setup** from the toolbar.
- Put the values for End Time (Tend), Min Time Step (Hmin), and Max Time Step (Hmax).

Note: The minimum step time taken for the simulation should be less than the time period of smallest sample in the circuit. On violation of this condition may lead to discrepancies in the output responses.

Step 5: Simulate the design and check results.

- Click the **Simulate setup** icon in the toolbar to run the simulation.
- Check results by creating rectangular reports form the **Results** icon under the project tree in **Project Manager Window**.

Following the above procedure the PWM-VSI drive circuit for 3-ϕ induction motor has been created as shown in the figure 3.14.

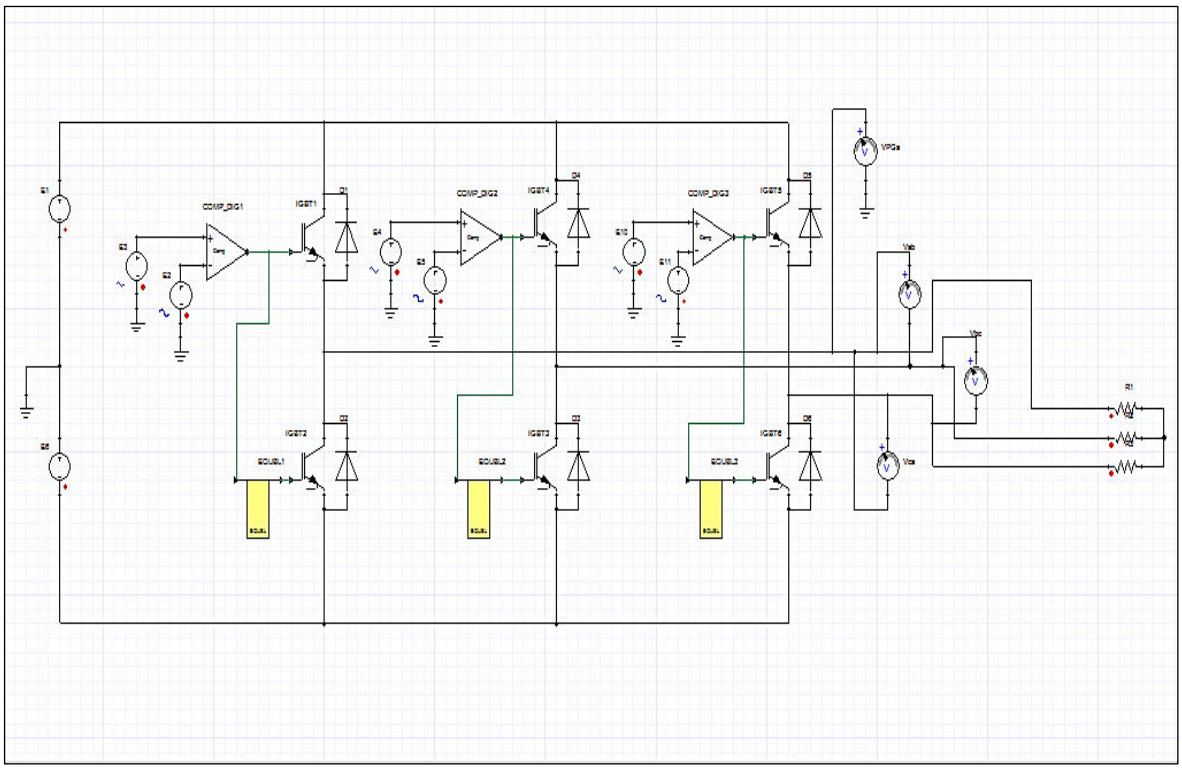

Fig. 3.14 PWM-VSI drive circuit for 3-ϕ induction motor

3.3.4 Co-Simulation of Maxwell 2D and Simplorer design tool

For integrating the induction machine and the drive circuit, a Transient-Transient simulation is set by creating a dynamic link between the Maxwell Transient design and Simplorer through the Simplorer user interface. This Simplorer interface permits RMxprt, Maxwell 2D, and 3D designs to be linked as dynamic components. The mechanism of coupling between the Maxwell 2D and Simplorer design tool is shown in the figure 3.15.

The Transient solvers of Maxwell 2D design tool integrate circuit equations with the finite element system of equations. Maxwell and Simplorer use the loop form and nodal form of the circuit equations respectively. At each time step, Simplorer generates a Norton-equivalent of the drive circuit at the links between the drive system and the Maxwell component. Consequently, Maxwell converts this Norton equivalent to Loop matrix, solves the finite element equations, and then generates a Thevenin equivalent for the next time step. And thus solves machine characterstics for each time step.

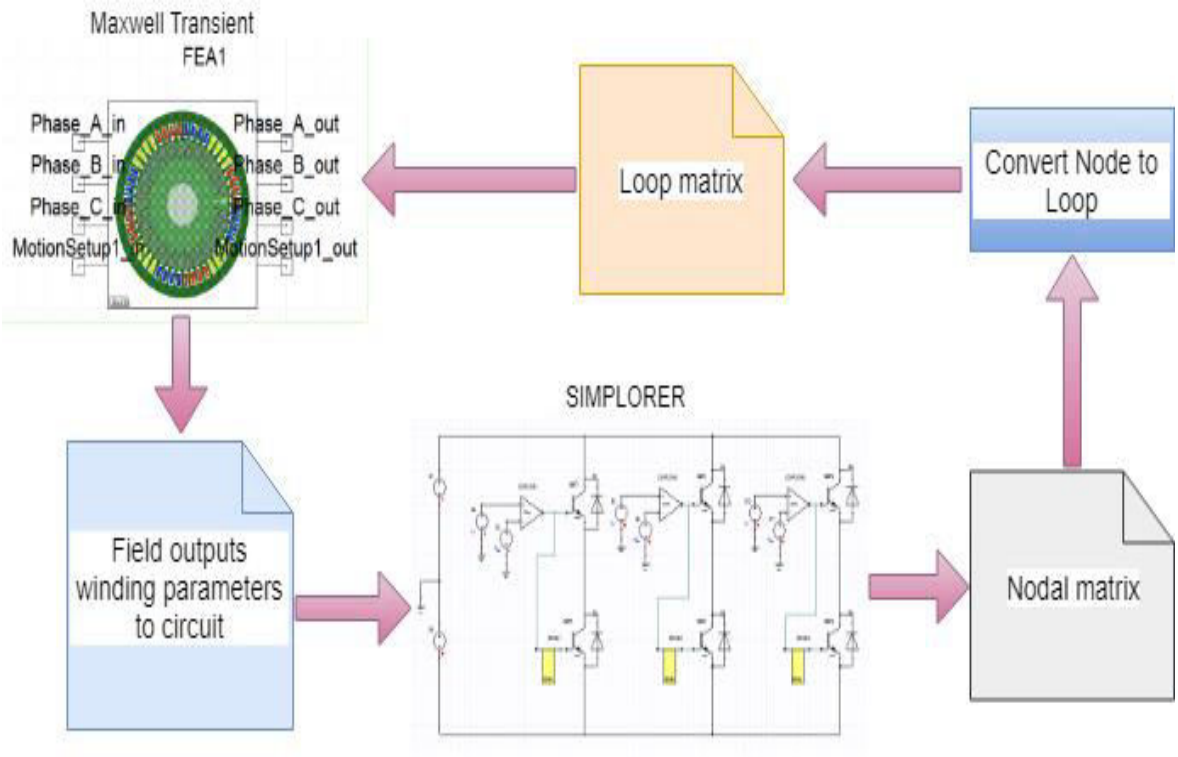

Fig. 3.15 Schematic diagram of co-simulation process

To set a Transient-Transient co-simulation:

Step 1: Simplorer Design tool settings.

- On the **Simplorer Circuit** main menu
  Select Subcircuit>Maxwell Component>Add Transient Co-simulation
- In the **Selection** panel of the **Link Description** tab, click the […] button to load the Maxwell file.
- Select the **Design** and the related **Solution** in the **Link Description tab.**
- Connect the pins with the drive circuit.
- Set the analysis setup for the simulation.

Step 2: Maxwell Design tool settings.

- Enable the Transient-Transient simulation settings
  Select Maxwell 2D>Design Settings>Advanced Product Coupling>Enable transient-transient link with Simplorer
- Set the analysis setup for the simulation.

RESULTS AND DISCUSSION

CHAPTER 4 RESULTS AND DISCUSSION

In the last chapter 3, we have already discussed the material and methods used for the design, modelling and co-simulation of the three phase induction motor drive system. In this chapter 4, the simulation results of performance analysis of IM drive system are presented and discussed. In addition, the inverter fault analysis has been carried out by open circuiting and short circuiting the inverter IGBT.

4.1 Simulation Results

The machine model has been created in ANSYS tools and further investigation for performance and fault analysis has been carried out in the proposed study. The simulation results have been obtained for various operations and finally the performance and fault analysis is done for the drive system.

4.1.1 Machine parameters for different operations in RMxprt design tool

The machine is tested under various operating conditions like no-load, rated load, locked-rotor and break-down operation. The parameters are obtained for each operation and are listed in the tabular forms as follows.

Table 4.1 Machine response at locked-rotor operation

Locked-Rotor Torque	101.612 N-m
Locked-Rotor Phase Current	126.251 A
Locked-Rotor Torque Ratio	2.1005
Locked-Rotor Stator Resistance	0.605669 ohm
Locked-Rotor Stator Leakage Reactance	0.77326 ohm
Locked-Rotor Rotor Resistance	0.342486 ohm
Locked-Rotor Rotor Leakage Reactance	0.693826 ohm

Table 4.2 Machine response at break-down operation

Break-Down Torque	183.819 N-m
Break-Down Phase Current	79.7667 A

Table 4.3 Machine response at rated-load operation

Copper Loss of Stator Winding	318.183 W
Copper Loss of Rotor Winding	99.5516 W
Iron-Core Loss	123.026 W
Frictional and Windage Loss	97.4384 W
Stray Loss	75 W
Total Loss	713.199 W
Input Power	8.21365 kW
Output Power	7.50045 kW
Mechanical Shaft Torque	48.375 N-m
Efficiency	91.3169%
Power Factor	0.934432
Rated Slip	0.0129331
Rated Shaft Speed	1480.6 rpm

Table 4.4 Machine response at no-load operation

No-Load Iron-Core Loss	133.07 W
No-Load Input Power	331.819 W
No-Load Power Factor	0.113148
No-Load Slip	0.000157875
No-Load Shaft Speed	1499.76 rpm

Observations: With the proper estimation of machine geometry i.e. stator slots dimensions, rotor slots dimensions etc. the efficiency of the machine increased to approximately 91% at rated-load operation. In addition, the power factor reached close to its ideal value i.e. approximately 0.93 at rated-load operation

4.1.2 Induction machine characteristics in RMxprt design tool

Induction motor performance is analysed in the RMxprt tool and its corresponding characteristics are obtained as depicted in the figures 4.1 to 4.6.

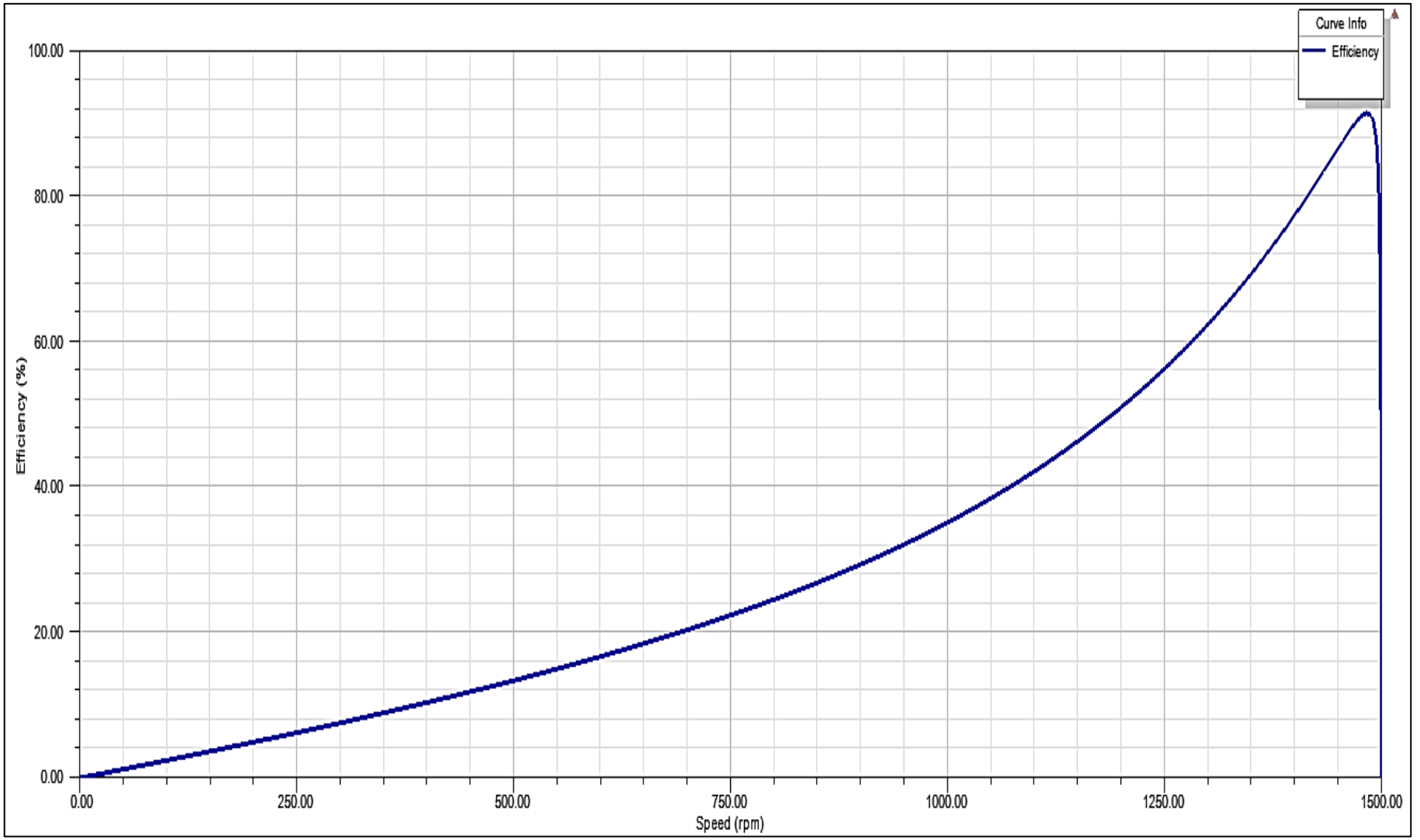

Fig. 4.1 Efficiency versus speed curve

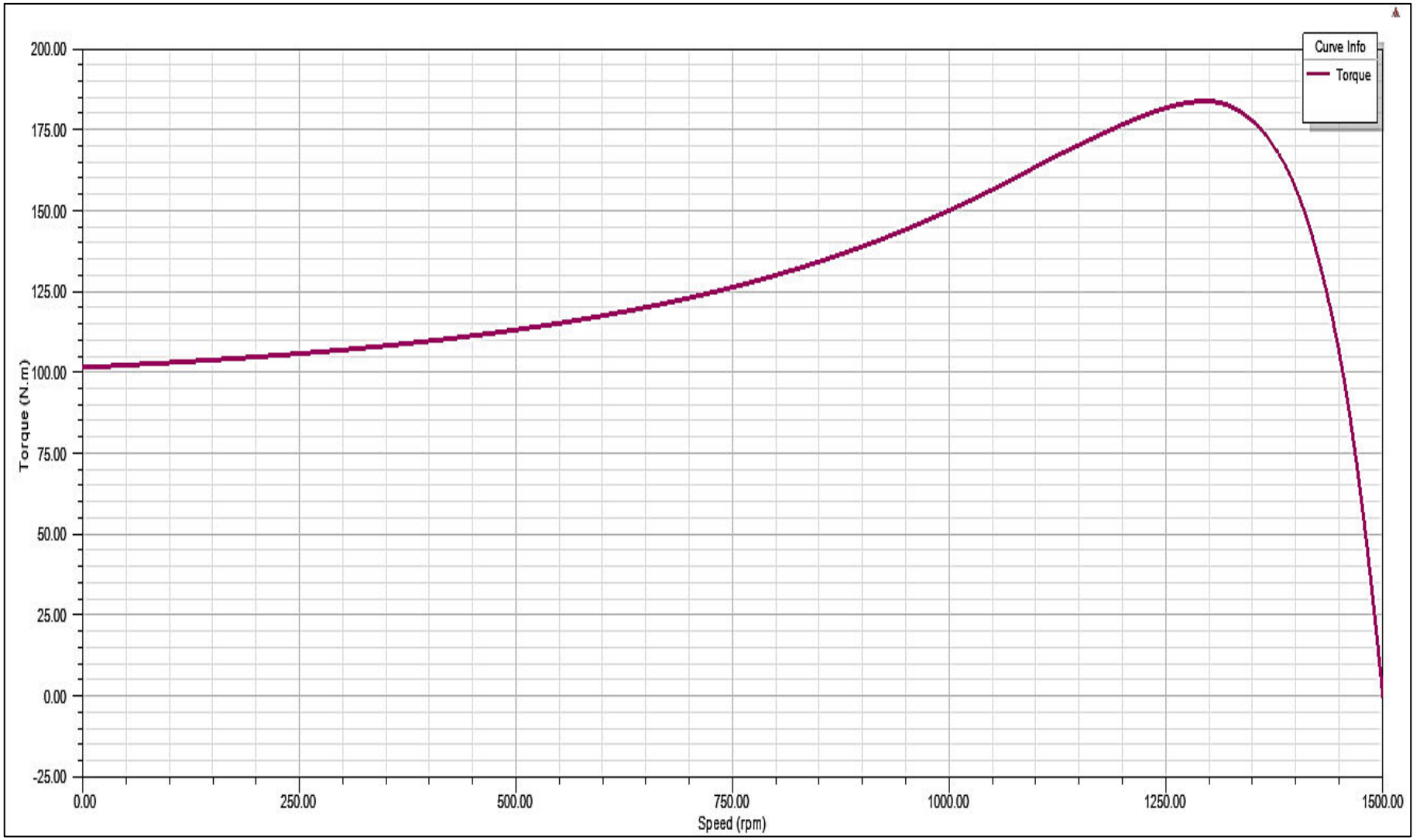

Fig. 4.2 Torque versus speed curve

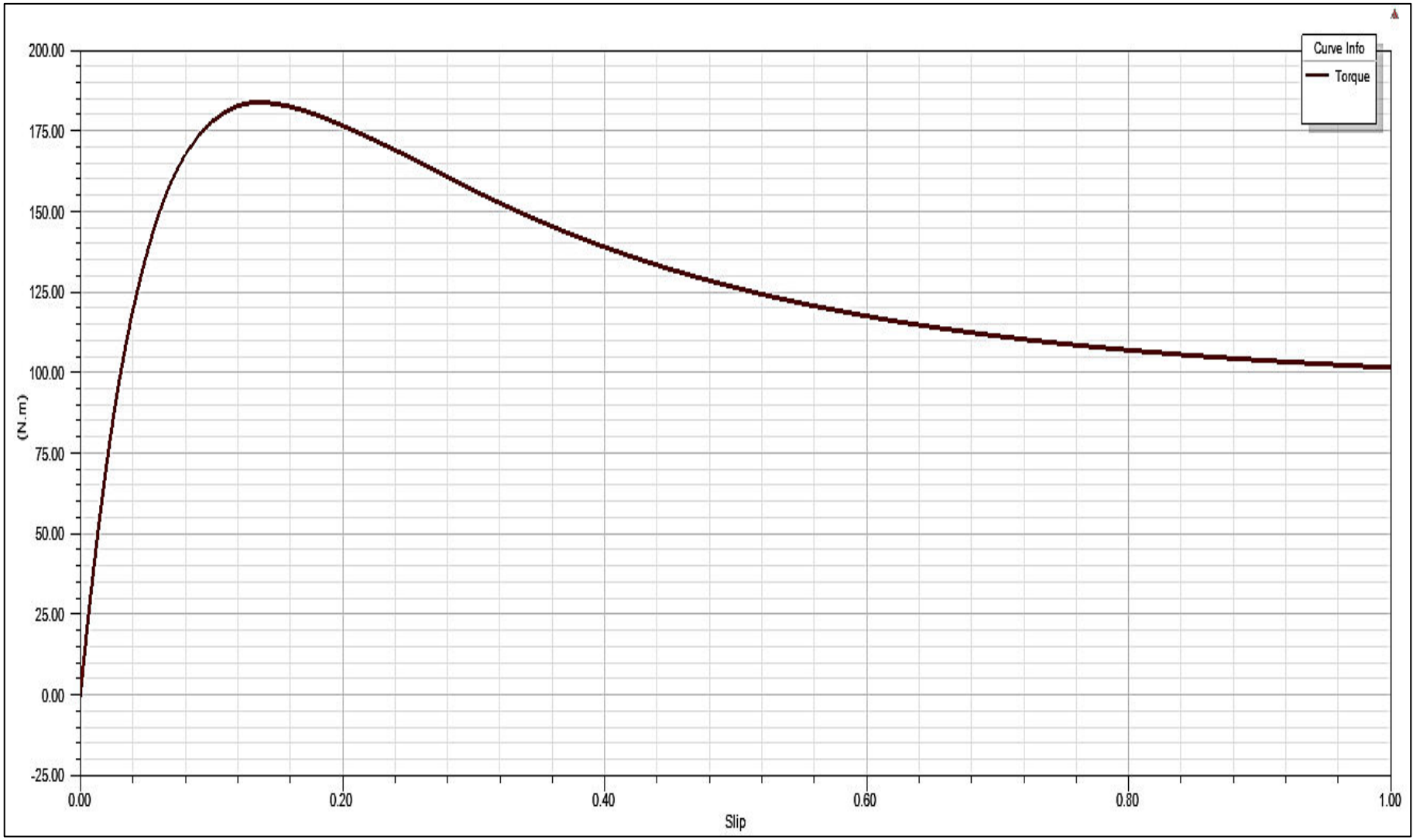

Fig. 4.3 Torque versus slip curve

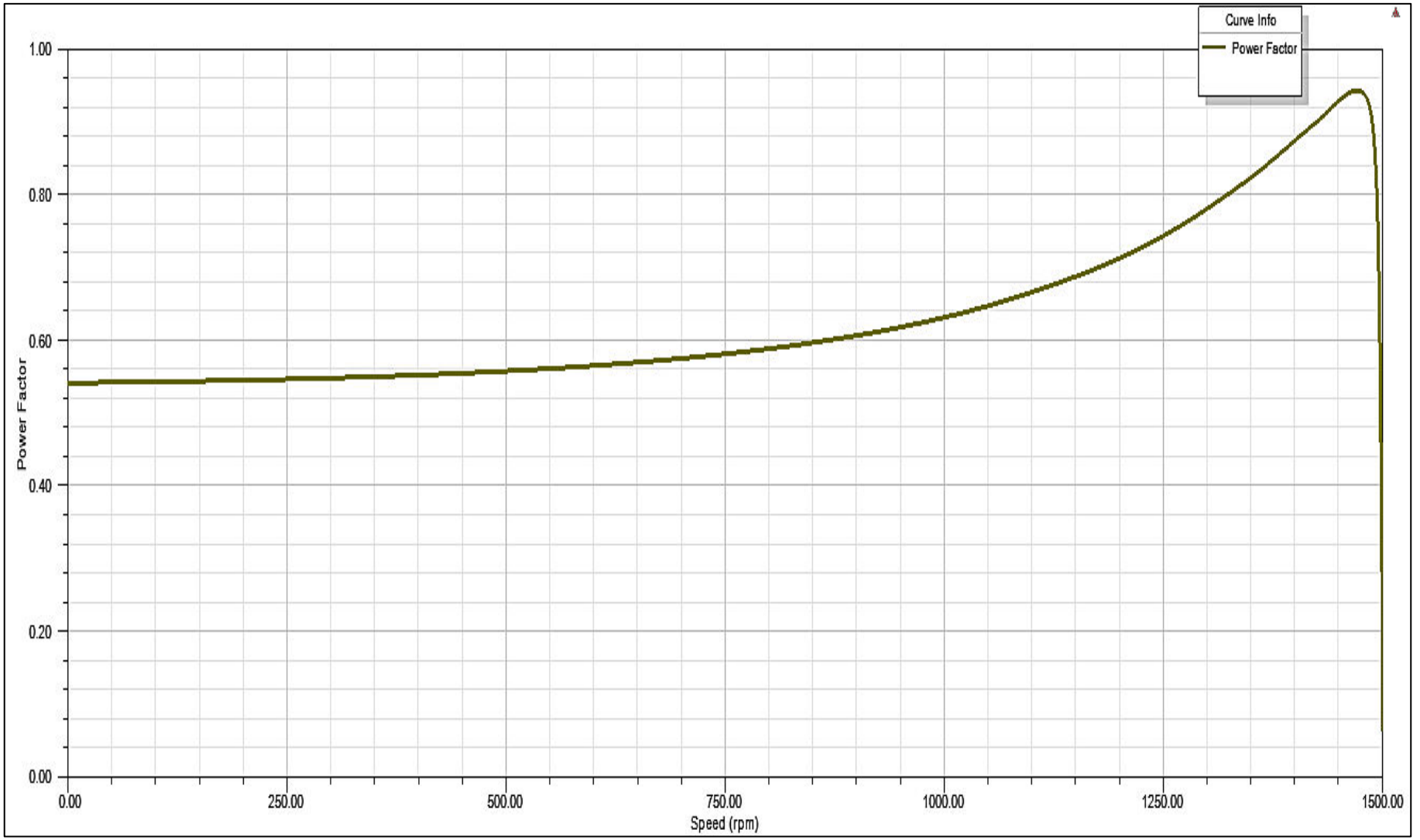

Fig. 4.4 Power factor versus speed curve

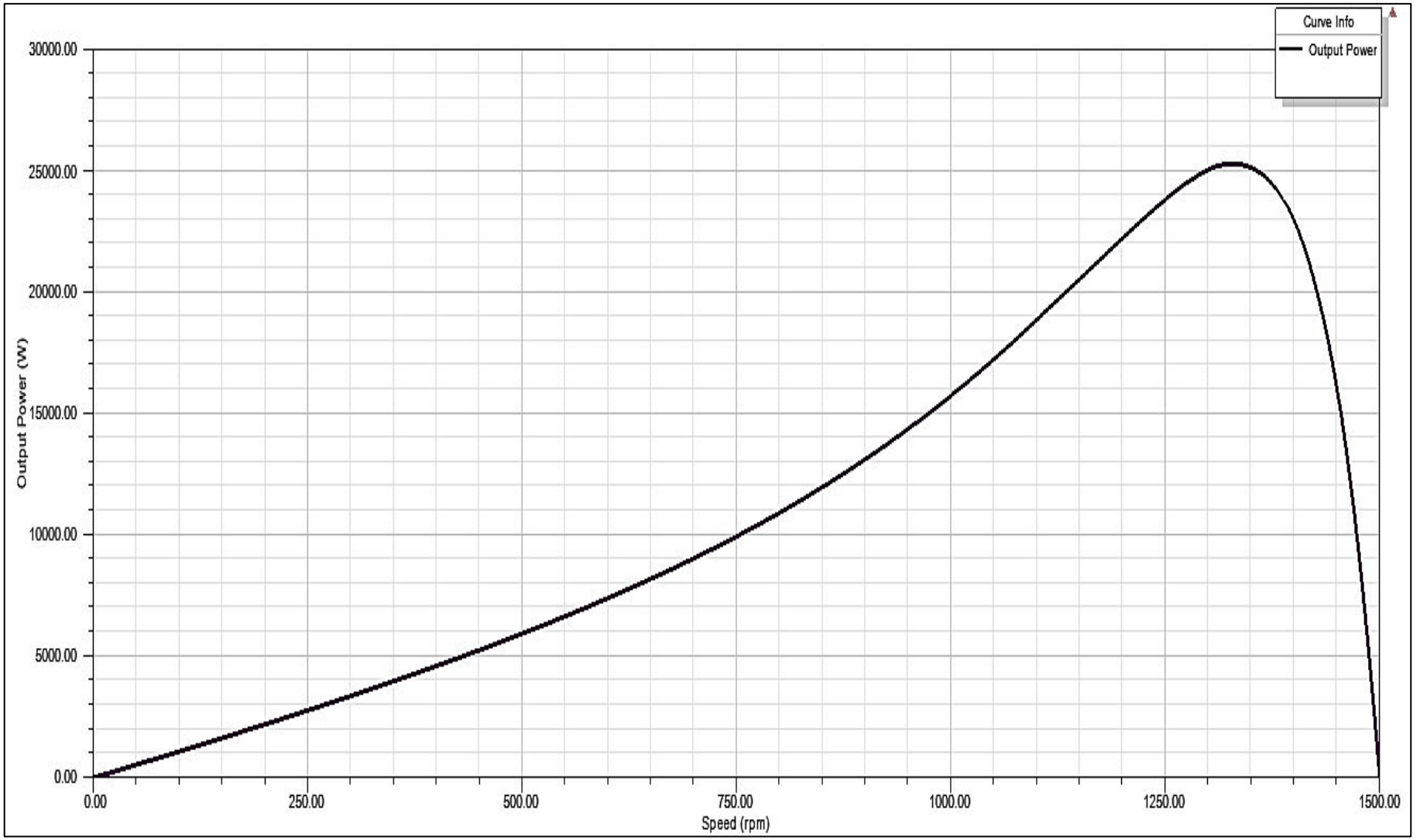

Fig. 4.5 Output power versus speed curve

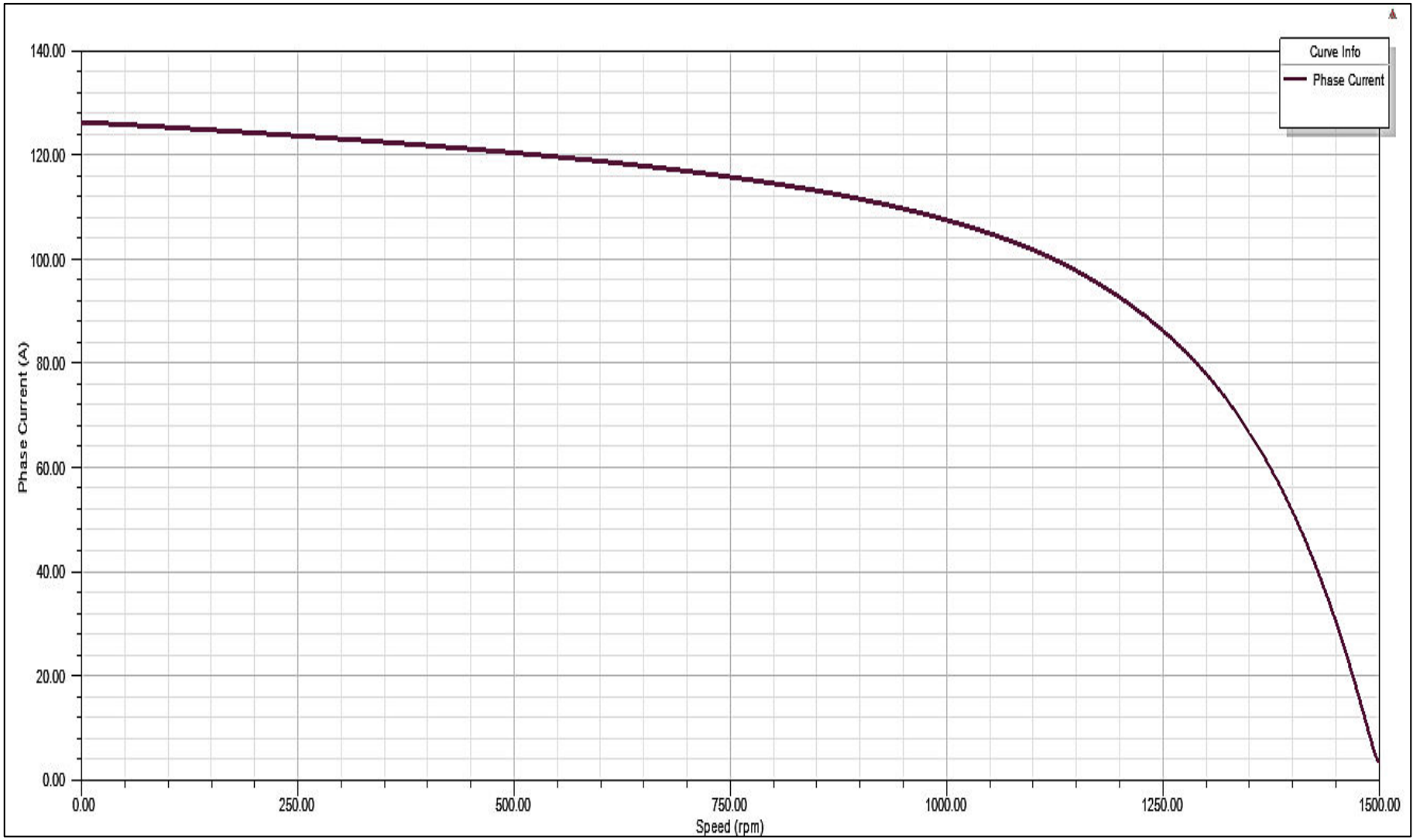

Fig. 4.6 Phase current versus speed curve

Observations:

These performance characteristics were obtained for the 7.5 kW of 3-ϕ induction motor in RMxprt design tool. The efficiency versus speed curve shows slight exponentially increasing nature with respect to speed and finally achieves maximum value of approximately 94% at about 1480 rpm. The torque versus speed curve shows the identical behaviour as for an ideal machine with the high starting torque of 102 N-m and reaches a maximum value of 185 N-m at 1300 rpm rotor speed. Similarly, the torque versus slip characteristic shows the mirror image of torque versus speed curve with the maximum torque of 185 N-m at slip approximately equal to 0.13. The power factor versus speed characteristic initially shows constant behaviour till 750 rpm and then attains an exponentially increasing nature thereafter acquiring the maximum power factor of 0.92 at rotor speed equal to 1480 rpm. The output power at shaft end initially demonstrates a sluggish exponentially increasing behaviour with respect to speed till 750 rpm and finally acquires a maximum output power of 25 kW 1325 rpm. The phase current versus speed characteristic initially shows a high starting current of 126 A at 0 rpm and decays slightly till 1000 rpm which exponentially decays to 4A thereafter.

4.1.3 SPWM technique controlled VSI results in Simplorer design tool

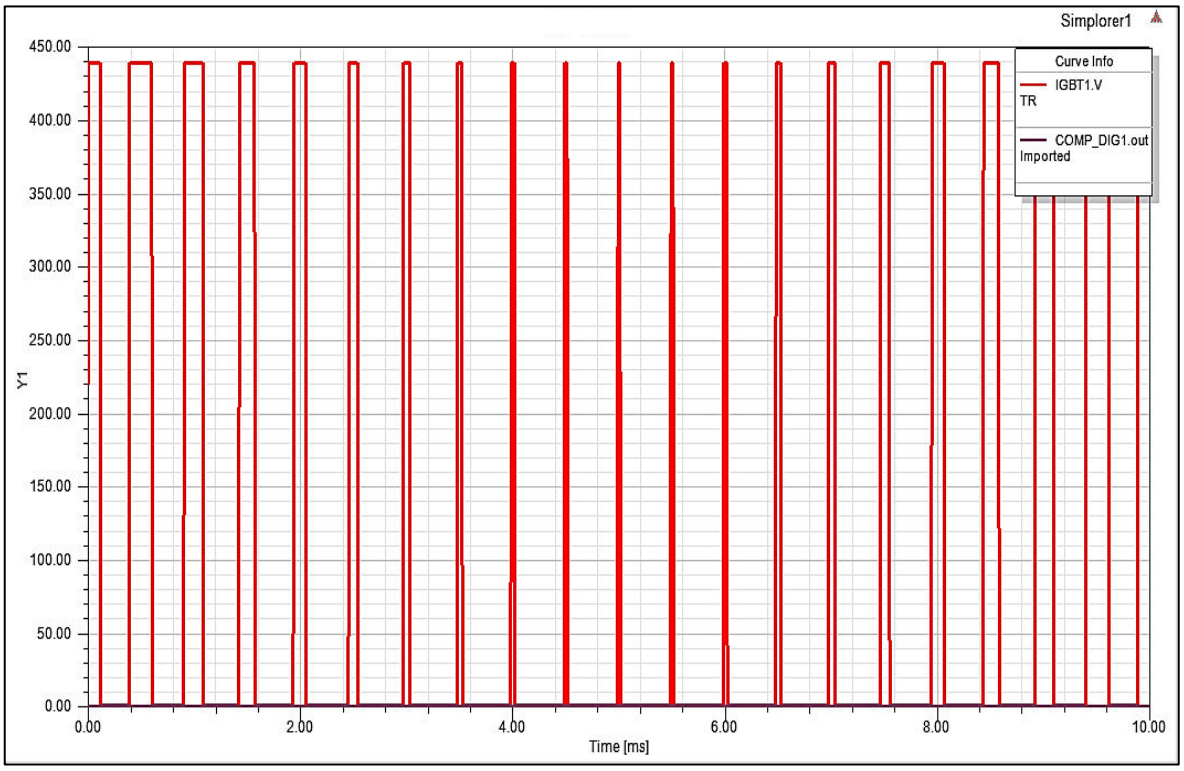

Fig. 4.7 IGBT1 and COMP1 switching

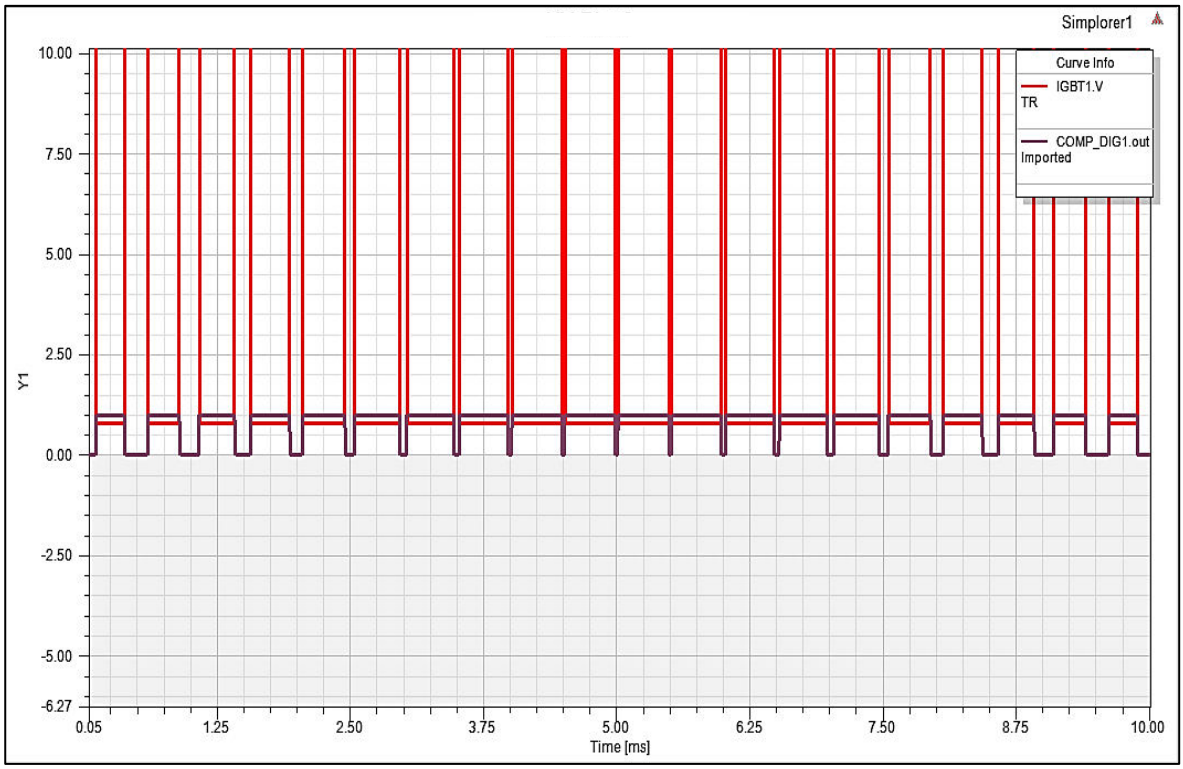

Fig. 4.8 Extended view of IGBT1 and COMP1 switching pattern

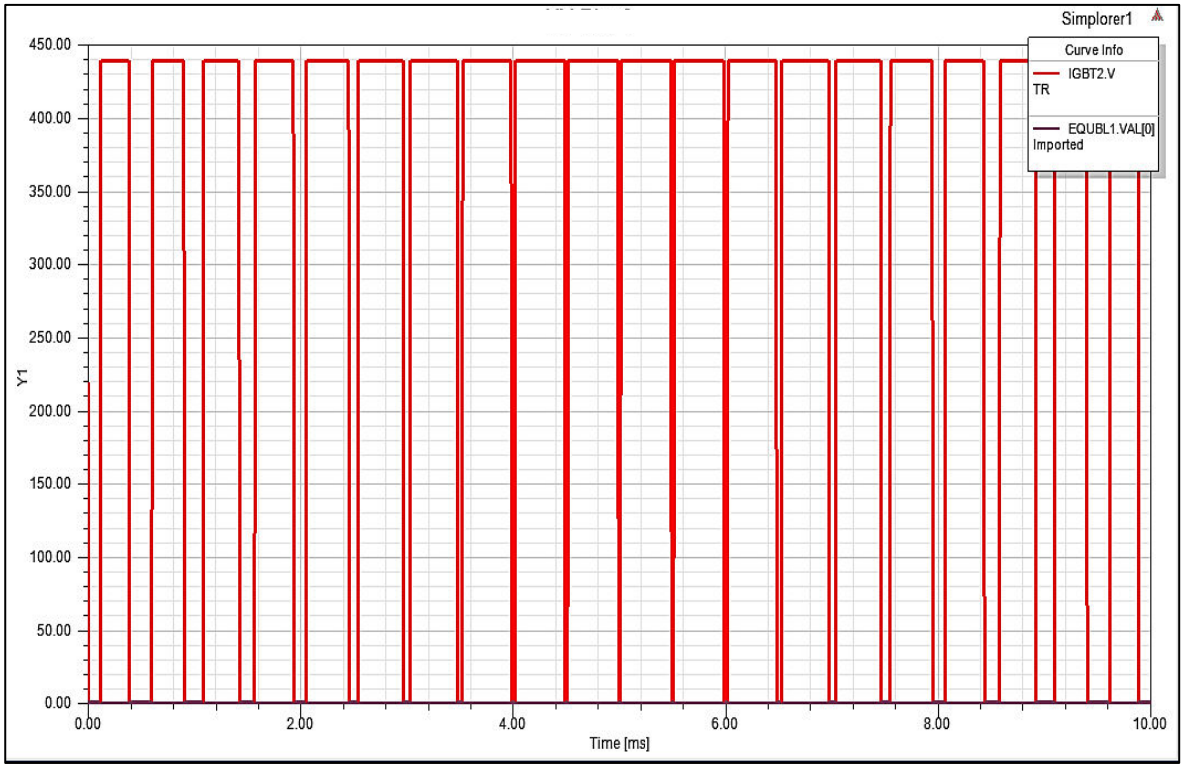

Fig. 4.9 IGBT2 and COMP2 switching

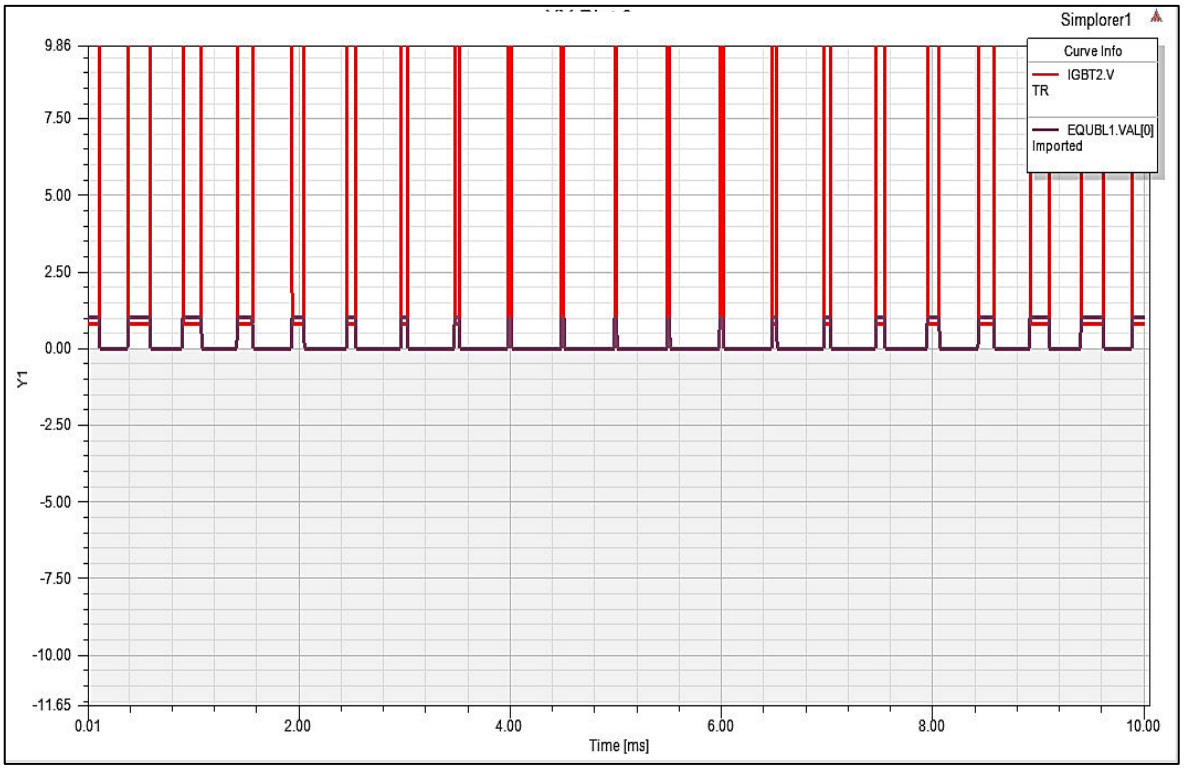

Fig. 4.10 Extended view of IGBT2 and COMP2 switching pattern

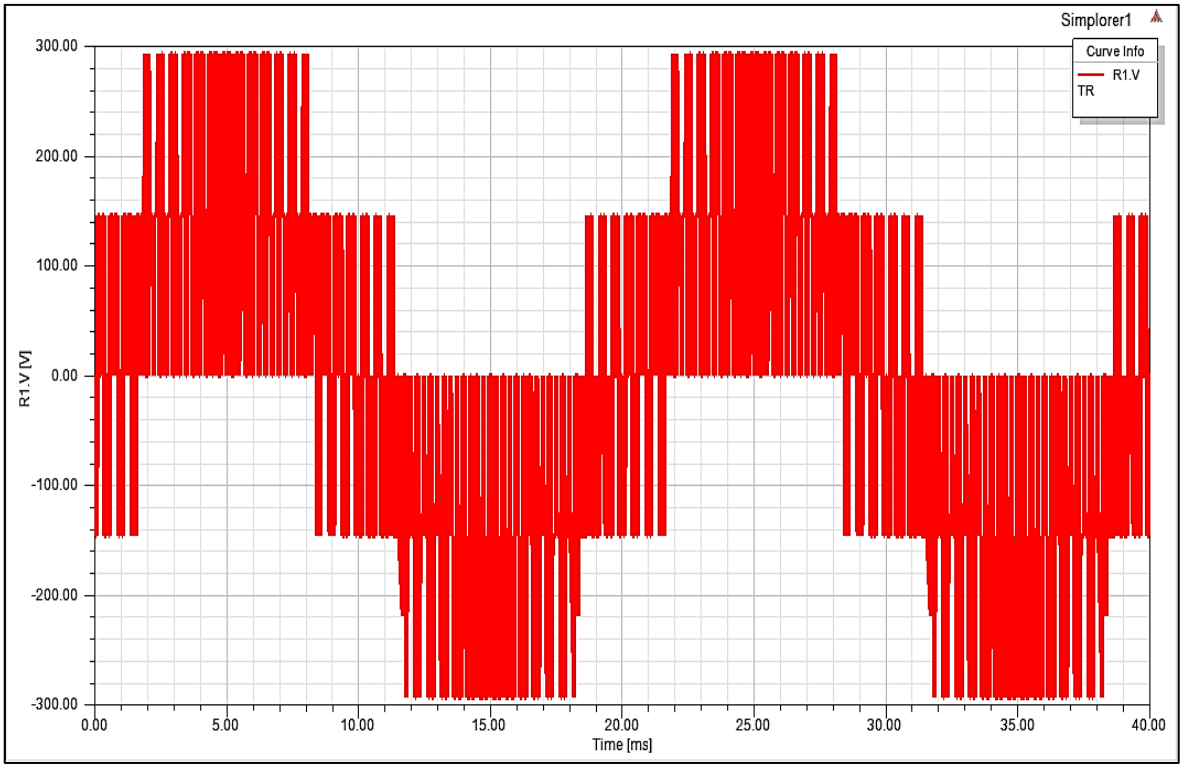

Fig. 4.11 Phase a line to neutral voltage

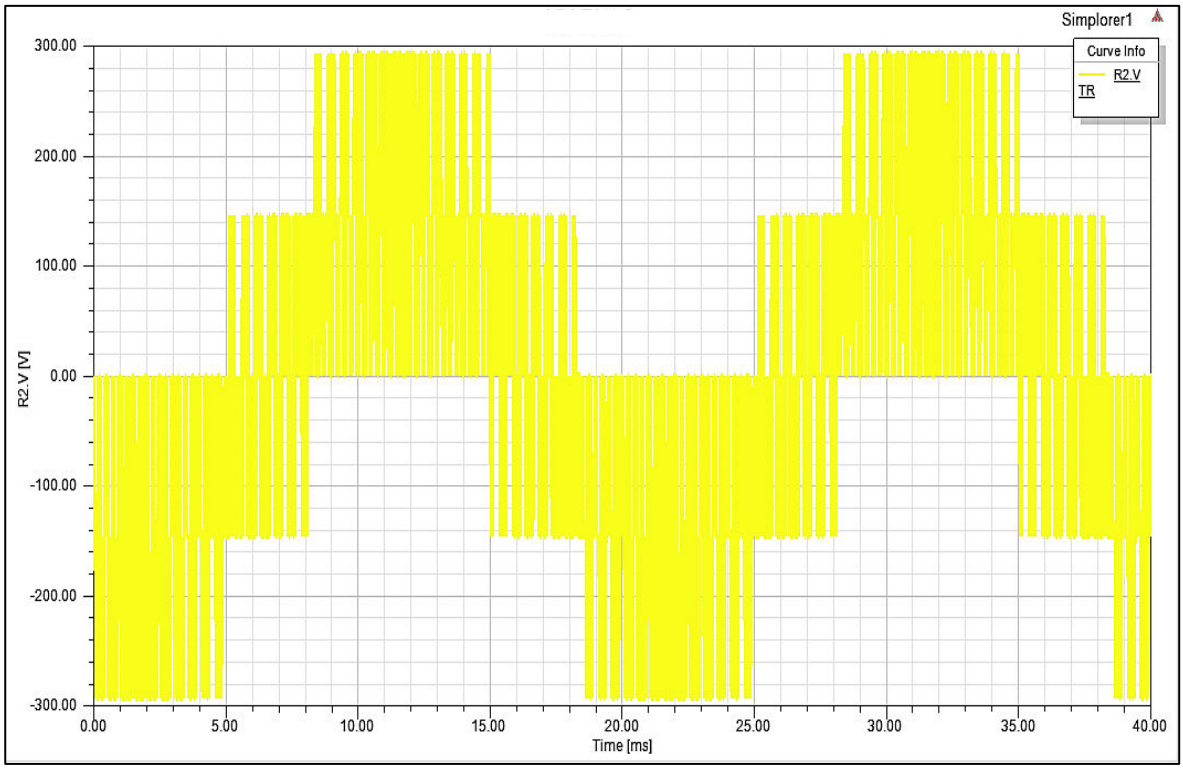

Fig. 4.12 Phase b line to neutral voltage

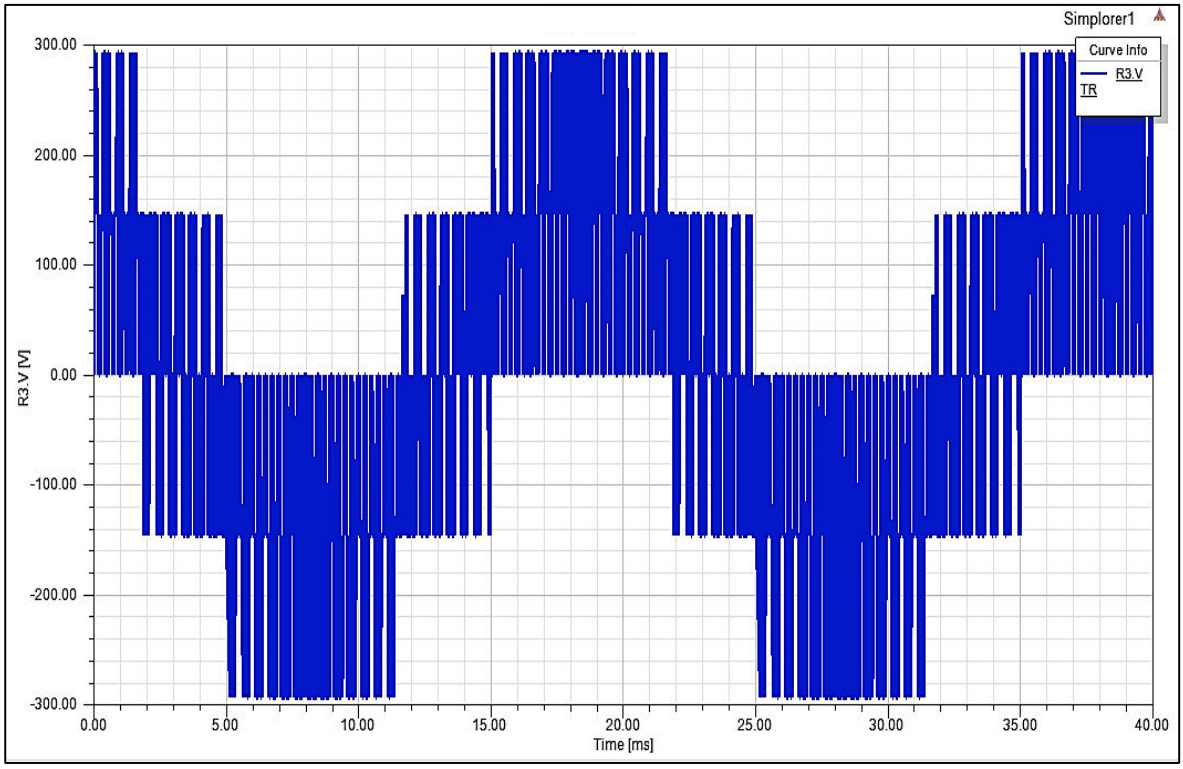

Fig.4.13 Phase c line to neutral voltage

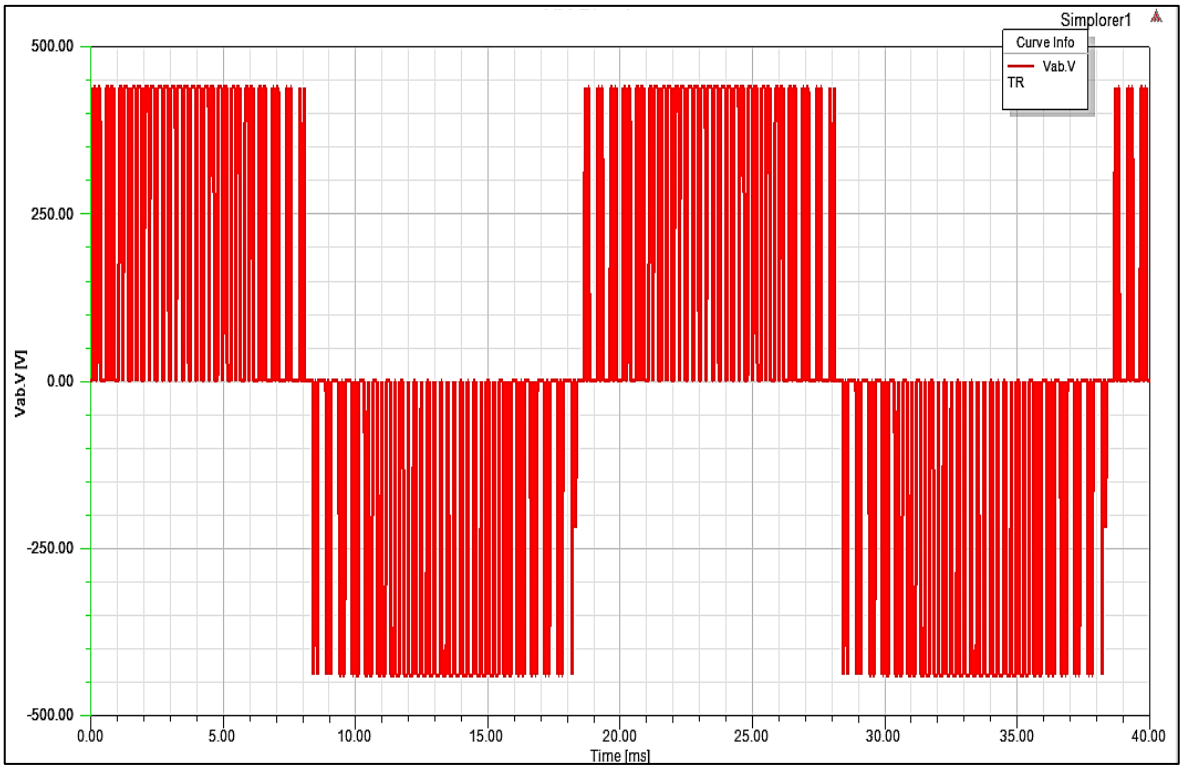

Fig. 4.14 Phase a-b line to line voltage of VSI

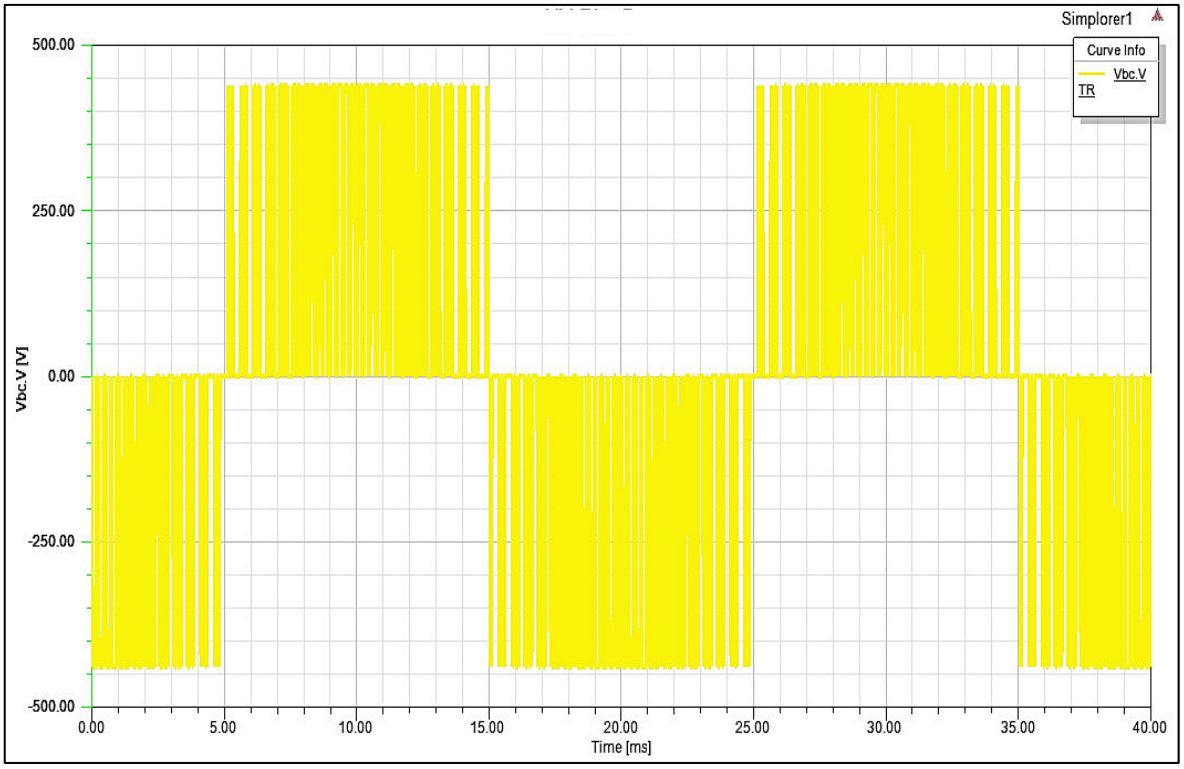

Fig. 4.15 Phase b-c line to line voltage of VSI

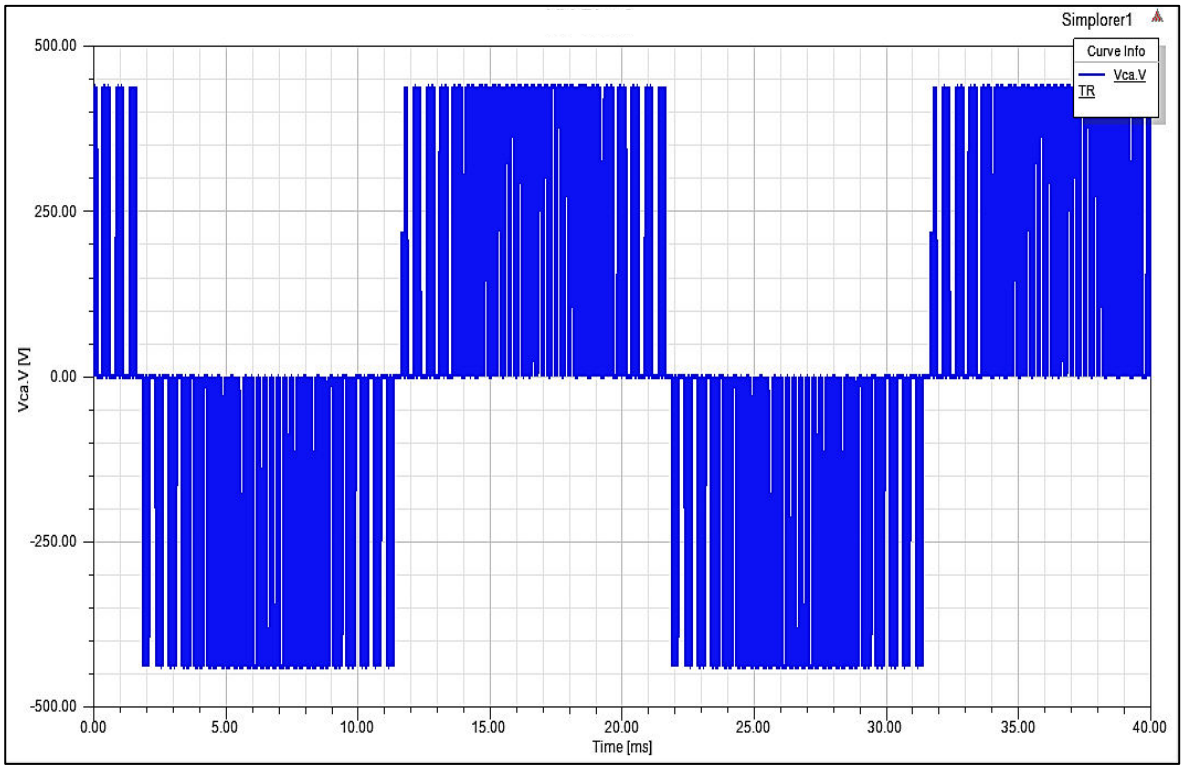

Fig. 4.16 Phase c-a line to line voltage of VSI

Observations:

The SPWM controlled VSI circuit is designed in the Simplorer design tool for the carrier frequency equal to 2 kHz. Each leg of the 3-ϕ inverter comprises two parallel connected power diode and IGBT which are joined to each other in series. The upper half switch i.e. IGBT1 is supplied with gate pulses from the comparatar (COMP1) for the instants when sinusoidal modulated signal has high magnitude than the triangular carrier signal. The reverse logic of the aforementioned technique is supplied for the gate pulses of the lower half switch i.e. IGBT2. The switching patterns of the comparator and IGBT switches of first leg are as shown in figures 4.7 to 4.10. The same switching patterns are observed for the other two legs of the inverter. The only difference remains for each leg is that the carrier signals are displaced by 120 ° from each other. The 3-ϕ output responses of the inverter for the phase and line to line voltages are as shown in the figures 4.11 to 4.16.

4.1.4 Open-loop induction machine drive results

The machine model and the drive circuit are integrated by co-simulating both the Maxwell and Simplorer tools and the drive responses are obtained as can be seen in the figures 4.17 to 4.27.

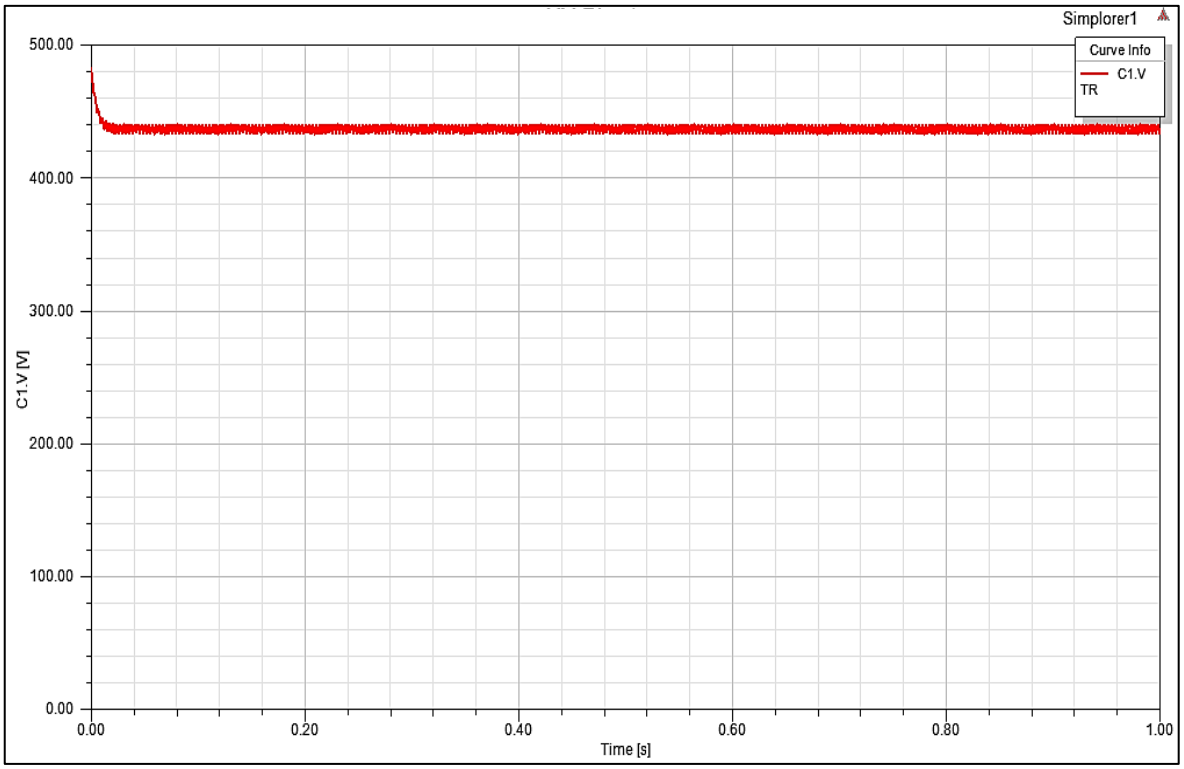

Fig. 4.17 DC link voltage of the drive system

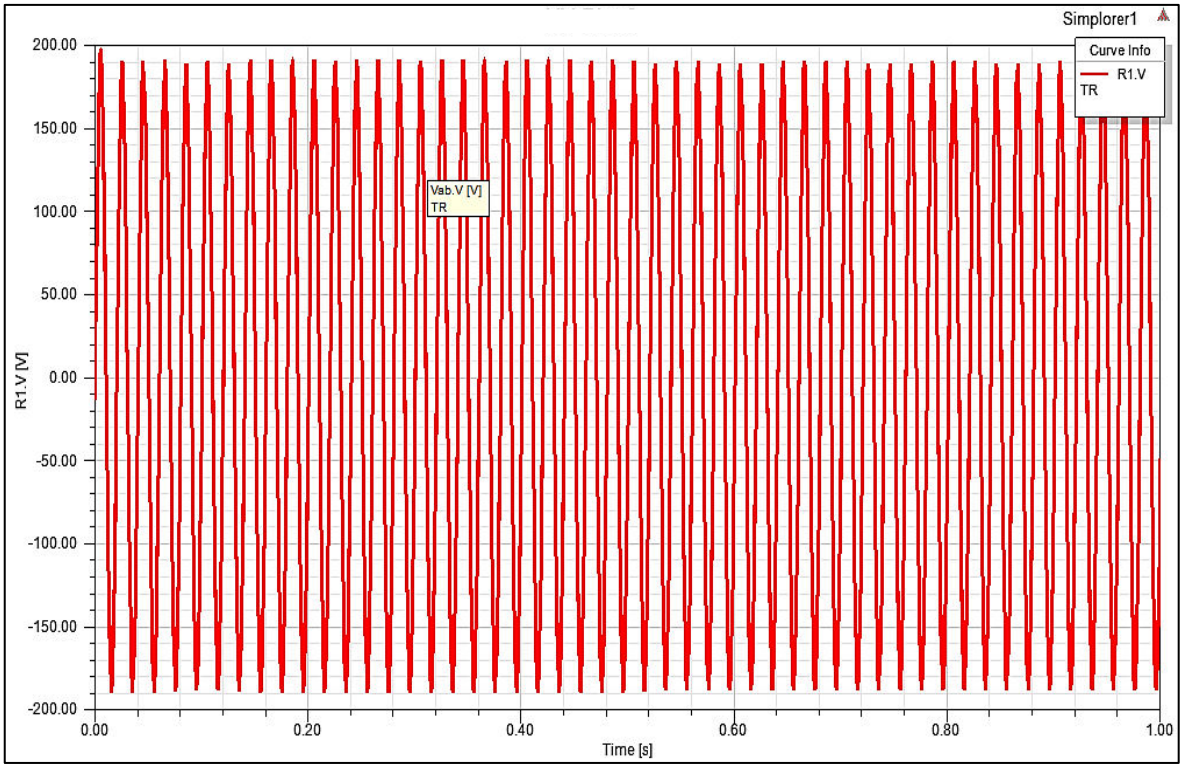

Fig. 4.18 Phase a voltage of the inverter

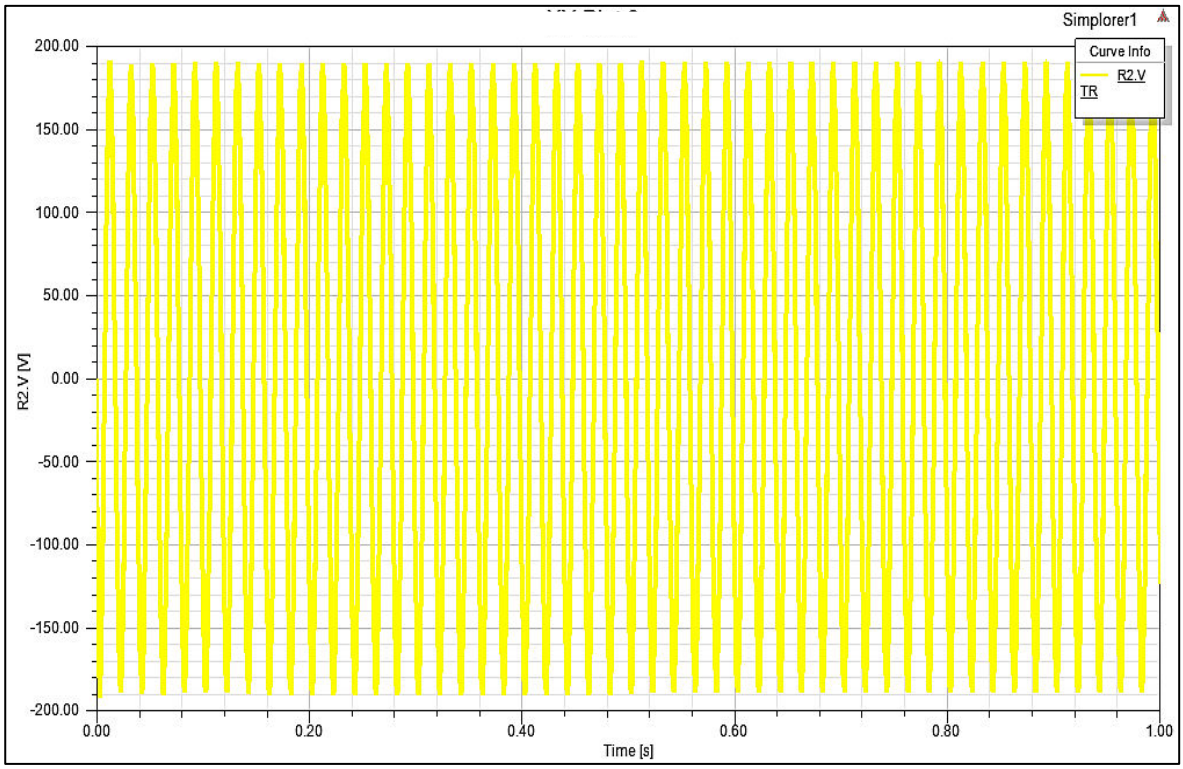

Fig. 4.19 Phase b voltage of the inverter

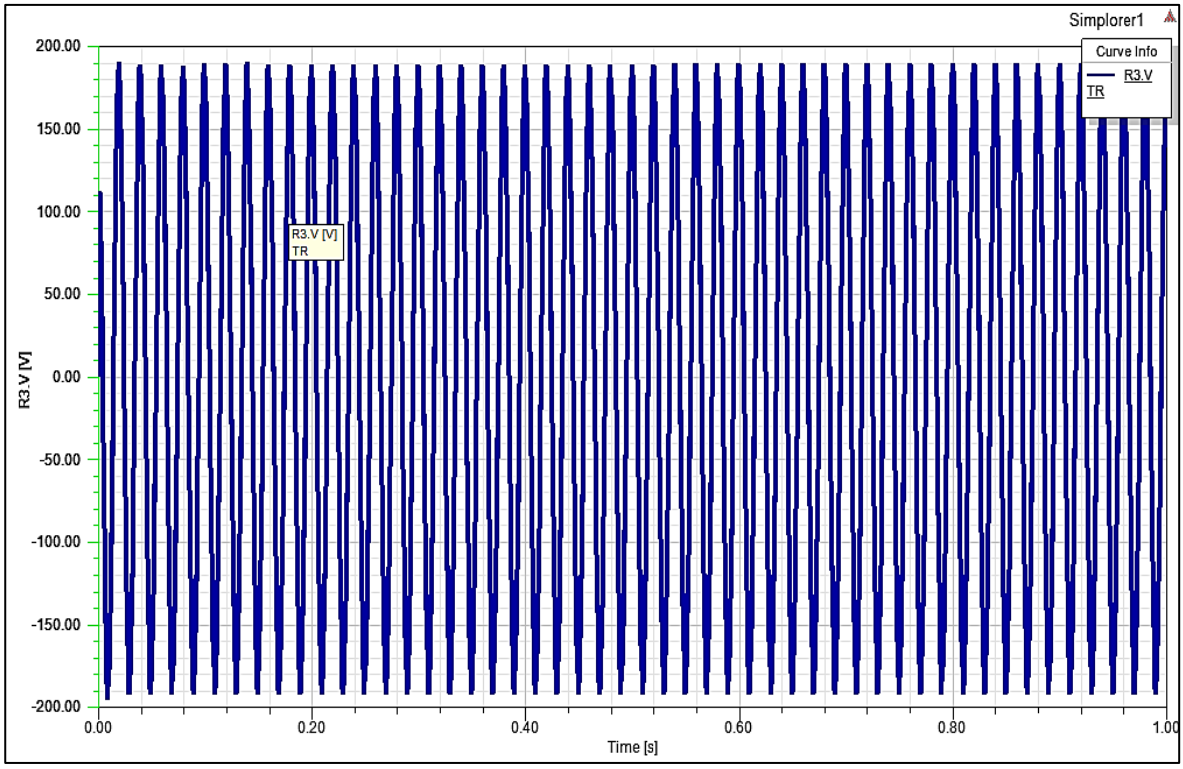

Fig. 4.20 Phase c voltage of the inverter

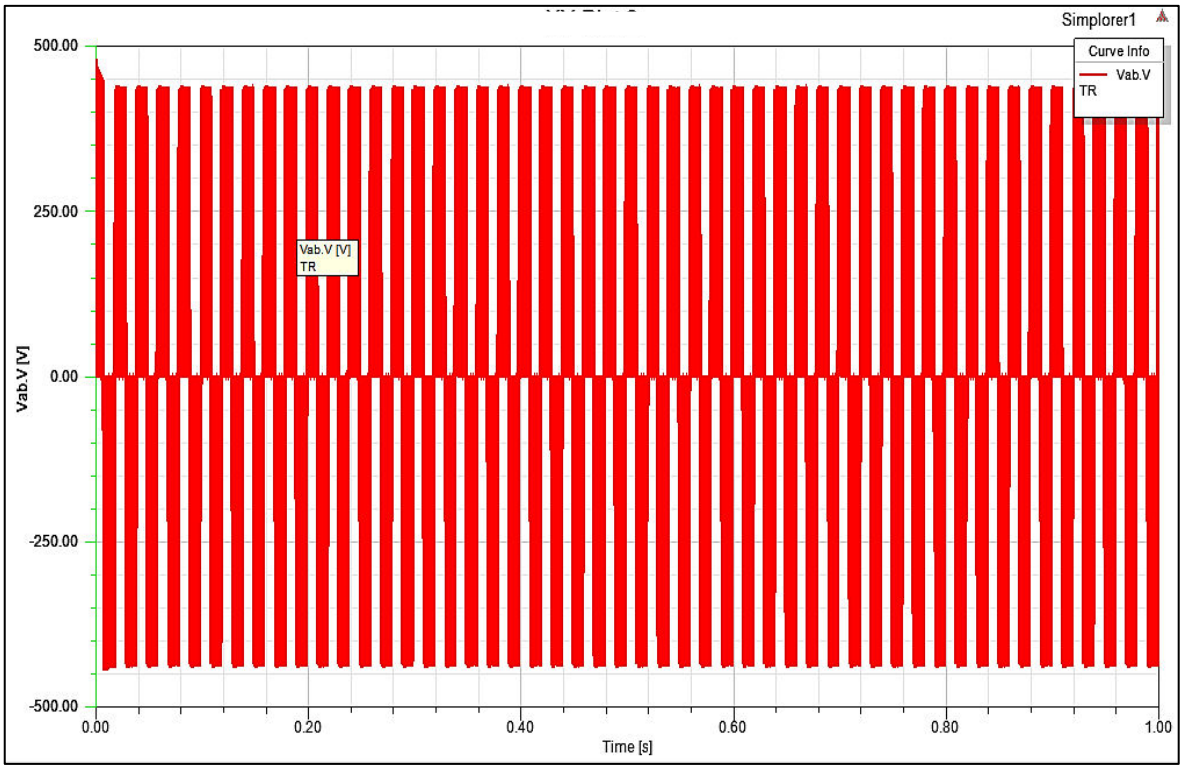

Fig. 4.21 Phase a-b line to line voltage of the inverter

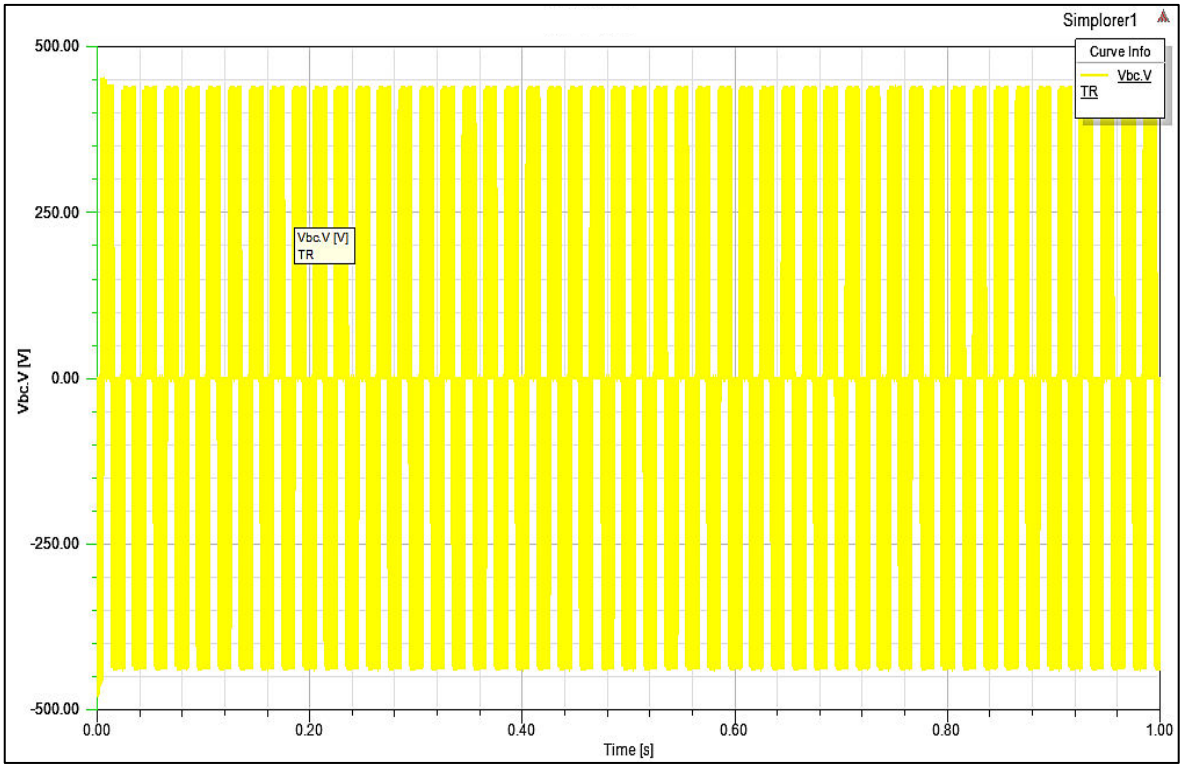

Fig. 4.22 Phase b-c line to line voltage of the inverter

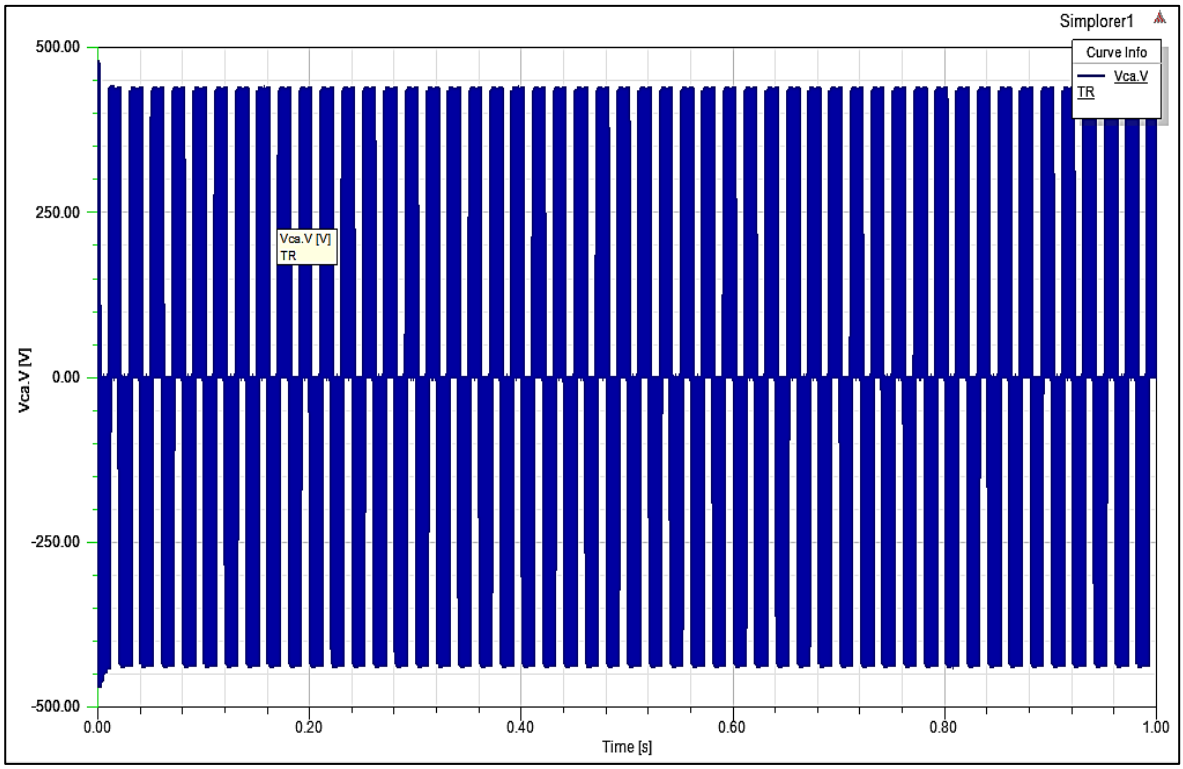

Fig. 4.23 Phase c-a line to line voltage of the inverter

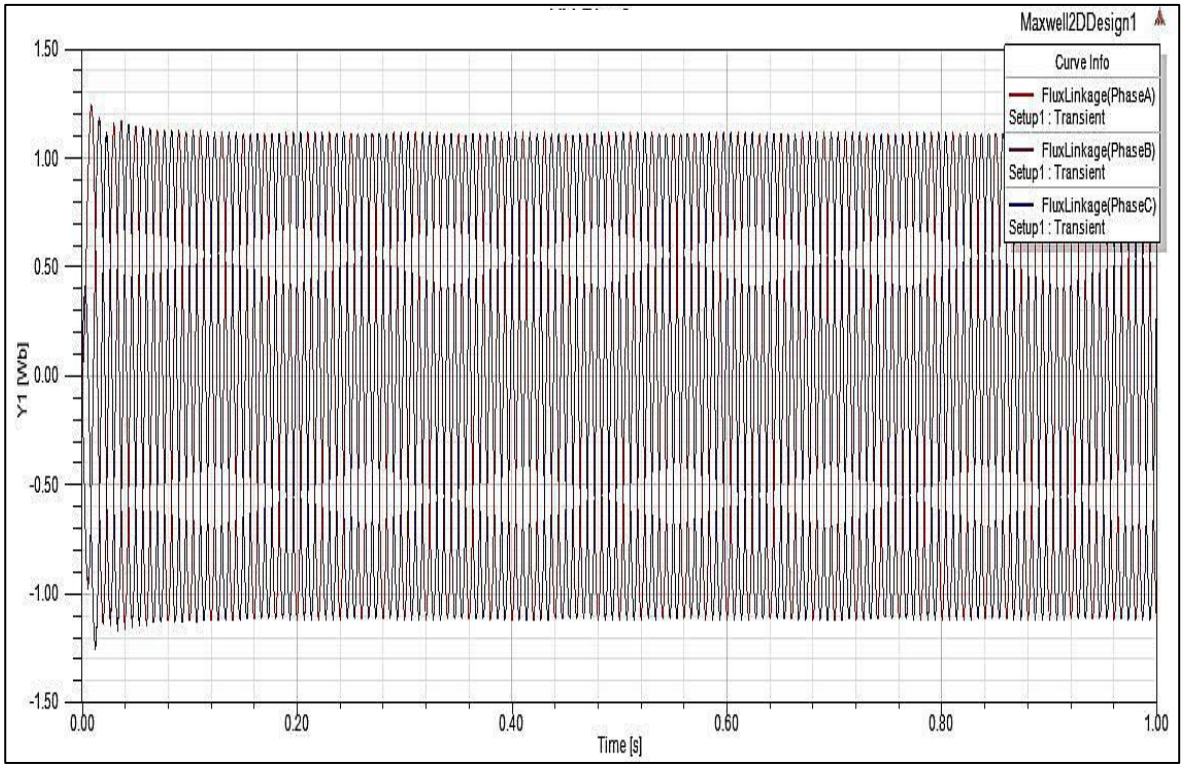

Fig. 4.24 Flux linkages in IM

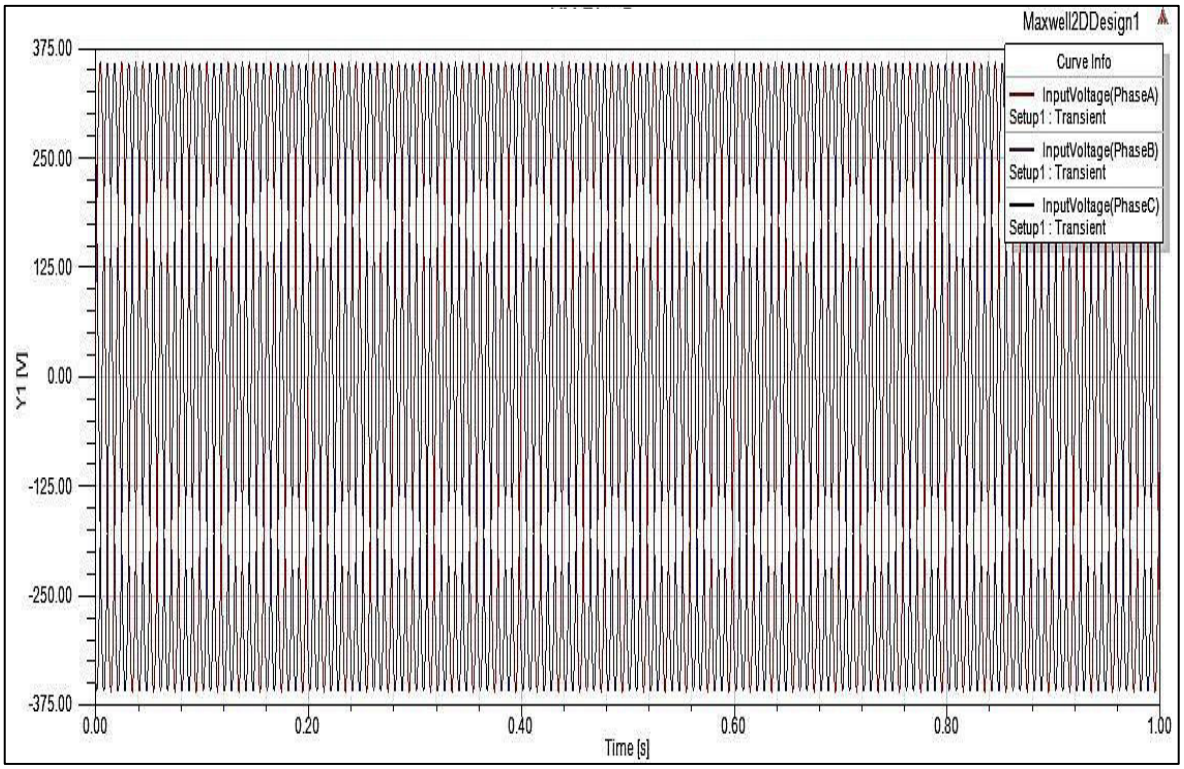

Fig. 4.25 Input voltages at the stator windings

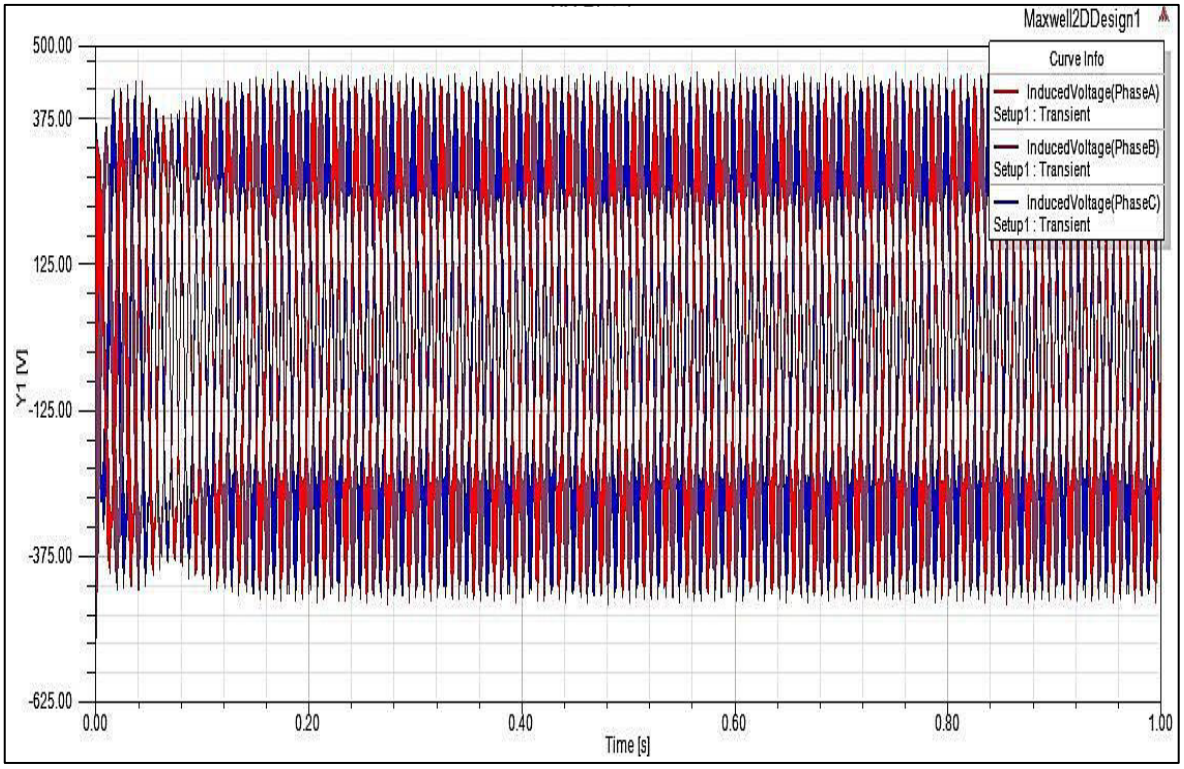

Fig. 4.26 Induced voltages in rotor conductors

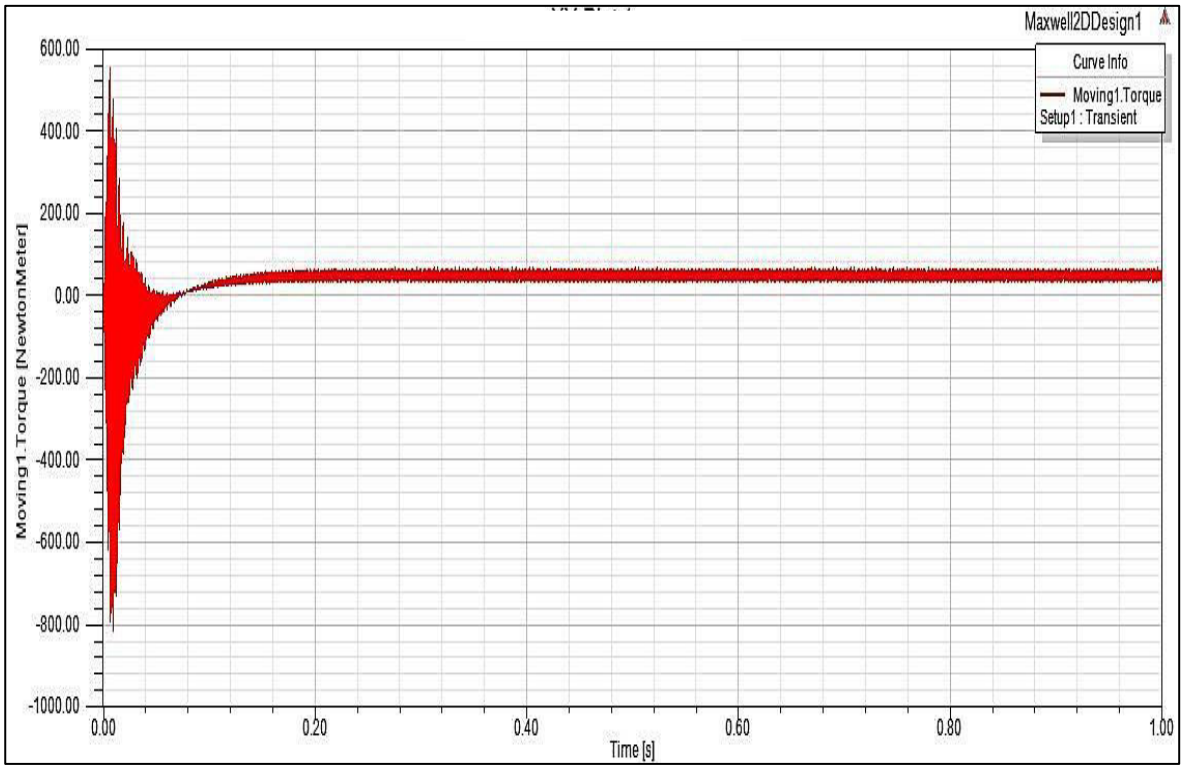

Fig. 4.27 Generated torque in IM

Observations:

The 2D model of the IM in Maxwell 2D design tool and PWM-VSI circuit in Simplorer design tool are integrated by co-simulating both the tools. Thus, the investigation of the performance characteristics of the complete open-loop drive system is done. The input response of the rectifier circuit is as shown in figure 4.17. The dc link voltage of the rectifier circuit provides a slightly pulsating dc supply of 440 V at the input terminals of the inverter however, the pulsation is very small ranging from the 339.25 V to 440 V. This dc voltage is fed to the inverter terminals which converts it into 3-ϕ ac supply as shown in the figures 4.18 to 4.23. This creates the sinusoidal flux linkages in the motor as shown in figure 4.24 having the maximum flux value of 1.2 Wb. The input voltages supplied to the stator windings are as shown in the figure 4.25 attaining the peak values of approximately 380 V. Due to the induction phenomenon, the voltages are induced in the rotor copper bars as shown in figure 4.26. The generated torque in the motor shows the transient behaviour for the 0.04 time period and attains the overshoot and under shoot values of 600 N-m and 800 N-m respectively at 0.001 sec of time instant. This torque characteristic finally becomes steady after this and acquires a pulsating nature ranging between the values 40 N-m to 50 N-m for the no-load operation.

4.1.5 PWM-VSI results in open-circuit fault condition

The proposed study has been done for the fault analysis of the inverter circuit power switches faults. Two cases of IGBT faults i.e. open-circuit and short-circuit of the switch have been considered in the present work. For this, the faults are incurred in the upper IGBT switch of the third leg in inverter by connecting a switch in parallel and series for short-circuit and open-circuit fault operation. Initially the normal operation of the drive circuit is considered till t= 0.5 sec then at this instant the switch in series with IGBT is kept open to incur the open-circuit fault in the inverter. The output responses of the inverter input and output terminals i.e. dc link voltage, phase voltages and phase currents are analysed. Although, the dc link voltage undergoes the minor changes due to the occurrence of the open-circuit fault however, the phase voltages and currents show the significant changes. The voltages of healthy phases of the inverter dip by small values during the fault operation while the positive half of the faulty phase voltage gets clipped off as the fault occurs.

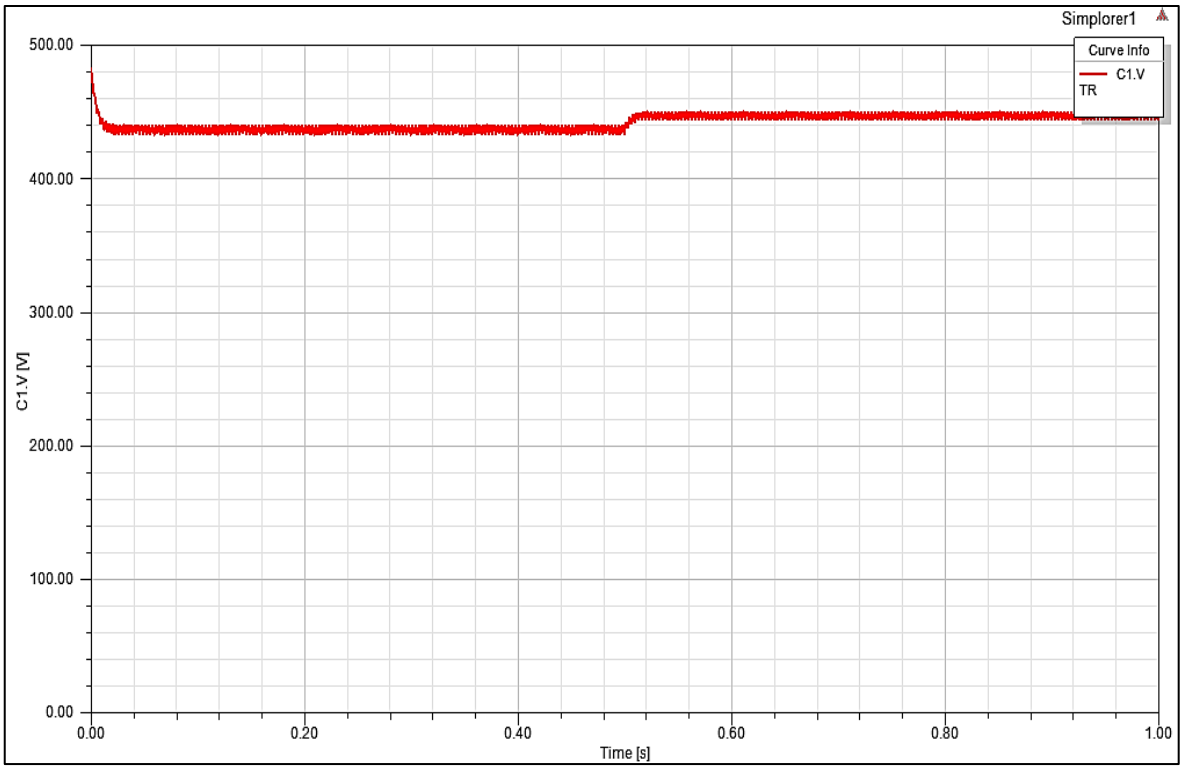

Fig. 4.28 DC link voltage under open-circuit fault operation

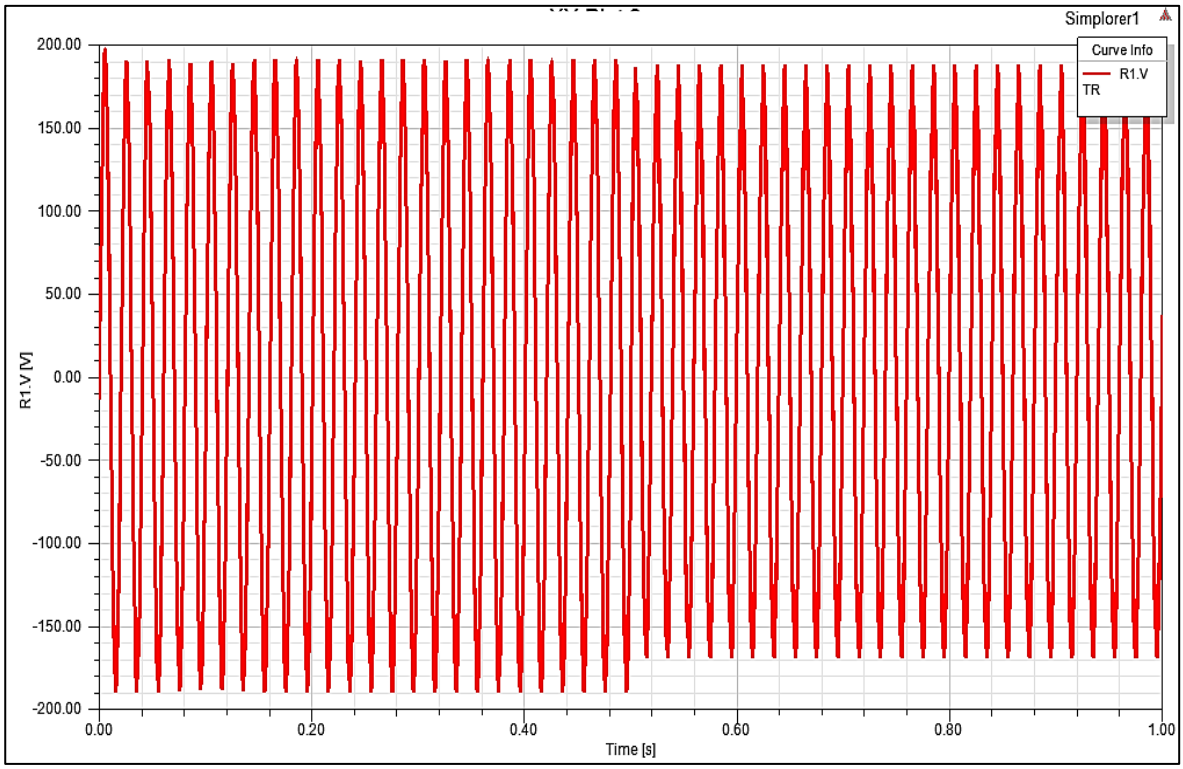

Fig. 4.29 Phase a voltage under open-circuit fault operation

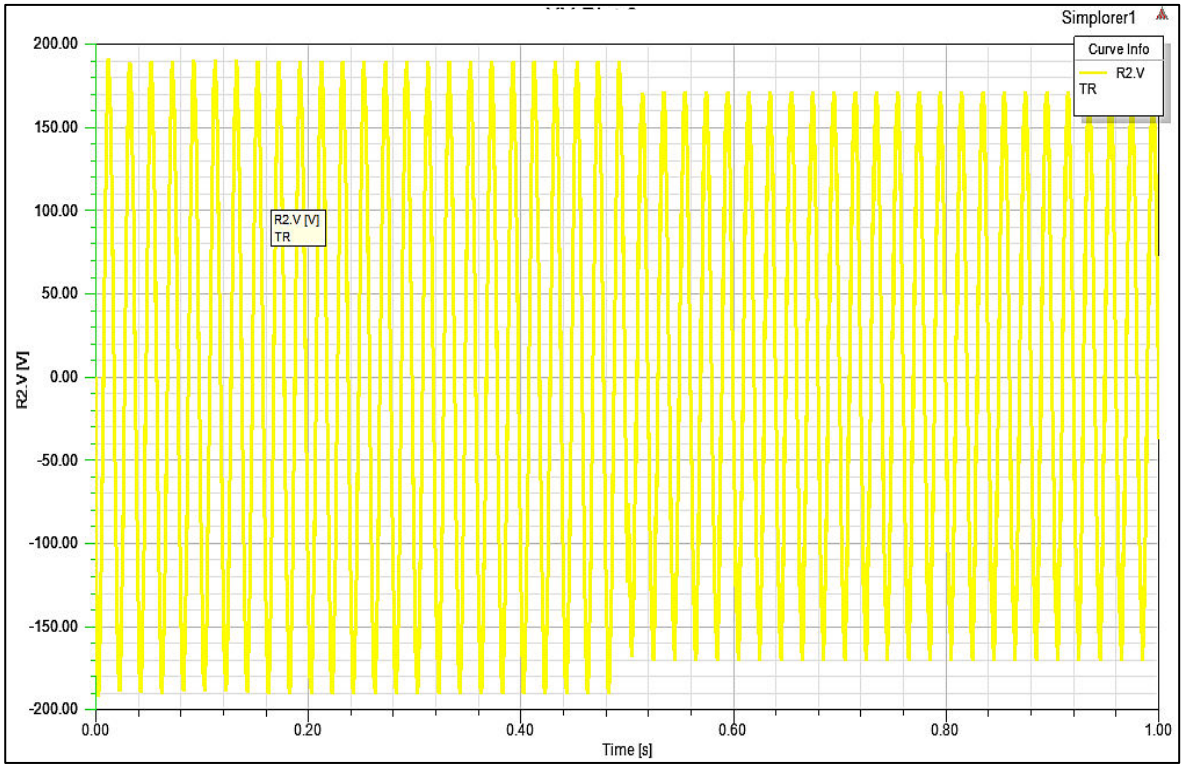

Fig. 4.30 Phase b voltage under open-circuit fault operation

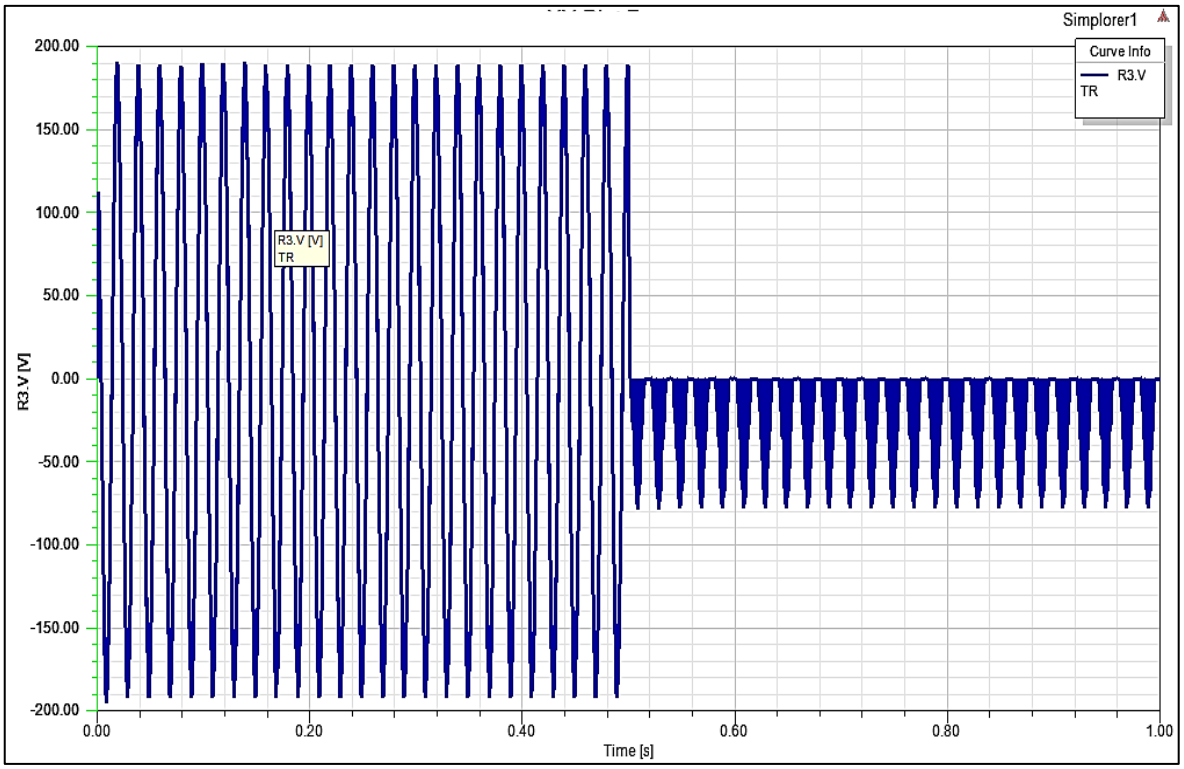

Fig. 4.31 Phase c voltage under open-circuit fault operation

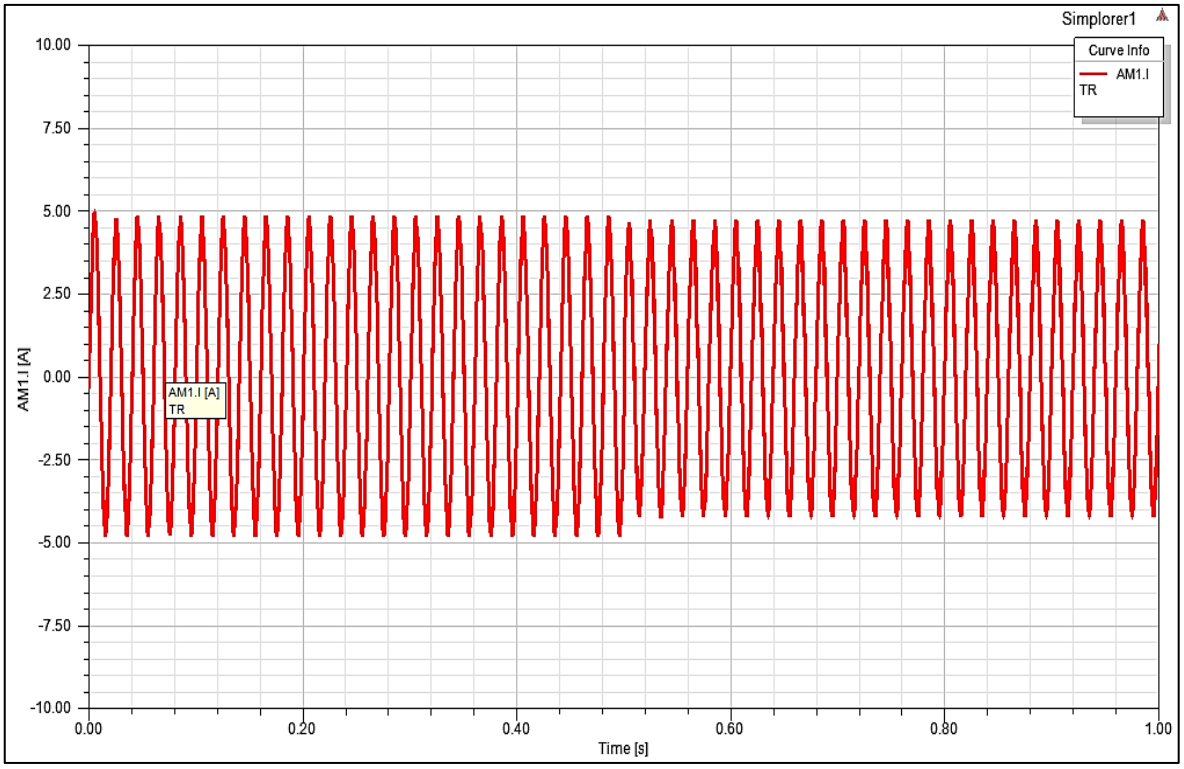

Fig. 4.32 Phase a current under open-circuit fault operation

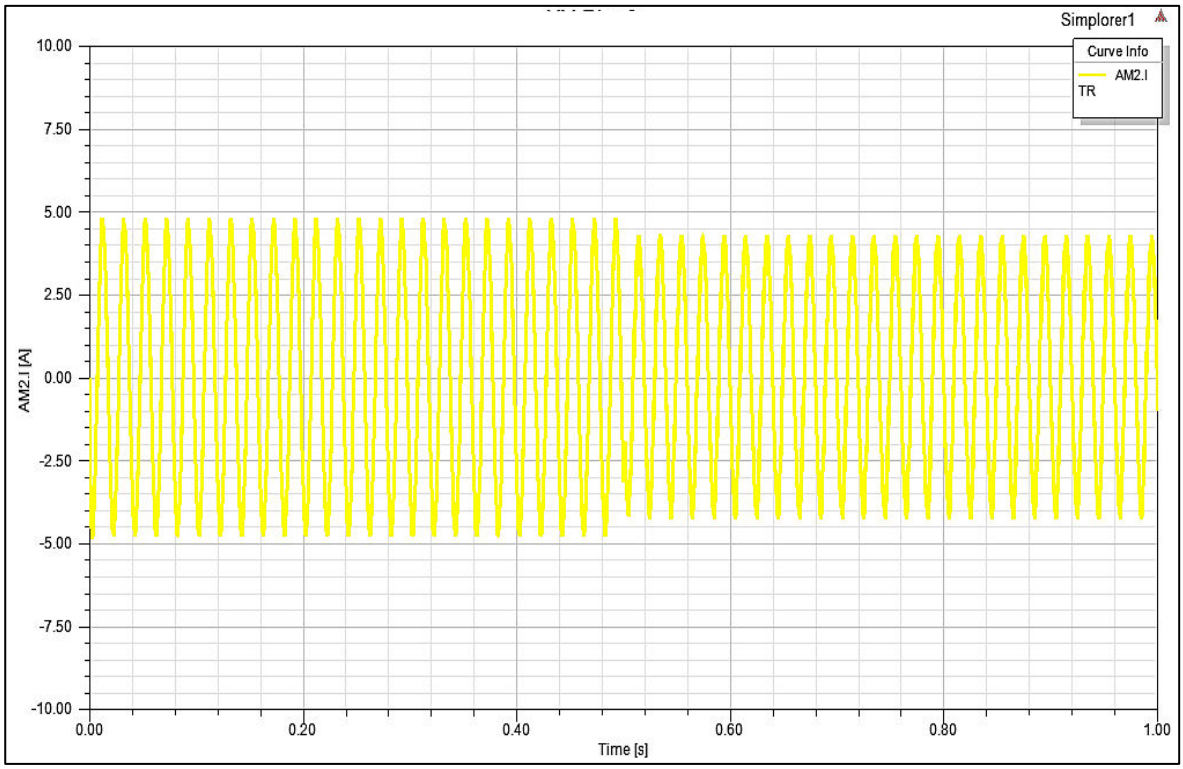

Fig. 4.33 Phase b current under open-circuit fault operation

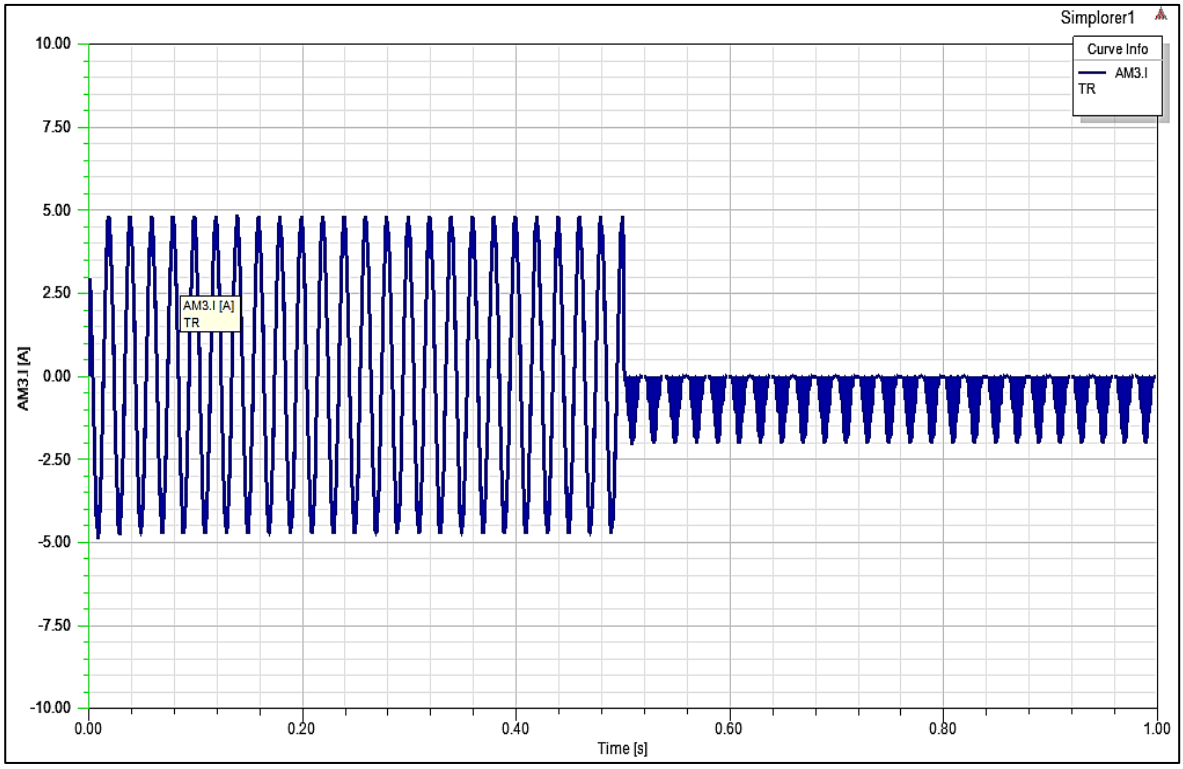

Fig. 4.34 Phase c current under open-circuit fault operation

Observations:

The following tables demonstrate the comparable changes in inverter parameters i.e. dc link voltage, phase voltages and currents under normal and open-circuit fault operation for the simulation time of 1 sec.

Table 4.5 Performance analysis at normal operation

Parameter values under normal operation		
Parameters	Maximum value	Minimum value
DC link voltage	440 V	399.25 V
Phase a voltage	185 V	- 185 V
Phase b voltage	185 V	- 185 V
Phase c voltage	185 V	- 185 V
Phase a current	4.55 A	- 4.55 A
Phase b current	4.55 A	- 4.55 A
Phase c current	4.55 A	- 4.55 A

Table 4.6 Performance analysis at open-circuit fault operation

Parameter values under open-circuit fault operation		
Parameters	Maximum value	Minimum value
DC link voltage	450 V	449.25 V
Phase a voltage	180 V	- 170 V
Phase b voltage	170 V	- 170 V
Phase c voltage	0 V	- 80 V
Phase a current	4.55 A	- 4.25 A
Phase b current	4.25 A	- 4.25 A
Phase c current	0 A	- 2 A

4.1.6 PWM-VSI results in short-circuit fault condition

After the open-circuit fault analysis, the short-circuit fault is incurred in the inverter by closing the switch which is connected in parallel across the first IGBT of the third leg of inverter. At t= 0.5 sec the switch gets closed thus the whole assembly of the power diode and IGBT gets bypassed i.e. the current instead of flowing through the IGBT gets a least resistive path across the switch. After the occurrence of fault, the inverter parameters i.e. dc link voltage, phase voltages and currents are analysed. Unlike the open-circuit fault case, the dc link voltage here shows significant changes in its characteristics i.e. pulsate between the voltage values of 360 V and 165 V. The healthy phase voltages also have immense impacts on its characteristics due to the fault in the unhealthy phase. Phase 'a' and 'b' voltages though remains sinusoidal in nature however their positive half magnitudes reduce by almost by 50%. The faulty phase voltage shifts upward with the maximum and minimum values of 165 V and 30 V respectively. Similar changes are witnessed in the phase currents after the occurrence of short-circuit fault in inverter.

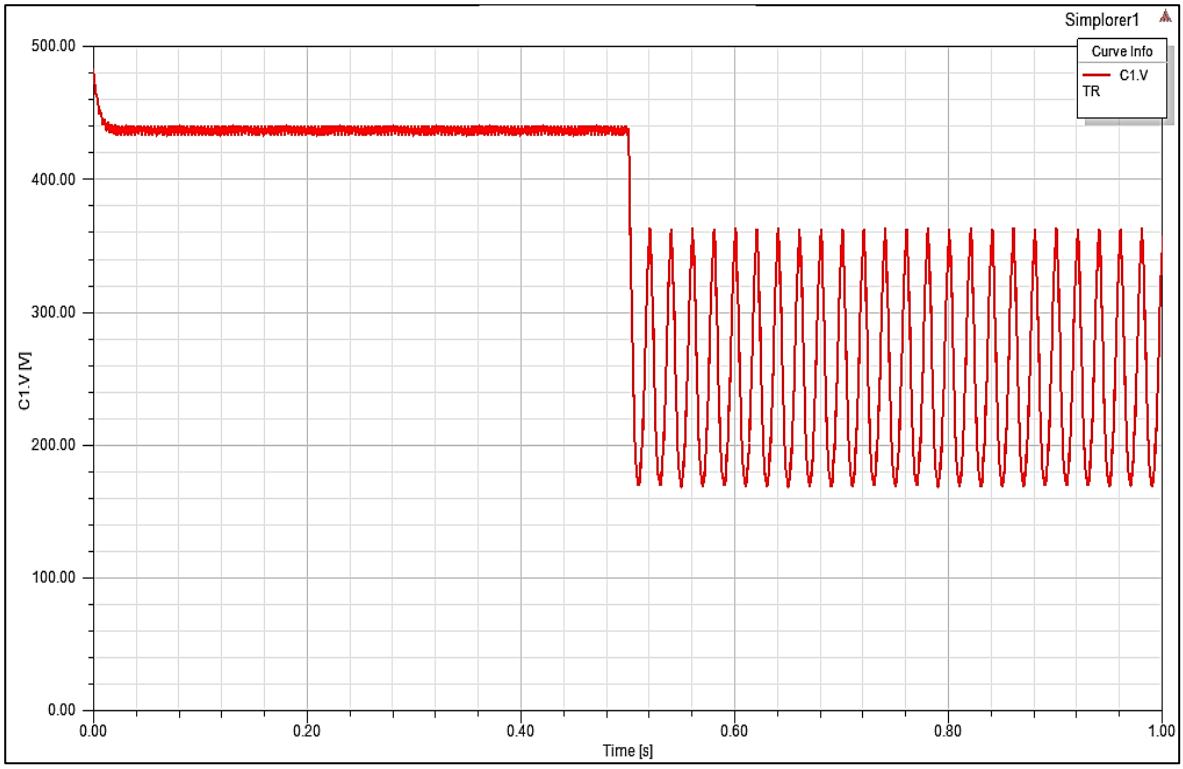

Fig. 4.35 DC link voltage under short-circuit fault operation

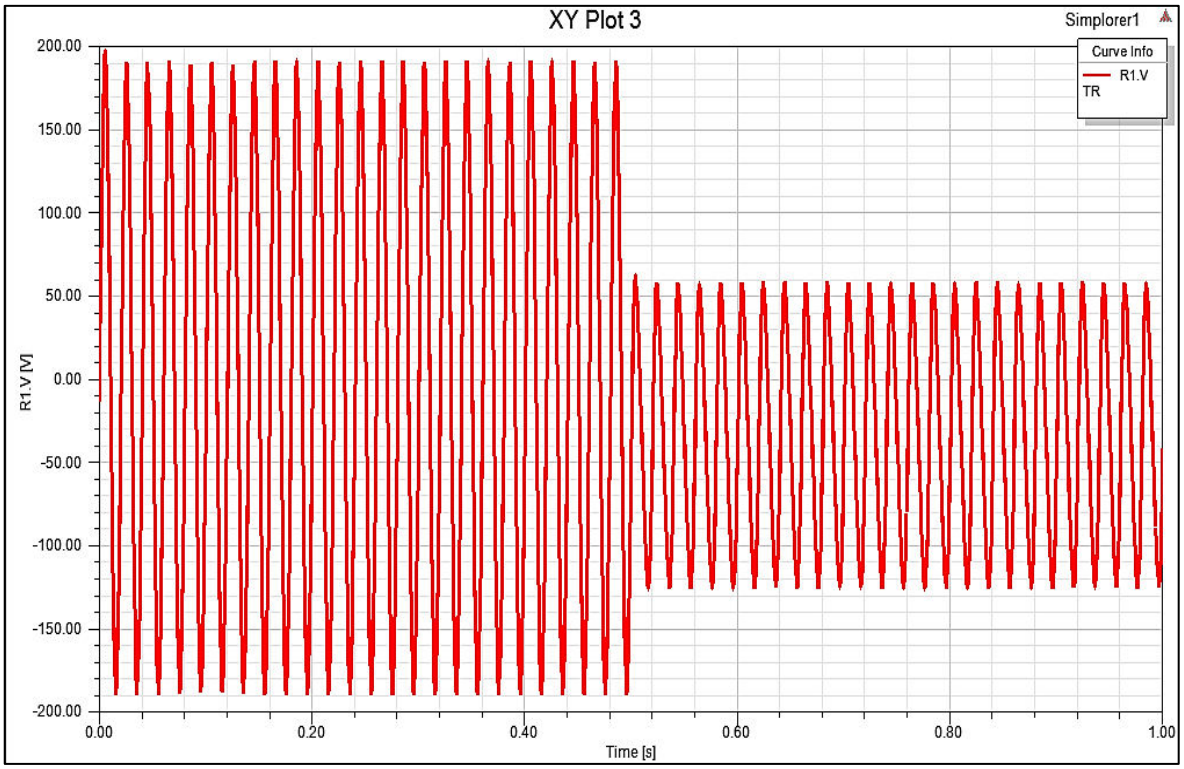

Fig. 4.36 Phase a voltage under short-circuit fault operation

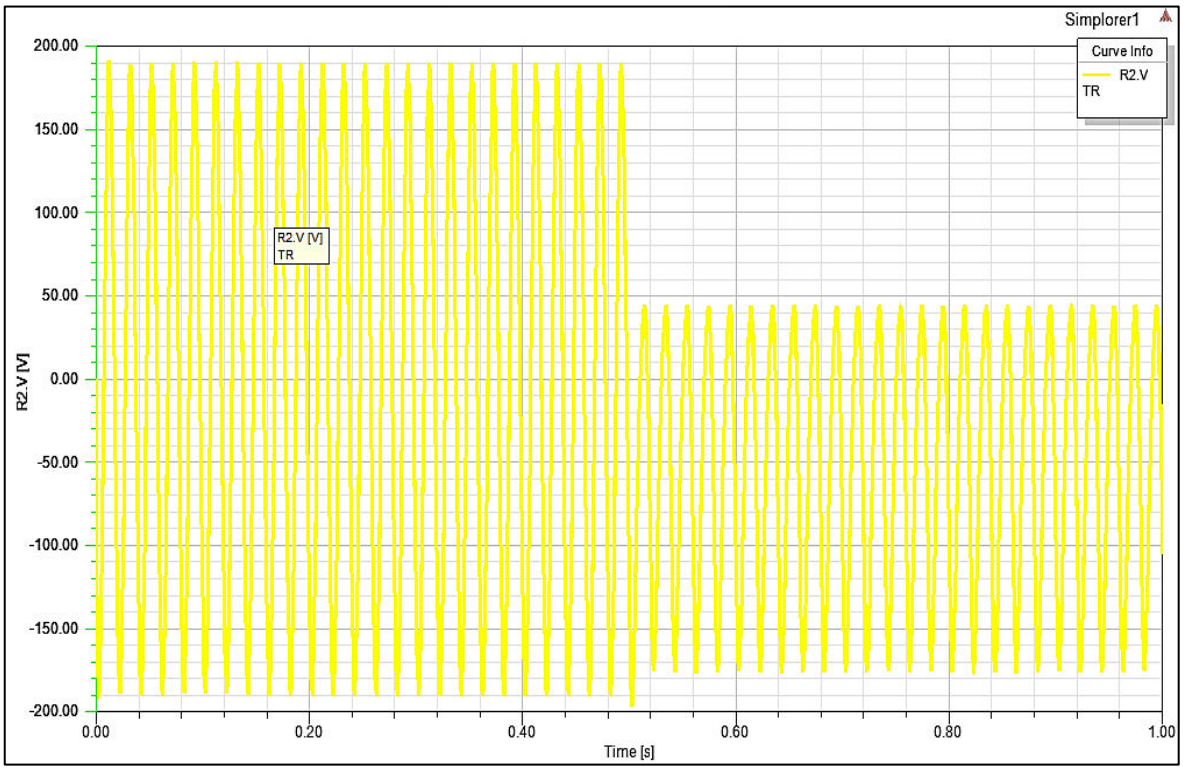

Fig. 4.37 Phase b voltage under short-circuit fault operation

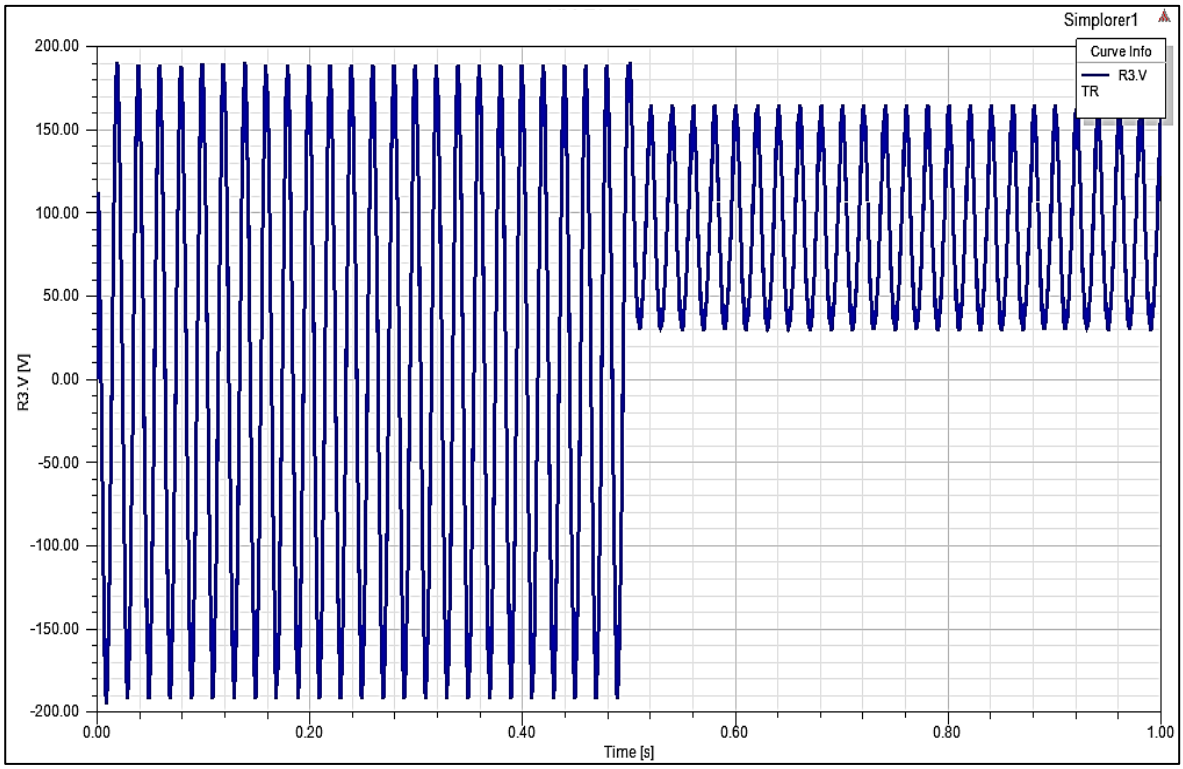

Fig. 4.38 Phase c voltage under short-circuit fault operation

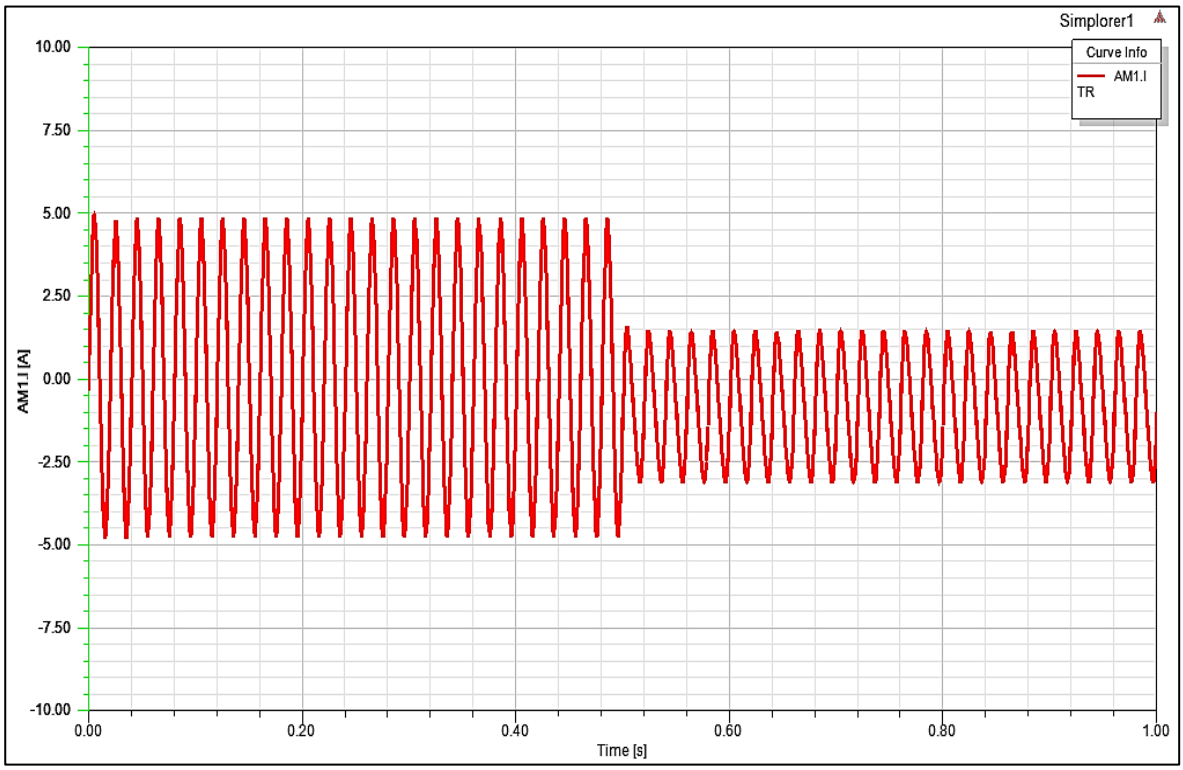

Fig. 4.39 Phase a current under short-circuit fault operation

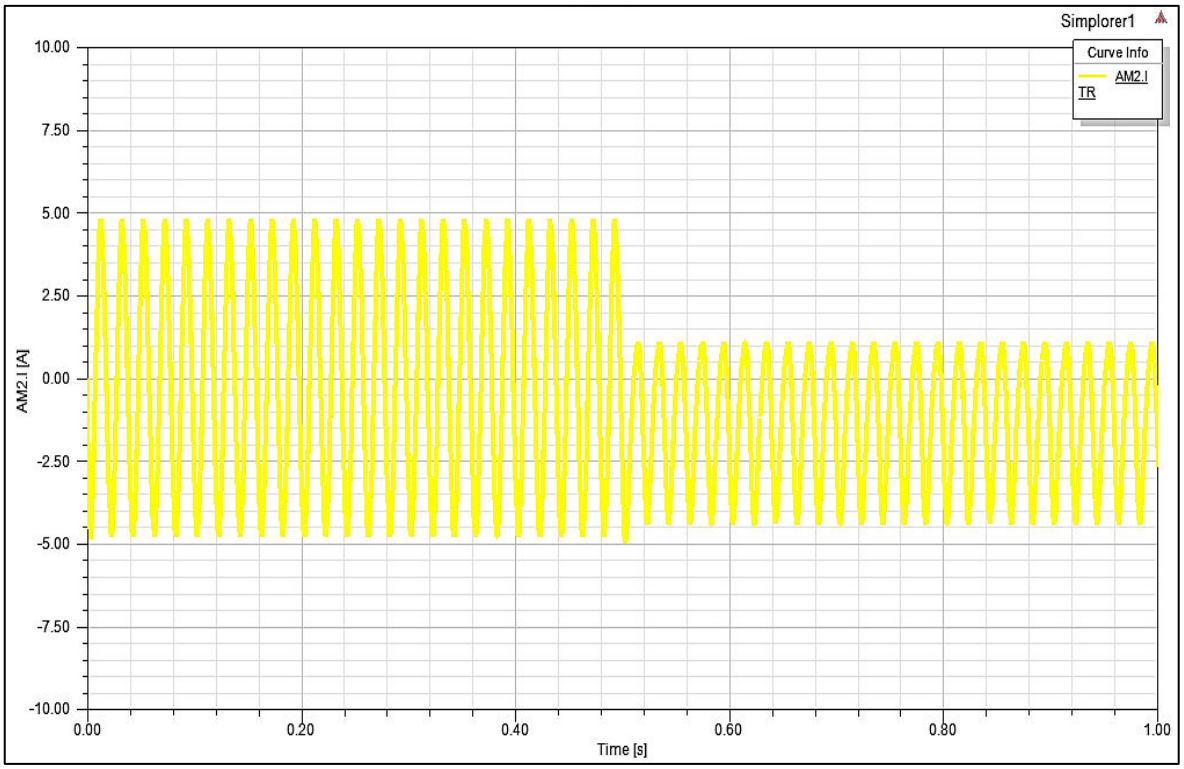

Fig. 4.40 Phase b current under short-circuit fault operation

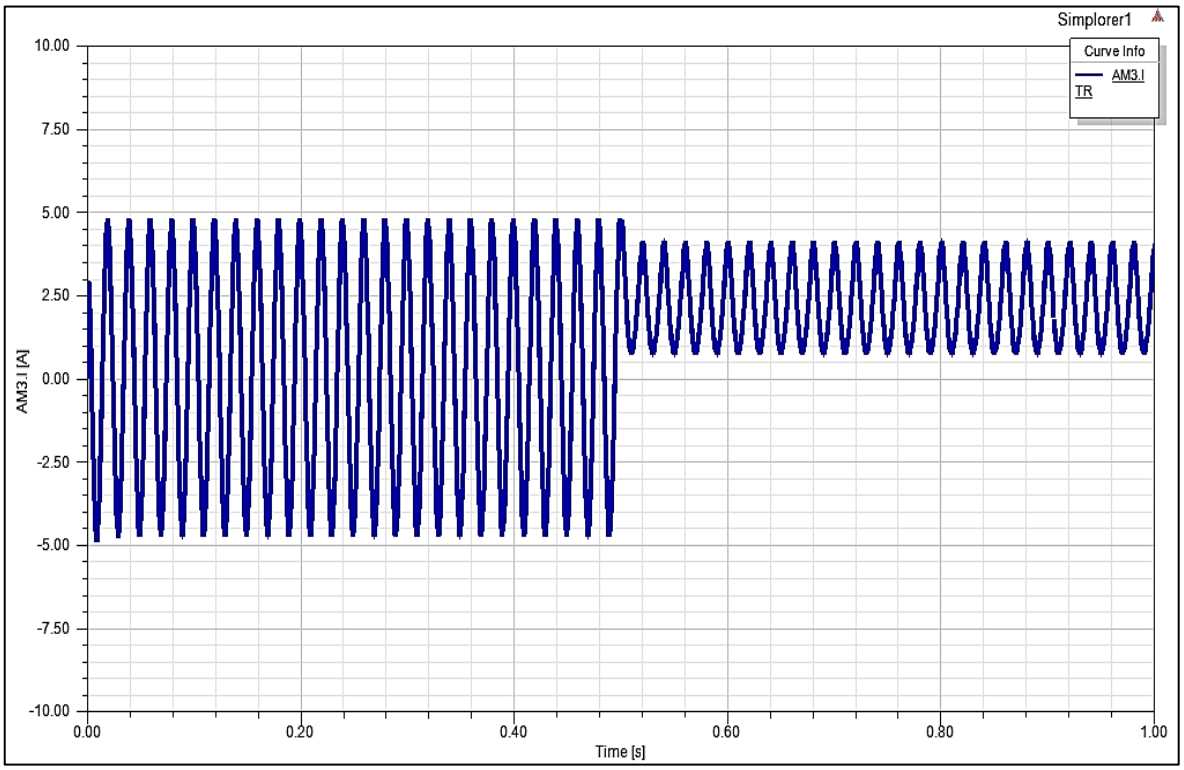

Fig. 4.41 Phase c current under short-circuit fault operation

Observations:

The following tables demonstrate the comparable changes in inverter parameters i.e. dc link voltage, phase voltages and currents under normal and short-circuit fault operation for the simulation time of 1 sec.

Table 4.7 Performance analysis at normal operation

Parameter values under normal operation		
Parameters	Maximum value	Minimum value
DC link voltage	440 V	399.25 V
Phase a voltage	185 V	- 185 V
Phase b voltage	185 V	- 185 V
Phase c voltage	185 V	- 185 V
Phase a current	4.55 A	- 4.55 A
Phase b current	4.55 A	- 4.55 A
Phase c current	4.55 A	- 4.55 A

Table 4.8 Performance analysis at short-circuit fault operation

Parameter values under short-circuit fault operation		
Parameters	Maximum value	Minimum value
DC link voltage	360 V	165 V
Phase a voltage	60 V	- 125 V
Phase b voltage	45 V	- 165 V
Phase c voltage	165 V	30 V
Phase a current	1.5 A	- 3.1 A
Phase b current	1 A	- 4.5 A
Phase c current	4.2 A	0.6 A

SUMMARY AND CONCLUSIONS

CHAPTER 5 SUMMARY AND CONCLUSION

5.1 Summary

The induction motor has pioneered in industrial applications due to its reliability, robust nature, low cost, efficiency and self-starting capability. With all these advantages, the IM had emerged as an unbeatable competitor despite of several other special motors in the market. The rapid developments in the power electronic sector have extended the horizons for the applications of IM in industries. The semiconductor power devices like IGBT on the virtue of its high efficiency, fast switching, high current tolerant capacity and easy gate-signal commutations control has laid the path for the IM in variable speed applications. The PWM-VSI fed 3-ϕ induction motor drives are widely used in industries for variable speed applications. However, these IM drives are sensitive to various types of inverter faults like IGBT switch open circuit and short circuit. Therefore, it becomes more important to trace the inverter faults so as to design the control strategies for avoiding the hindrance in the drive system occurring due to faults.

In the present study, two cases of inverter faults i.e. IGBT open circuit and short circuit are analysed and the results are plotted sequentially in chapter 4. Here, the IM prototype of 7.5 kW is first designed in the RMxprt design tool by considering the complete geometry of the machine. The 2D model of the machine is then designed in the Maxwell 2D design tool for the finite element analysis. Further, the drive circuit of the motor comprising a VSI controlled by SPWM technique is modelled in the Simplorer design tool. The output responses of the PWM-VSI are first analysed for the resistive load. Then, the drive circuit is then integrated with the motor by co-simulating the Maxwell 2D design tool and Simplorer design tool for investigating the performance of the complete drive system. Finally, the fault analysis is carried out for the inverter by introducing the faults in inverter IGBT switches and tracing the output responses of the inverter terminals. To achieve the above said purpose, the simulation was conducted in ANSYS software.

5.2 Conclusions

The conducted study provides a thorough comprehension of the design and simulation aspects of the open-loop IM drive system. The work effectively aids in predicting the performance of the drive under normal and different inverter fault operation. While designing the 7.5 kW prototype of 3-ϕ induction motor in RMxprt design tool, it was observed that the efficiency and motor characteristics improvisation could be done by altering the stator and rotor slot configurations. At the circuit modelling level, it was concluded that the 3-ϕ output responses of the inverter improved by taking appropriate values for the carrier frequency. Different fault conditions have been analysed for the inverter and the result justifies the significant changes observed at the inverter terminals. The IGBT open-circuit and short-circuit faults can be easily traced by noticing the responses of DC link voltage, phase voltages, and phase currents of inverter circuit. Recognising these changes in parameters will be a help in designing the fault control algorithm in future.

5.3 Recommendation for Further Work

The possible extension of the study could be to develop the fault diagnosis algorithms of the inverter IGBT faults in open-loop PWM-VSI fed IM drive system by recognising the significant changes at the inverter terminals during fault operation

REFERENCES

LITERATURE CITED

Apostoaia, C. M. (2012, November). Co-simulation platform for AC drives control systems. *In WASET 2012-ICEMDS International Conference on Electric Machines and Drive Systems (No. 71, pp. 1879-1886).*

de Araujo Ribeiro, R. L., Jacobina, C. B., Da Silva, E. R. C., & Lima, A. N. (2004). Fault-tolerant voltage-fed PWM inverter AC motor drive systems. *IEEE Transactions on Industrial Electronics*, *51*(2), 439-446.

Estima, J. O., & Cardoso, A. M. (2010, September). A new approach for real-time multiple open-circuit fault diagnosis in voltage source inverters. *In Energy Conversion Congress and Exposition (ECCE), 2010 IEEE (pp. 4328-4335). IEEE.*

Fuchs, F. W. (2003). Some diagnosis methods for voltage source inverters in variable speed drives with induction machines-a survey. *Industrial Electronics Society, (3), 1378-1385.*

Georgakopoulos, I. P., Mitronikas, E. D., & Safacas, A. N. (2011). Detection of induction motor faults in inverter drives using inverter input current analysis. IEEE Transactions on Industrial Electronics, 58(9), 4365-4373.

Guan, Y., Sun, D., & He, Y. (2007, May). Mean current vector based online real-time fault diagnosis for voltage source inverter fed induction motor drives. *In Electric Machines & Drives Conference, 2007. IEMDC'07. IEEE International (Vol. 2, pp. 1114-1118). IEEE.*

Islam, M. S., Raju, N. I., & Ahmed, A. U. (2013). Sinusoidal PWM signal generation technique for three phase voltage source inverter with analog circuit & simulation of PWM inverter for standalone load & micro-grid system. *International Journal of Renewable Energy Research (IJRER), 3(3), 647-658.*

Klima, J. (2005). Time and frequency domain analysis of fault-tolerant space vector PWM VSI-fed induction motor drive. *IEE Proceedings-Electric Power Applications*, *152*(4), 765-774.

Kumar, N.P., Isha, T. B., and Balakrishnan, P.(2016), "Radial electromagnetic field analysis of induction motor under faulty condition using FEM," *2016 Biennial International Conference on Power and Energy Systems: Towards Sustainable Energy (PESTSE), Bangalore, 2016, pp. 1-6.*

Kumar, N. P., and Isha T.B., (2016), "Electromagnetic field analysis of 3-Phase induction motor drive under broken rotor bar fault condition using FEM," *2016 IEEE International Conference on Power Electronics, Drives and Energy Systems (PEDES), Trivandrum, 2016,pp. 1-6.*

Kumar, N. P., Sreemathi, R., Chandar, K. R., Vaijayanthi, V., & Kumar, S. P. (2017, August). PWM inverter switch open-circuit fault analysis in three phase induction motor drive using FEM. *In 2017 International Conference on Energy, Communication, Data Analytics and Soft Computing (ICECDS) (pp. 1244-1248). IEEE.*

Lee, S., & Yun, J. (2017, August). Influence of electrical steel characteristics on efficiency of industrial induction motors. *In Electrical Machines and Systems (ICEMS), 2017 20th International Conference on (pp. 1-4). IEEE.*

Lu, B., & Sharma, S. (2008, October). A literature review of IGBT fault diagnostic and protection methods for power inverters. *In Industry Applications Society Annual Meeting, 2008. IAS'08. IEEE (pp. 1-8). IEEE.*

Mini, V. P., & Ushakumari, S. (2012, December). Rotor fault analysis of an induction motor using FEM. *In Power, Control and Embedded Systems (ICPCES), 2012 2nd International Conference on (pp. 1-7). IEEE.*

Najafabadi, T. A., Salmasi, F. R., & Jabehdar-Maralani, P. (2011). Detection and isolation of speed-, DC-link voltage-, and current-sensor faults based on an adaptive observer in induction-motor drives. *IEEE Transactions on Industrial Electronics, 58(5), 1662-1672.*

Prieto, J., Jones, M., Barrero, F., Levi, E., & Toral, S. (2011). Comparative analysis of discontinuous and continuous PWM techniques in VSI-fed five-phase induction motor. *IEEE Transactions on Industrial Electronics, 58(12), 5324-5335.*

Sreeja V„ Mini.V.P., Sreedevi.G., (2015, September) Fault analysis of induction motor drive system using Maxwell-Simplorer. *International Journal of Electrical, Electronics and Data Communication, Volume-3, Issue-9*

Srinivasan, J., Selvaraj, K., Chitrarasu, J., & Resmi, R. (2016, October). Design and analysis of squirrel cage induction motor in short pitch and full pitch winding configurations using FEA. *In Emerging Technological Trends (ICETT), International Conference on (pp. 1-10). IEEE.*

Trabelsi, M., Boussak, M., Mestre, P., & Gossa, M. (2011, June). An improved diagnosis technique for IGBTs open-circuit fault in PWM-VSI-fed induction motor drive. *In Industrial Electronics (ISIE), 2011 IEEE International Symposium on (pp. 2111-2117). IEEE.*

Vujacic, M., Hammami, M., Srndovic, M., & Grandi, G. (2018). Analysis of dc-Link Voltage Switching Ripple in Three-Phase PWM Inverters. *Energies, 11(2), 471.*

Yu, O. S., Park, N. J., & Hyun, D. S. (2006, November). A novel fault detection scheme for voltage fed PWM inverter. *In IEEE Industrial Electronics, IECON 2006-32nd Annual Conference on (pp. 2654-2659). IEEE.*

Zhang, J., Zhao, J., Zhou, D., & Huang, C. (2014). High-performance fault diagnosis in PWM voltage-source inverters for vector-controlled induction motor drives. *IEEE Transactions On Power Electronics, 29(11), 6087-6099.*

VITA

The author of this manuscript, ***Mr. Rajat Sharma*** *was born on 22nd November, 1994 in Ghaziabad, Uttar Pradesh. He passed his High School examination in 2010 and Intermediate examination in 2012 from R.R.C.S Gadarpur, Uttarakhand. He completed his B.Tech. in Electrical & Electronics Engineering from Amrapali Institute of Technology & Sciences, Haldwani, Uttarakhand in 2016. He joined M.Tech. in Electrical Engineering in 2016 with major in Electrical Energy System in the College of Post Graduate Studies, G. B. Pant University of Agriculture & Technology, Pantnagar, Uttarakhand. He is the recipient of MHRD GATE Scholarship during M.Tech Programme.*

Address:

Rajat Sharma,
H.No. 90/11, Yellow Quarters,
Lohia Nagar, Ghaziabad,
Distt. – Ghaziabad, Pin-201001
Uttar Pradesh, India
Phone: 8859844314
Email: rajatsharmagbpuat@yahoo.com

ABSTRACT

Name	:	Rajat Sharma	Id. No.	:	50912
Sem. &Year	:	1st Sem, 2016-17	Degree	:	M.Tech.
Major	:	Electrical Energy System	Department	:	Electrical Engineering
Thesis Title	:	Design, Modelling and Fault Analysis of Induction Motor Drive System using ANSYS			
Advisor	:	Dr. Rajiv Singh			

Induction motors have wide applications in industries by virtue of its reliability, efficiency, robustness, self-starting capability and low cost. With rapid developments in power electronics over the past few years, the 3-ϕ induction motor has acquired a unique place in the variable speed application drives. The PWM-VSI fed 3-ϕ induction motor drives have pioneered in industrial applications for variable speed operations such as traction, robotics, aeronautics and railway. The fast switching, high efficiency, simple gate-signal commutations control and ability to manage high short-circuit current of power switches like IGBT have created wide applications of VSIs for the drives. However, these IM drives are prone to different types of faults like IGBT switch short-circuit and open-circuit fault. On an approx. nearly 53% failures occur in the control circuit while 38% failures are majorly associated with the power components of variable speed drives. Thus, it becomes crucial to investigate the complete design, modelling and fault analysis of the IM drive system. This thesis presents a comprehensive performance analysis of PWM-VSI fed IM drive system under normal and fault operation. This work is an attempt to encompass various aspects of design, modelling, simulation and analysis of the IM drive circuit. Typical cases of IGBT open-circuit and short-circuit faults have been analysed in the proposed work. The 7.5 kW prototype of SCIM has been designed in RMxprt and Maxwell 2D design tools for finite element analysis. While the SPWM controlled inverter circuit has been designed in the Simplorer design tool. The Maxwell 2D motor model and Simplorer circuit design are then co-simulated in order to investigate the performance of the open-loop drive system and analysis of the open-circuit and short-circuit faults in inverter IGBT.

(Rajiv Singh)
Advisor

(Rajat Sharma)
Author

नाम	: रजत शर्मा	पहचान संख्या	: 50912
प्रवेश वर्ष	: 2016	उपाधि	: एम. टेक.
प्रमुख	: विद्युत अभियांत्रिकी	विभाग	: विद्युत अभियांत्रिकी
थीसिस शीर्षक	: एएनएसवाईएस का उपयोग कर प्रेरण मोटर ड्राइव सिस्टम का डिजाइन, मॉडलिंग और दोष विश्लेषण		
सलाहकार	: डॉ राजीव सिंह		

सारांश

इंडक्शन मोटर्स की विश्वसनीयता, दक्षता, मजबूती, आत्म-प्रारंभिक क्षमता और कम लागत के आधार पर उद्योगों में व्यापक अनुप्रयोग हैं। पिछले वर्षों में शक्ति इलेक्ट्रॉनिक्स में तेजी से विकास के साथ, 3-ϕ इंडक्शन मोटर ने परिवर्तनीय गति अनुप्रयोग ड्राइव में एक अद्वितीय जगह हासिल की है। पीडब्लूएम-वीएसआई ने 3-ϕ इंडक्शन मोटर ड्राइव की आपूर्ति की है, जो ट्रैक्शन, रोबोटिक्स, एयरोनॉटिक्स और रेलवे जैसे परिवर्तनीय गति संचालन के लिए औद्योगिक अनुप्रयोगों में अग्रणी है। तेजी से स्विचिंग, उच्च दक्षता, सरल गेट-सिग्नल कम्यूटेशन नियंत्रण और आईजीबीटी जैसे शक्ति स्विच के उच्च शॉर्ट-सर्किट प्रवाह को प्रबंधित करने की क्षमता ने ड्राइव के लिए वीएसआई के व्यापक अनुप्रयोग बनाए हैं। हालांकि, ये आईएम ड्राइव आईजीबीटी स्विच शॉर्ट-सर्किट और ओपन-सर्किट दोष जैसे विभिन्न प्रकार के दोषों से ग्रस्त हैं। नियंत्रण सर्किट में लगभग 53% विफलता होती है, जबकि 38% असफलता परिवर्तनीय गति ड्राइव के पावर घटकों से मुख्य रूप से जुड़ी होती है। इस प्रकार, आईएम ड्राइव सिस्टम के पूर्ण डिजाइन, मॉडलिंग और दोष विश्लेषण की जांच करना महत्वपूर्ण हो जाता है। यह थीसिस सामान्य और दोष ऑपरेशन के तहत पीडब्ल्यूएम-वीएसआई आपूर्ति आईएम ड्राइव सिस्टम का एक व्यापक प्रदर्शन विश्लेषण प्रस्तुत करता है। यह काम आईएम ड्राइव सर्किट के डिजाइन, मॉडलिंग, सिमुलेशन विश्लेष के विभिन्न पहलुओं को शामिल करने का प्रयास है। आईजीबीटी ओपन-सर्किट और शॉर्ट-सर्किट दोषों के विशिष्ट मामले का प्रस्तावित काम में विश्लेषण किया गया है। इसके लिए, एससीआईएम आईएम का 7.5 किलोवाट प्रोटोटाइप आरएमएक्सप्रेट और मैक्सवेल 2 डी डिज़ाइन टूल्स में परिमित तत्व विश्लेषण के लिए डिज़ाइन किया गया है, जबकि एसपीडब्ल्यूएम नियंत्रित इन्वर्टर सर्किट को सिम्प्लोरर डिज़ाइन टूल में डिज़ाइन किया गया है। दो मैक्सवेल 2 डी और सिम्पलोरर डिज़ाइन को इन्वर्टर आईजीबीटी में ओपन सर्किट और शॉर्ट सर्किट दोषों के लिए पूरे ओपन-लूप ड्राइव सिस्टम के प्रदर्शन और गलती विश्लेषण की जांच करने के लिए सह-अनुकरण किया जाता है।

(राजीव सिंह)
सलाहकार

(रजत शर्मा)
लेखक